Analysis of Resonant Structures in the pK_S^0-channel at HERMES

Analyse resonanter Strukturen im pK_S^0-Kanal bei HERMES

Master-Thesis

im Studiengang M.Sc. Physik

vorgelegt von

Marian Stahl

Gießen, im Juli 2013

AG Düren

II. Physikalisches Institut

Justus-Liebig-Universität Gießen

Zusammenfassung

Die Analyse resonanter Strukturen im pK^0_S ($\bar{p}K^0_S$) Kanal, im Zusammenhang mit der Suche nach dem Θ^+ ($\overline{\Theta}^-$) Pentaquark, wurde mit HERMES Daten aus quasi-reeller Photoproduktion von Wasserstoff- und Deuteriumtargets wiederholt. Für die Analyse wurden bereits veröffentlichte (HERA I) und neue (HERA II) Daten verwendet. Die gesammelte Statistik am Deuteriumtarget konnte um einen Faktor 2.15 gegenüber den publizierten Daten verbessert werden. Die Wasserstoffdaten sind neu, unveröffentlicht und umfassen im Vergleich mit Deuteriumdaten etwa die doppelte Statistik. Alte und neue Daten wurden mit verbesserten Spurrekonstruktions- und Teilchenidentifikationsalgorithmen analysiert. Dabei wurden Selektionskriterien mit Hilfe zweier unterschiedlicher Philosophien in einer blinden Analyse bestimmt, welche die Abschätzung systematischer Unsicherheiten durch die Selektionskriterien erlauben. Eine der Philosophien strebt optimierte Statistik an, während die andere auf höhere Reinheit und vorsichtigere Selektionskriterien ausgelegt ist. Zusätzlich wurden weitere systematische Studien durchgeführt, darunter die Optimierung von Teilchenidenfikationsparametern für Proton-Kandidaten, Studien an Parametern des Proton-Vertex, Kontamination des pK^0_S-Kanals durch andere Teilchenzerfälle und kinematische Korrelationen. Die pK^0_S Spektren beider Philosophien zeigen an Deuteriumdaten ein schmales Signal bei ~ 1522 MeV, während kein Signal in Wasserstoffdaten zu sehen ist. Die globale Signifikanz des Signals aus den Deuteriumdaten für den Datensatz mit optimierter Statistik wurde zu $3.1\,\sigma$ berechnet. Die Spektren beider Philosophien und das 2004 publizierte Resultat sind zueinander kompatibel. Für das Verhältnis von Signalereignissen in Wasserstoff zu Deuterium wurde ein 95 % Konfidenzniveau berechnet. Zusätzlich wurde die Kompatibilität von Deuterium- zu Wasserstoffdaten als $\mathrm{CL_s}$-Wert und Gaußsche Signifkanz mit Hilfe des direkten Quotienten von Deuterium- zu Wasserstoffdaten oder einer Bayesschen MARKOV-Ketten-Monte-Carlo Methode quantifiziert. Die strangeness des Signals wurde durch die Suche einer nicht-exotischen Resonanz im $\Lambda\pi^+$-Kanal getestet, wobei eine obere Grenze an die Größe $\mathcal{B} = \frac{\Gamma(\Theta^+ \to \Lambda\pi^+)}{\Gamma(\Theta^+ \to pK^0_S)}$ berechnet wurde. Das Signal in den Deuteriumdaten kann, inbesondere mit Hinblick auf systematische Unsicherheiten aufgrund der Modellierung des Untergrundes, nur als Hinweis auf eine reale Resonanz bei ~ 1522 MeV gedeutet werden. Die statistische Signifikanz des Signals ist aber nicht ausreichend um es als Entdeckung zu bezeichnen.

Abstract

The analysis of resonant structures in the pK^0_S ($\bar{p}K^0_S$) channel, associated with a search for the light pentaquark Θ^+ ($\overline{\Theta}^-$), using HERMES data from quasi-real photoproduction off hydrogen and deuterium targets has been redone. The analysis included previously published (HERA I) and new (HERA II) data. The statistics taken on a deuterium target could be improved by a factor of 2.15 and the data taken on a hydrogen target is new, unpublished data with about twice as much statistics as the combined deuterium data. Old and new data were analyzed with refined tracking and particle identification algorithms. Selection criteria were determined by following two different philosophies in a blind analysis which provide a benchmark for systematic uncertainties due to the selection criteria. One of the philosophies aims for optimized statistics, while the other intends a more careful approach reaching for higher purity. Additional systematic studies have been carried out, containing the optimization of PID parameters for the proton candidate, studies on parameters of the proton vertex, cross-feed from other channels and kinematic correlations. The pK^0_S spectra obtained by both philosophies from data taken on deuterium exhibited a narrow bump at ~ 1522 MeV, while no structure was seen in hydrogen data. The global significance of the bump on deuterium for the sample with optimized statistics was calculated to be $3.1\,\sigma$. The pK^0_S spectra of both philosophies and also the published result from 2004 are statistically compatible to each other. An upper limit of the ratio of signal events on hydrogen to deuterium has been calculated at the 95 % confidence level. In addition the compatibility of the results from deuterium and hydrogen targets has been quantified in terms of a $\mathrm{CL_s}$ value or a Gaussian significance using the direct ratio of both spectra or a Bayesian MARKOV-chain-Monte-Carlo approach. The strangeness of the bump has been tested by a search for a non-exotic resonance in the $\Lambda\pi^+$-channel, where an upper limit to $\mathcal{B} = \frac{\Gamma(\Theta^+ \to \Lambda\pi^+)}{\Gamma(\Theta^+ \to pK^0_S)}$ was set. The bump on deuterium, with regard to systematic uncertainties coming from the background shape, is a hint that there might be a real resonance in the data at ~ 1522 MeV, but it is not strong enough to claim the observation of a particle.

Table of contents

1 Introduction

This chapter will give a brief "folkloristic" introduction to particle physics and shortly discuss the QCD-Lagrangian and its exact, approximate, broken and absent symmetries. The property of approximate $SU(3)$ flavor symmetry is then used to construct meson and baryon multiplets. Baryons in the limit of a chirally symmetric Lagrangian are addressed in a summary of the basic properties of the SKYRME model which eventually led to the prediction of a light and narrow pentaquark.

After the identification of electrons (e^-) as particles in 1897 by THOMPSON, RUTHERFORD discovered in 1909 the nuclear structure in atoms. In 1917 he found hydrogen-like particles in the nuclear reaction of pure nitrogen with α-particles. This experiment led him to the postulation that the hydrogen nucleus is a fundamental particle, and named it proton (p). Because of the electric repulsion force of protons in nuclei, RUTHERFORD predicted neutrons (n) which compensate this force. In 1932 CHADWICK was able to confirm the existence of the neutron. In the same year HEISENBERG introduced the isospin I as a new quantum number to explain symmetries between protons and neutrons, like mass and interaction strength. In the limit of isospin-symmetry, the potentials needed to form the nucleus collapse from three – namely p-p, p-n and n-n – to two types of interaction, where nucleons couple to $I = 0$ or $I = 1$. In 1935 YUKAWA formulated the internuclear interaction of protons and neutrons by means of the exchange of heavy bosons which he named mesons, and which were confirmed in 1947 by the discovery of charged pions ($\pi^\pm$) in Bristol by POWELL *et al.* [1]. The neutral pion (π^0) was discovered two years later at the cyclotron of the University of California [2]. As a consequence of the DIRAC-equation, the discovery of the positron (e^+) and its identification as anti-electron 1932 by ANDERSON, anti-protons ($\bar{p}$) and anti-neutrons ($\bar{n}$) were expected to exist. And indeed, the $\bar{p}$ was discovered in 1955 at the Berkley Bevatron by SEGRÈ *et al.* [3] and the $\bar{n}$ shortly after that by CORK *et al.* [4].
With this set of hadrons and leptons the picture of (elementary) particle physics could have been complete[1], but there were some unforeseen discoveries in the meantime. First, the muon (μ) was discovered in cosmic radiation by ANDERSON and NEDDERMEYER in 1936 [6] and, because of its mass, thought to be the meson predicted by YUKAWA in 1935. But later studies with "μ-mesons" showed that it did not interact with the nuclear force (i.e. strong force). Even 9 years after its observation, RABI posed the question "*Who ordered that?*" at his Nobel laureate to express the ongoing confusion about the nature of muons. YUKAWA's theory of nuclear forces reached its limitations as well. When probing the interaction at short distances, experimental data indicated higher attraction between nucleons, which led to the prediction of an isoscalar scalar meson (the σ or f_0 – which is still not completely understood) and an isoscalar and isovector vector meson (ω and ρ), discovered in the early 1960s.
In addition strangeness was observed. First in the V-shaped decay of a Kaon (K) in a cloud chamber photograph from cosmic rays impinging on a lead plate in 1947 by ROCHESTER and BUTLER [7]. A different strange particle, the Λ-baryon, decaying into $p\pi^-$, was discovered at the Cal Tech facility by SERIFF *et al.* [8]. Further studies have shown that these strange particles were produced in pairs following certain rules: a Λ was e.g. produced together with a K^+, but never with a K^-. To explain this behavior a new quantum number, the strangeness, was introduced. The strangeness is conserved in the production processes of the strong interaction, but violated in the weak decay, providing a link to the β-decay where the isospin conservation is violated. More particle discoveries followed, like an isospin-quadruplet originating from πN interactions, known as Δ-resonances, a strange iso-triplet, the Σ-baryons, and a doubly strange iso-doublet, the Ξ-baryons and excitations of these states.

[1] The discovery of electron-neutrinos, hypothesized by PAULI to explain the β decay, followed in 1956 by COWAN *et al.* [5].

The whole zoo of strongly interacting particles was divided into mesons, originating from the Greek word $\tau\grave{o}\ \mu\acute{\epsilon}\sigma o\nu$, meaning intermediate – due to the mass of mesons with respect to the electron and nucleons – and baryons, originating from the Greek word $\beta\alpha\rho\acute{\upsilon}\zeta$, meaning heavy – analogue to the naming for mesons. Different approaches in the classification and in understanding the interactions of all these particles were pursued, from which two seemingly different types of theories/philosophies describing strong interactions emerged, which persisted until today.
One of these two main philosophies, the string theory, educed from arranging particles in straight REGGE trajectories, which relate mass and spin of a particle. Together with the S(cattering)-matrix theory, developed by HEISENBERG in 1943, the idea that everything could be built up by modes of energetic strings was derived. In such a theory, point-like elementary particles would not exist. With the advent of Quantum ChromoDynamics (QCD), string theory was put in the dustbin for making wrong predictions for some experimental findings. Later it was realized, that this theory could be a candidate for a Theory Of Everything (TOE), combining the theory of gravity with the standard model or a grand unified theory beyond the standard model. It would be thrilling to see how string theory (in all its variations) and the principles of QCD fit together in a consistent picture.
The other philosophy followed the ancient concept of elementary particles, i.e. particles that can not be further divided. The basic idea was to introduce a generalization of isospin and arrange it, similar to the $SU(2)$ properties of isospin, in an $SU(3)$ group. In 1956, SAKATA proposed (p, n, Λ) to be the building blocks of matter [9]. In this model mesons are formed by the combination of baryon and anti-baryon. The model had some difficulties, such as the description of long-range baryon-baryon interaction in the YUKAWA-picture, and the description of the Σ-triplet and the Ξ-doublet as higher representations of (p, n, Λ) containing an additional baryon-anti-baryon pair.
In 1961 GELL-MANN and independently NE'EMAN extended the ideas of SAKATA in a more abstract approach, where elementary baryons and mesons do not exist [10, 11]. In his paper GELL-MANN established the term eightfold way for the octet representation of baryons along with the term gluon to describe coupling of the strong force. In addition GELL-MANN made some remarkable predictions: He anticipated the existence of the η and ω meson, and predicted the Ω^- baryon in a corollary – a particle with a strangeness of -3 and a mass of ~ 1680 MeV [12]. The Ω^-, discovered in 1964 [13], was the missing "puzzle piece" in the decuplet representation of meson-nucleon scattering; all other 9 particles of this multiplet were known.
The question arose why baryons and mesons fit into multiplets while their fundamental representation is a unitary triplet **3**, collapsing to an isospin-doublet (u, d) and a strange singlet (s). Using the fundamental representation GELL-MANN and ZWEIG independently postulated three new particles, called quarks or aces. Despite the elegant description of hadrons by the eightfold way, the quark model had some serious problems and was doubted by many physicists until the mid 1970s. One major objection was, that no individual isolated quarks could be discovered (until now). This phenomenon is known as the confining nature of strong interactions, but the underlying mechanism remains illusive. A second major problem were the "edges" of the baryon decuplet, which seemed to violate the PAULI exclusion principle. The today well established principle of color charge, proposed in 1964 by GREENBERG [17] as a way out of this dilemma, was comprehensively perceived as a technical sleight at that time. And although high energy experiments in the 1960s at the SLAC and CERN facilities indicated the substructure of the proton and suggested that its charge is concentrated in three lumps, almost half of its energy was carried by neutral particles, which was not anticipated. These deep-inelastic-scattering experiments were commonly described by the parton model proposed by FEYNMAN in 1969, which did not introduce additional hypotheses like quarks. Although partons can now be associated with quarks and gluons, the parton model persisted and is still an active field of study.

With the discovery of the J/Ψ meson and thus the charm quark in 1974 [18, 19], the quark model eventually prevailed. The existence of a fourth type of quarks was initially claimed by BJØRKEN and GLASHOW [20] – unfortunately for the wrong reasons. A different approach by GLASHOW, ILIOPOULOS and MAIANI in 1970 (the GIM mechanism) [21] needed the existence of a charm quark and was later generalized by KOBAYASHI and MASKAWA in the CABIBBO-KOBAYASHI-MASKAWA matrix which successfully describes the transition between quark types in the electroweak interaction and plays an important role in the understanding of $\mathcal{CP}$-violation.

1.1 QCD and its Symmetries

In 1954 YANG and MILLS formulated a gauge theory based on the non-abelian $SU(2)$ isospin-symmetry group to explain strong interactions [22]. The formalism can be extended to any compact semi-simple LIE groups, such as $SU(N)$.
Let $\{\phi_r(x)|r = 1, ...f\}$ be a set field operators, denoted as f-dimensional vector $\phi(x)$, which transforms under a $N^2 - 1$-dimensional gauge group $SU(N)$ like

$$\phi(x) \to \exp\left[i \sum_{a=1}^{N^2-1} \theta^a(x) T_a\right] \phi(x) \,, \tag{1.1}$$

with T_a being the generators of the gauge group. Note that the gauge shift $\theta^a(x)$ in a local symmetry depends on space-time, which is not the case in global symmetries. Thus local gauge invariance is a more stringent requirement. In order to construct a gauge invariant Lagrangian, the derivatives of the field operators must transform like the field operators themselves. Using the EINSTEIN summation convention henceforth, the gauge covariant derivative transforms like

$$\mathscr{D}_\mu \phi(x) \to \exp\left[i\theta^a(x) T_a\right] \left[\mathscr{D}_\mu \phi(x)\right] \,. \tag{1.2}$$

It is known from differential geometry that this condition is fulfilled by

$$\mathscr{D}_\mu \phi(x) = \left[\partial_\mu + igA^a_\mu(x) T_a\right] \phi(x) \,. \tag{1.3}$$

Thus the condition of local gauge invariance of the Lagrangian naturally introduces $N^2 - 1$ gauge vector fields $A^a_\mu(x)$, the quanta of which are called gauge- or exchange bosons, and a coupling of $\phi(x)$ to $A_\mu(x)$ with strength g. The gauge field transformation is most easily expressed in terms of

$$A^a_\mu(x) T_a \to A^a_\mu(x) \left[e^{i\theta^b(x)T_b} T_a e^{-i\theta^b(x)T_b}\right] + \frac{i}{g}\left[\partial_\mu e^{i\theta^b(x)T_b}\right] e^{-i\theta^b(x)T_b} \,. \tag{1.4}$$

In a YANG-MILLS theory the field strength tensor $F^a_{\mu\nu}(x)$ is defined by the commutator of the gauge covariant derivatives

$$\left[\mathscr{D}_\mu, \mathscr{D}_\nu\right] = -igT_a F^a_{\mu\nu}(x) \,. \tag{1.5}$$

Using the property

$$\left[T_a, T_b\right] = i f_{ab}{}^c T_c \tag{1.6}$$

of the LIE-algebra, with its structure constants $f_{ab}{}^c$ and equation (1.3), the field strength tensor reads

$$F^a_{\mu\nu}(x) = \partial_\mu A^a_\nu(x) - \partial_\nu A^a_\mu(x) + g f^a{}_{bc} A^b_\mu(x) A^c_\nu(x) \,. \tag{1.7}$$

The field strength tensor transforms as a gauge vector – hence is no observable quantity – but the product

$$\mathscr{L}_{\mathrm{gf}}(x) = -\frac{1}{4} F_a^{\mu\nu}(x) F^a_{\mu\nu}(x) \,, \tag{1.8}$$

similar to quantum electrodynamics, is the demanded gauge invariant quantity, called gauge field Lagrangian. In the presence of a DIRAC field $\phi(x)$ the gauge invariant Lagrangian is given by

$$\mathscr{L}(x) = \mathscr{L}_{\mathrm{gf}}(x) + \mathscr{L}_0(x) = \mathscr{L}_{\mathrm{gf}}(x) + \overline{\phi}(x) \left(i \not{\mathscr{D}} - M \right) \phi(x) \,, \tag{1.9}$$

i.e. the gauge field Lagrangian plus the Lagrangian for a free DIRAC fermion with $\overline{\phi}(x) = \phi^\dagger(x)\gamma^0$ being the PAULI adjoint spinor and the gauge covariant derivative $\mathscr{D}_\mu$, using the FEYNMAN slash notation $\not{\mathscr{D}} = \gamma^\mu \mathscr{D}_\mu$.
QCD is described as a YANG-MILLS theory with an underlying $SU(3)_{\mathrm{c}}$ color charge group. Experimental results verified the color charge hypothesis and determined the number of colors to be $N_{\mathrm{c}} = 3$. The only compact semi-simple LIE group having 3-dimensional irreducible real and complex representations is $SU(3)$. The complex representations are needed to account for the anti-color, carried by anti-quarks and gluons. Applying equation (1.9) to the $SU(3)_{\mathrm{c}}$ color charge group of QCD, the decomposed Lagrangian reads

$$\begin{aligned}
\mathscr{L}_{\mathrm{QCD}}(x) = &-\frac{1}{4} \left(\partial_\mu G^a_\nu(x) - \partial_\nu G^a_\mu(x) \right) \left(\partial^\mu G_a^\nu(x) - \partial^\nu G_a^\mu(x) \right) + \bar{q}^\alpha_f \left(i \not{\partial} - M_f \right) q^\alpha_f \\
&+ g \bar{q}^\alpha_f \not{G}^a(x) \left(\frac{\lambda_a}{2} \right)_{\alpha\beta} q^\beta_f \\
&+ \frac{g}{2} f_a{}^{bc} \left(\partial_\mu G^a_\nu(x) - \partial_\nu G^a_\mu(x) \right) G^\mu_b(x) G^\nu_c(x) \\
&- \frac{g^2}{4} f^{abe} f_{cde} G^\mu_a(x) G^\nu_b(x) A^c_\mu(x) G^d_\nu(x) \,,
\end{aligned} \tag{1.10}$$

with the color indices α, β, the 8 gauge field indices a, the flavor index f of the quark field and the DIRAC indices μ, ν, which are omitted on the fermion spinors. The generators $T_a = \frac{\lambda_a}{2}$ of $SU(3)$ are given by the GELL-MANN matrices λ_a [10]. To link the formal gauge field $A^a_\mu(x)$ and the field operator $\phi(x)$ to QCD, the notation $G^a_\mu(x)$ for the gluon field and $q(x)$ for the quark field was chosen. The coupling g is the gauge coupling and should not be confused with the effective running coupling $\alpha_{\mathrm{s}}(Q^2)$. In the quark mass term $-\bar{q}^\alpha_f M_f q^\alpha_f$ the "bare" quark masses, generated via the HIGGS mechanism, enter in the mass matrix[1]. It is also seen that a term $\sim m^2 G^\mu_a G^a_\mu$ does not appear and would violate gauge invariance (c.f. eq. (1.4)). Thus gluons, and in general gauge vector bosons in a YANG-MILLS theory, must be massless. Nevertheless, the physical quantities of the gauge fields can acquire mass by symmetry breaking [23–25]. The first line in equation (1.10) contains the kinetic terms for quark and gluon fields; the second line describes the color interaction between quarks and gluons and line 3 and 4 give rise to self-interaction of 3rd and 4th order of the gluons. These terms come from the non-vanishing commutator of the LIE-algebra in equation (1.7) and appear even in the absence of other fields. In the quantized Lagrangian additional fields appear due to gauge fixing (c.f. e.g. [26]). For further considerations in this work these additional fields are not needed, but the properties of the quantized quark and gluon fields shall be briefly discussed.

[1] The matrix is commonly assumed to be diagonal $M_f = M_{ff'} \delta_{ff'}$.

Table 1.1 summarizes important properties of the quantized quark fields. The masses therein are taken from [27], and were, with exception of the top quark, theoretically calculated by means of the modified minimal subtraction ($\overline{MS}$) renormalization scheme. The flavor quantum numbers are the third component of the isospin I_3, strangeness S, charm C, bottomness/beauty B' and topness/truth T. The flavor states in table 1.1 are eigenstates with respect to the strong interaction. In the electroweak sector of the standard model these eigenstates are rotated in flavor-space and, contrary to QCD, transitions from up-type (u,c,t) to down-type (d,s,b) quarks and vice versa are allowed. Quarks are spin $\frac{1}{2}$ fermions with, by convention, positive parity and a baryon number of $\frac{1}{3}$. Anti-quarks have complementary quantum numbers. Quarks are the only standard model particles to experience all four fundamental interactions, namely electromagnetic, weak, strong and gravitational interaction.

I		II		III	
u	up $I_3 = +\frac{1}{2}$ $2.3^{+0.7}_{-0.5}$ MeV	c	charm $C = +1$ 1.275 ± 0.025 GeV	t	top $T = +1$ $173.5 \pm 0.6 \pm 0.8$ GeV
d	down $I_3 = -\frac{1}{2}$ $4.8^{+0.7}_{-0.3}$ MeV	s	strange $S = -1$ 95 ± 5 MeV	b	bottom $B' = -1$ 4.18 ± 0.03 GeV

Table 1.1: Properties of quark states. The generation number is given on top. Name, flavor quantum number and the quark mass entering in the QCD-Lagrangian are given next to the symbol of the quark. The up-type (u,c,t) quarks carry an electric charge of $+\frac{2}{3}e$ and the down-type (d,s,b) quarks $-\frac{1}{3}e$.

In a $SU(N)$ gauge theory the gauge fields $A^a_\mu(x)$ are vector fields in the adjoint representation, which is N^2-1-dimensional. For the color charge group $SU(3)_\mathrm{c}$ this means that eight linear independent gluons exist, which carry color and anti-color. Gluons themselves are colored objects, contrary to a photon in QED which is not charged. Hence they are able to change the color charge state of strongly interacting fields.

As mentioned earlier, quarks have not been directly observed in an experiment. Although scattering off point-like constituents of hadrons is possible, the physically observable final state is a color neutral object. This phenomenon is known as confinement. Up to now, the only unambiguous directly observed color neutral strong interacting objects are baryons and mesons, i.e. bound states of three quarks or a quark and an anti-quark. Because QCD conserves the flavor quantum number (flavor-blindness), hadrons can be labeled by their minimum (valence) quark content, but are dynamically "dressed" with (sea-)quarks and gluons from the QCD vacuum. Confinement does not limit strongly interacting states to be qqq-baryons or $q\bar{q}$-mesons, so combinations like tetraquarks $(qq)(\bar{q}\bar{q})$, mesonic molecules $(q\bar{q})(q\bar{q})$, pentaquarks $qqqq\bar{q}$, hybrid mesons $qg\bar{q}$, glueballs gg, etc. are not forbidden.

1.1.1 Construction of Hadrons

Prior to the color charge model of strong interaction, the $SU(3)$ group structure was used by Gell-Mann and Ne'man in the eightfold way to organize baryons and mesons in multiplets [10, 11]. They utilized the approximate mass-degeneration of states in the resulting multiplets, and hence treated the quark fields as flavor symmetric. The flavor group $SU(3)_\mathrm{f}$ has two independent fundamental representations $\mathbf{3}$ and $\bar{\mathbf{3}}$. These representations are usually plotted as weight diagrams in the (I_3, Y)-plane (fig. 1.1), where I_3 is the third component of the isospin and Y, the sum of strangeness and baryon number, is the (strong) hypercharge.

The nodes in the **3** ($\bar{\mathbf{3}}$) diagram correspond to the three quark flavors u, d and s ($\bar{u}, \bar{d}$ and $\bar{s}$). The black solid lines between the nodes correspond to the lowering and raising operators which move between the different weight vectors, each forming a $SU(2)$ subalgebra.

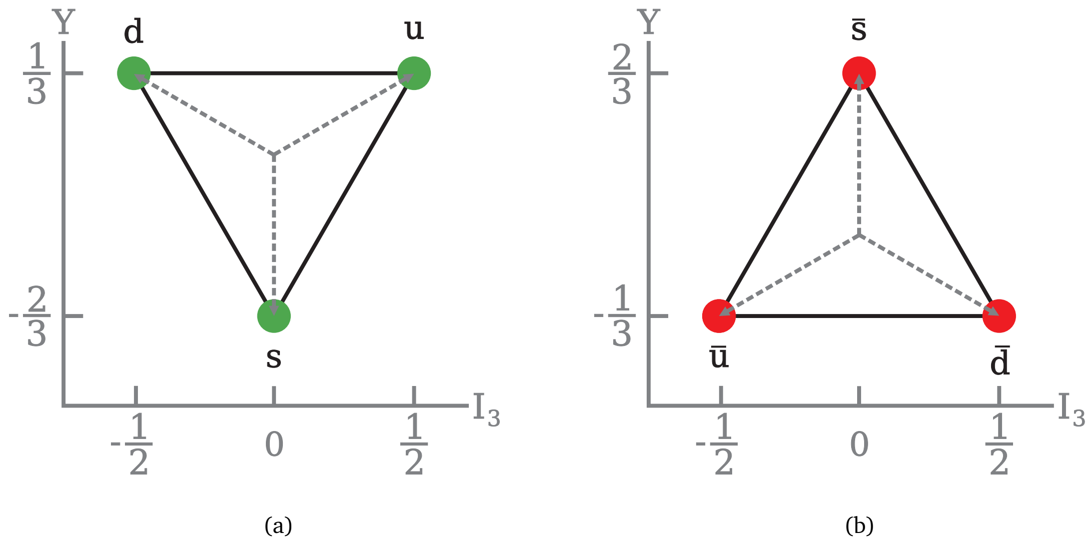

Figure 1.1: Weight diagram of quarks and anti-quarks. (a) The fundamental **3** representation of the $SU(3)_f$ group. (b) Weight diagram for the $\bar{\mathbf{3}}$ representation of $SU(3)_f$.

Mesons can now be graphically constructed by adding one fundamental representation, with center $(0,0)$, to the nodes of the other which is equivalent to a shift of the three gray dashed vectors to each node. This has been done in figure 1.2.

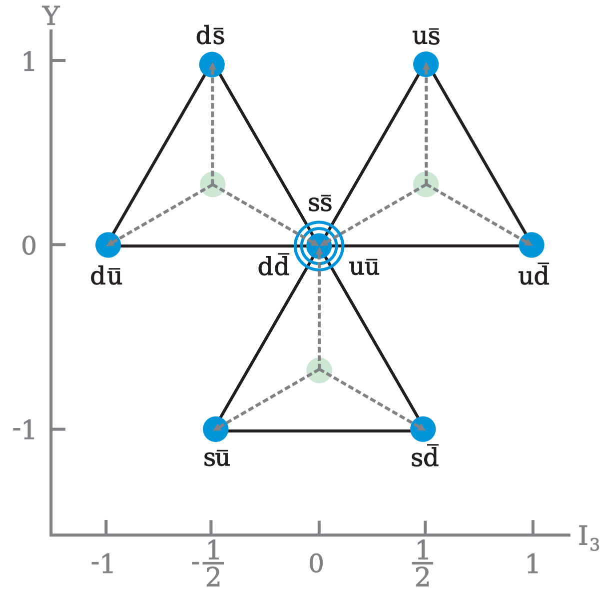

Figure 1.2: Meson octet plus singlet $\mathbf{3} \otimes \bar{\mathbf{3}} = \mathbf{8} \oplus \mathbf{1}$ representation of the $SU(3)_f$ group. The $\bar{\mathbf{3}}$ representations have been added to the nodes of the **3** representation, which are depicted in light green.

The graphical construction however, is not able to reproduce all group theoretical properties of the multiplets. The decomposition of the multiplets into irreducible representations is discussed e.g. in [28]. For mesons, the irreducible representations are an octet and a singlet representation coming from the direct product of quark- and anti-quark representation $\mathbf{3} \otimes \bar{\mathbf{3}} = \mathbf{8} \oplus \mathbf{1}$. The next step is to identify the nodes in the weight diagrams of irreducible multiplets with $SU(3)_f$-symmetric states, whose wave functions can be computed using tensor algebra [29]. For some reason the $SU(3)_f$-symmetric wave functions of the iso-singlet from the octet representation and the singlet do not correspond to physical observables and mix. This mixing is empirically described by an angle θ, and its decomposition is an active area of research (c.f. e.g. [30, 31]). In the case of vector-mesons almost ideal mixing $\left(\tan\theta \approx \frac{1}{\sqrt{2}}\right)$ is measured, such that the observable ϕ and ω mesons can approximately be written as $s\bar{s}$ and $\frac{1}{\sqrt{2}}(u\bar{u} + d\bar{d})$ respectively.
The (graphical) construction of baryons is straightforward, and as an intermediate step an object consisting of two quarks is formed, plotted in 1.3.

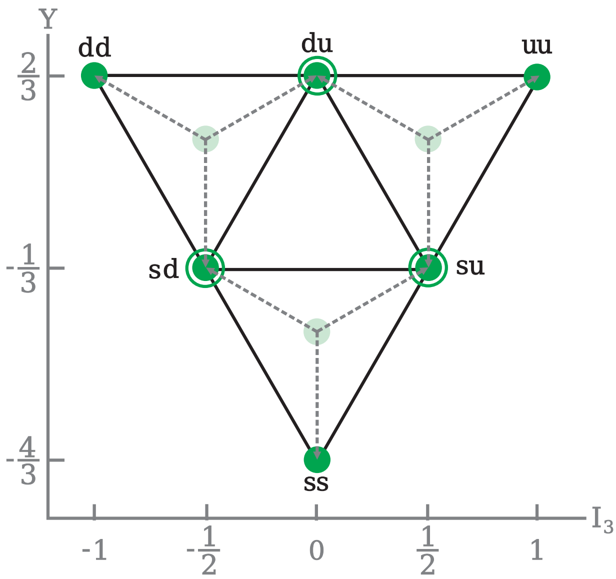

Figure 1.3: Diquark sextet plus anti-triplet $\mathbf{3} \otimes \mathbf{3} = \mathbf{6} \oplus \bar{\mathbf{3}}$ representation. The $\mathbf{3}$ representations have been added to the nodes of the $\mathbf{3}$ representation, which are depicted in light green.

The bound configurations of two quarks are known as diquarks. Although diquarks can not be observed directly, they play an important role in some effective QCD models, where e.g. baryons consist of a diquark and a spectator quark. Lattice QCD calculations seem to support these models [32].
The addition of a third quark to the sextet representation of two quarks yields a decuplet and an octet representation, shown in figure 1.4. In addition to $\mathbf{6} \otimes \mathbf{3} = \mathbf{10} \oplus \mathbf{8}$, the product of a quark with the second diquark representation $\mathbf{3} \otimes \bar{\mathbf{3}} = \mathbf{8} \oplus \mathbf{1}$ is already known from the construction of mesons. Thus the baryonic $SU(3)_f$ states are given by

$$\mathbf{3} \otimes \mathbf{3} \otimes \mathbf{3} = (\mathbf{6}_S \oplus \bar{\mathbf{3}}_A) \otimes \mathbf{3} = \mathbf{10}_S \oplus \mathbf{8}_M^{(2)} \oplus \mathbf{1}_A \,, \tag{1.11}$$

where the subscripts A, S and M denote antisymmetric, symmetric and mixed symmetric flavor representations respectively, and the superscript denotes the multiplicity of a multiplet.

The symmetry of the representations play an important role in the construction of the wave functions. Because baryons obey Fermi-Dirac statistics, their wave function which is given by

$$\Psi_{\text{total}} = \zeta_{\text{flavor}} \otimes \xi_{\text{space}} \otimes \phi_{\text{color}} \otimes \chi_{\text{spin}} \tag{1.12}$$

has to be antisymmetric. Octet and decuplet baryons are spatially symmetric (positive parity) and the color wave function of every observable state is antisymmetric due to confinement. Confinement is mathematically equivalent to a color singlet representation, hence a strongly interacting object can only be an observable state if the decomposition of the color representation contains a singlet. The fundamental representations $\mathbf{3}_c$ and $\bar{\mathbf{3}}_c$ of the $SU(3)_c$ group are equivalent to the fundamental representations of $SU(3)_f$. It is clear that diquarks, or e.g. $qq\bar{q}$ are no physical observables, since their decomposition into irreducible representations $\mathbf{3}_c \otimes \mathbf{3}_c = \mathbf{6}_c \oplus \bar{\mathbf{3}}_c$ and $\mathbf{3}_c \otimes \mathbf{3}_c \otimes \bar{\mathbf{3}}_c = (\mathbf{6}_c \oplus \bar{\mathbf{3}}_c) \otimes \bar{\mathbf{3}}_c = \overline{\mathbf{10}}_c \oplus \mathbf{8}_c \oplus \bar{\mathbf{6}}_c \oplus \mathbf{3}_c$ do not contain color singlet states. The spin wave functions are composed by the product of the three quark spins ($\frac{1}{2}$ each) and are symmetric if the spin couples to $\frac{3}{2}$, and of mixed symmetry if it couples to $\frac{1}{2}$. In order to obey the Pauli exclusion principle for the octet states, $\zeta_{\text{flavor}} \otimes \chi_{\text{spin}}$, which are both of mixed symmetry, must be symmetric. If the flavor wave function is antisymmetric, the spin wave function also has to be antisymmetric. The configuration of a antisymmetric spin wave function at low energies is not realized in nature. The wave functions of the octet are thus constructed by a normalized linear combination of $\mathbf{8}_{\text{M}}^{(2)}$, which are symmetric in spin- and flavor-space. Since the flavor wave function of the singlet is antisymmetric, and the spin wave function must therefore be antisymmetric too, a singlet state is not observed, although it could be realized as a spatial excitation.

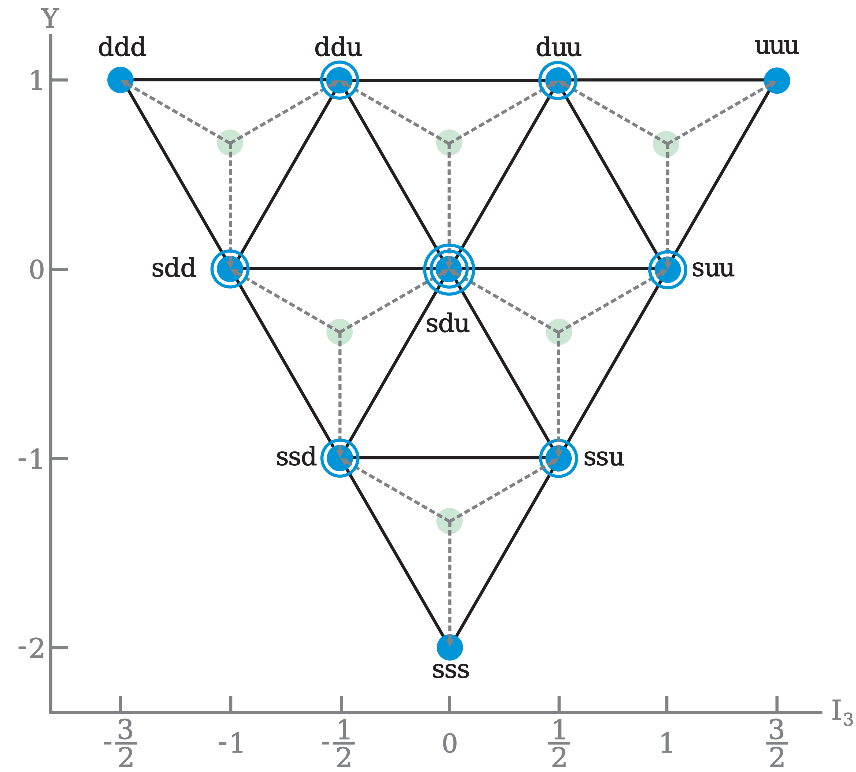

Figure 1.4: The baryon octet and decuplet originating from the diquark sextet, which is shown in light green. The wave functions of the outer nodes of the decuplet would violate the Pauli exclusion principle if there was no color quantum number.

From the group theoretical point of view, the $qqqq\bar{q}$ pentaquark states are constructed in a straightforward way. The product of the quark triplets, decomposed in irreducible representations reads

$$\mathbf{3} \otimes \mathbf{3} \otimes \mathbf{3} \otimes \mathbf{3} \otimes \bar{\mathbf{3}} = \mathbf{35} \oplus \mathbf{27}^{(3)} \oplus \overline{\mathbf{10}}^{(2)} \oplus \mathbf{10}^{(4)} \oplus \mathbf{8}^{(8)} \oplus \mathbf{1}^{(3)} \tag{1.13}$$

and the corresponding wave functions were calculated in [33].

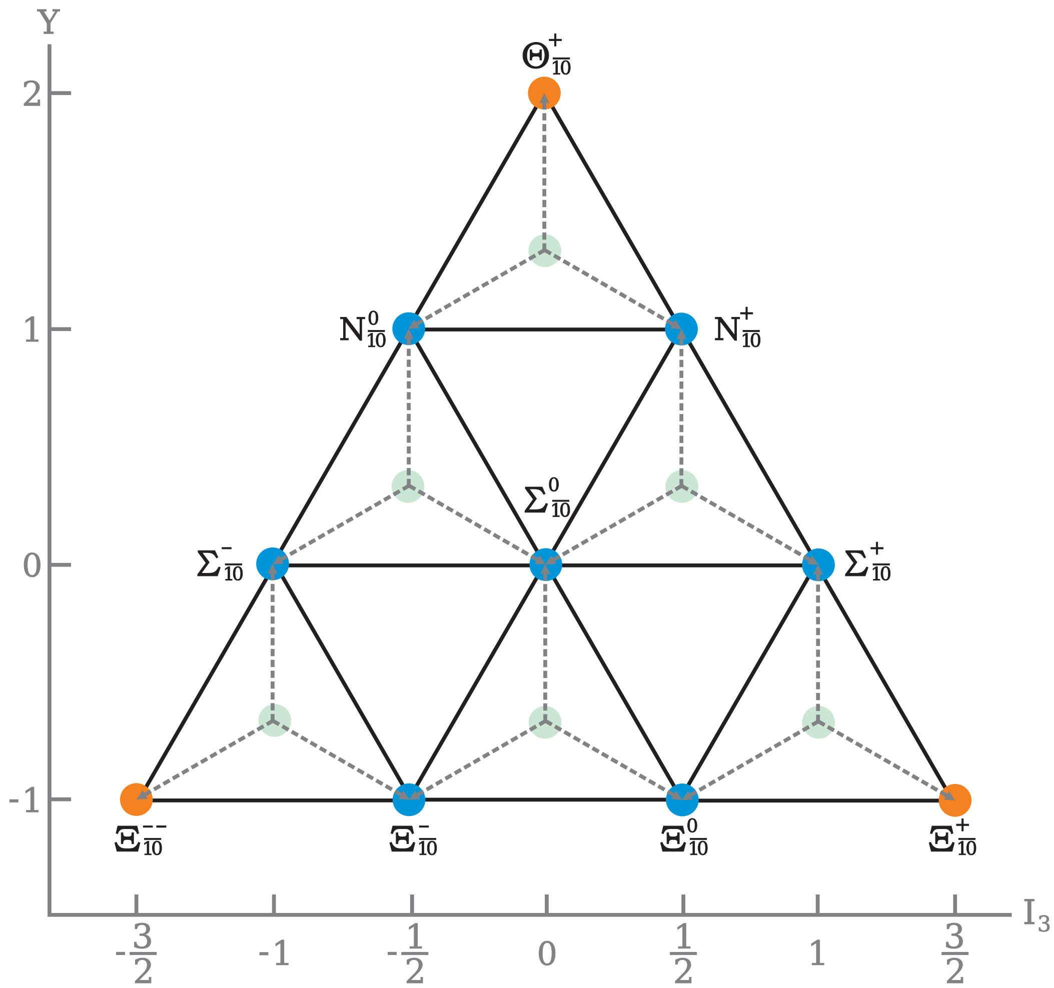

Figure 1.5: The exotic anti-decuplet originating from the $\bar{\mathbf{6}} \otimes \bar{\mathbf{3}} = \overline{\mathbf{10}} \oplus \mathbf{8}$ representation. The $\bar{\mathbf{6}}$ representation of a diquark-diquark combination is indicated in light green. The blue nodes comprise the octet representation, but their weights are omitted to clarify the notation. The corners of the anti-decuplet, depicted by orange nodes, are manifestly exotic.

The exotic Θ^+ baryon, subject to this work, is then located at the apex of the anti-decuplet $\overline{\mathbf{10}}$ representation and is also included in the **27**-plets and the **35**-plet, where the "outer ring" of its weight diagram entirely consists of manifestly exotic pentaquarks. Here the term exotic refers to a combination of (I_3, Y) quantum numbers which are not accessible for qq-baryon combinations. As an example, the Θ^+ has $Y = 2$ (or equivalently $S = +1$) and $I_3 = 0$, but in the quark model positive strangeness can solely be obtained by $\bar{s}$ valence-quarks. The Ξ^+ and Ξ^{--} baryons have no independently exotic (I_3, Y) quantum numbers, namely $Y = -1$ and $I_3 = \pm\frac{3}{2}$, but their combination is exotic. Non-exotic (I_3, Y) combinations in the $qqqq\bar{q}$ configuration are sometimes called cryptoexotic.

1.1.2 The Chiral Structure of QCD and the Skyrme Model

The concept of the – by construction – exact local $SU(3)_c$ gauge invariance of the QCD-Lagrangian and its approximate global $SU(3)_f$ symmetry were subject to the previous sections; but there exists yet another important symmetry in the limit of massless quarks, the chiral symmetry[1]. To consider light quarks u, d as massless is reasonable because their masses are small compared to the QCD scale $\Lambda_{\mathrm{QCD}} \approx 250$ MeV below which the effective coupling becomes large. The Dirac equation of massless fermions has solutions with positive and negative chirality [29], thus the remaining fermionic part of the Lagrangian (1.10) reads

$$\mathscr{L} = \bar{q}_{\mathrm{L}} \left(i\not{D}\right) q_{\mathrm{L}} + \bar{q}_{\mathrm{R}} \left(i\not{D}\right) q_{\mathrm{R}} \tag{1.14}$$

with left- and right-handed quark spinors $q_{\mathrm{L,R}} = P_{\mathrm{L,R}}(u,d)^T$ and $P_{\mathrm{L}} = \left(1-\gamma^5\right)/2$, $P_{\mathrm{R}} = \left(1+\gamma^5\right)/2$. The Lagrangian (1.14) is, in addition to its local $SU(3)_c$ symmetry, invariant under the unitary transformations $U(2)_{\mathrm{L}}$ and $U(2)_{\mathrm{R}}$, which act on the left- and right-handed quarks separately. The $U(2)_{\mathrm{L,R}}$ symmetry groups can be further divided into $SU(2)_{\mathrm{L,R}} \times U(1)_{\mathrm{L,R}}$, so that the currents associated with these symmetries, according to the Noether theorem are given by

$$j^{\mu}_{\mathrm{L,R}} = \bar{q}_{\mathrm{L,R}}\gamma^{\mu} q_{\mathrm{L,R}} \qquad (\text{"}U(1)\text{ current"}) \tag{1.15}$$

$$j^{\mu,a}_{\mathrm{L,R}} = \bar{q}_{\mathrm{L,R}}\gamma^{\mu}\tau^a q_{\mathrm{L,R}}\,, \qquad (\text{"}SU(2)\text{ current"}) \tag{1.16}$$

where $\tau^a = \sigma^a/2$ represent the generators of $SU(2)$ and σ^a are the Pauli matrices. The linear combinations of these currents give vector and axial vector currents for $U(1)$ and $SU(2)$ respectively

$$j^{\mu}_{\mathrm{V}} = \bar{q}\gamma^{\mu} q = j^{\mu}_{\mathrm{R}} + j^{\mu}_{\mathrm{L}} \tag{1.17}$$

$$j^{\mu,5}_{\mathrm{A}} = \bar{q}\gamma^{\mu}\gamma^5 q = j^{\mu}_{\mathrm{R}} - j^{\mu}_{\mathrm{L}} \tag{1.18}$$

$$j^{\mu,a}_{\mathrm{V}} = \bar{q}\gamma^{\mu}\tau^a q = j^{\mu,a}_{\mathrm{R}} + j^{\mu,a}_{\mathrm{L}} \tag{1.19}$$

$$j^{\mu,a,5}_{\mathrm{A}} = \bar{q}\gamma^{\mu}\gamma^5\tau^a q = j^{\mu,a}_{\mathrm{R}} - j^{\mu,a}_{\mathrm{L}}\,. \tag{1.20}$$

The vector transformations $SU(2)_{\mathrm{V}} \times U(1)_{\mathrm{V}}$ are (approximately) conserved symmetries of QCD, and the associated currents lead to the conservation of isospin (i.e. flavor) and the baryon number. The axial vector currents do not correspond to observed symmetries of the strong interaction. The singlet current (1.18) should be conserved in a classical theory but is broken in a quantum theory. This phenomenon is called chiral anomaly and has far-reaching consequences, such as the strong $\mathcal{CP}$ problem or the exceptionally high mass of the η' meson. The $SU(2)_{\mathrm{A}} \times SU(2)_{\mathrm{V}}$ symmetry group, which should be conserved theoretically, is spontaneously broken down to the subgroup of vector symmetries [34]. As a consequence the QCD vacuum is characterized by a non-vanishing quark condensate, to which u and d quarks are able to couple and acquire an effective mass. The major part of the observable mass of strongly interacting particles containing u and d quarks is generated because of the spontaneously broken $SU(2)_{\mathrm{A}} \times SU(2)_{\mathrm{V}} \to SU(2)_{\mathrm{V}}$ symmetry. Additionally to the spontaneous symmetry breaking, the chiral symmetry is explicitly broken by the small, but non-vanishing mass of u and d quarks appearing in the chiral Lagrangian (1.14).

Since the exotic anti-decuplet appears as solution in extensions of the Skyrme model, which generated renewed interest in exotics in the 1980s [35–37], it is worthwhile to discuss the properties of the model briefly.

[1] The $SU(3)_f$ symmetry is a consequence of the $SU(3)_{\mathrm{V}}$ invariance in the chiral limit.

In the early 1960s, even before the concept of quarks and color charge, Skyrme developed a rather heuristic model in which the fundamental fields consisted of just pions [38]. The original Skyrme model is thus an effective field theory of extended, rather than elementary point like objects, and later provided a link between QCD and the Yukawa picture of strong interactions in the (sub-) GeV regime. The Lagrangian of this model is composed such, that its solutions, sometimes called Skyrmions, are classical (topological) soliton configurations of the pion field. One remarkable aspect is that fermions, such as baryons, emerge from a theory built up from bosonic, i.e. meson fields without adding them explicitly to the model.

The Skyrme model became "popular" in the early 1980s after striking arguments from low energy QCD approximations. In 1974 't Hooft considered $1/N_c$, i.e. the inverse of the number of colors, as an expansion parameter for QCD at low energies and showed, that for large N_c QCD may be treated as a theory of weakly interacting mesons, in the sense that scattering amplitudes or quadrilinear coupling constants are of order $1/N_c$ [39, 40]. Witten recognized a different behavior of the effective coupling for interactions involving baryons which led to the conclusion that baryons can be regarded as solutions of an effective meson theory [41]. The Skyrme model also used properties of the non-linear realization of chiral symmetry, such that scalar fields do not appear at all [42, 43]. In a postmortem reconstructed talk, Skyrme illustrated his original motivations, mainly the unification of mesons and baryons, the desire to eliminate fermions from fundamental principles and the formulation of a field theory of extended objects, since quantum field theories of point-like particles introduced infinities which are "swept under the rug" by the renormalization process [44].

The extension of the classical Skyrme model to an $SU(3)$ model and the explicit supplementation of flavor symmetry breaking terms to the Lagrangian lead to solitons belonging to higher dimensional representations which contain a $Y = 1$ state, such as $\overline{\mathbf{10}}$, $\mathbf{27}$ and so forth [35]. This also implies sizable admixture of states from these representations to the classical octet and decuplet representations. In 1997 Diakonov, Petrov and Polyakov employ the chiral quark soliton model (χQSM) [45] to calculate the properties of the assumptive anti-decuplet $\overline{\mathbf{10}}$, yielding a relatively light and narrow exotic $J^P = \frac{1}{2}^+$, $S = +1$ particle, which was identified as the Θ^+ [46]. Since the χQSM can be regarded as an interpolation between the Skyrme model and the non relativistic constituent quark model [47], the anti-decuplet solutions of [46] can be considered as both, $qqqq\bar{q}$ and soliton states.

2 A Brief History of the Θ^+ Pentaquark

This chapter summarizes predictions of the Θ^+ pentaquark baryon in several theoretical models and – if given – its characteristics as well as experimental results on the subject. It should be noted, that the summary makes no claim to completeness.

2.1 Theoretical Predictions

The earliest notion of pentaquarks certainly came from GELL-MANN, who, in his first paper on quarks, pointed out that from **group theoretical considerations**, "*baryons can be constructed from quarks by using the combinations qqq, $qqqq\bar{q}$ etc*" [14].
Employing the **MIT bag model** [49], JAFFE claimed that ground state pentaquarks are cryptoexotic states in the octet representation, whereas real exotics should be heavier, further above threshold for a decay into qqq and $q\bar{q}$ and very broad due to strong coupling to the KN s-wave, if resonant at all [48]. He identified the lightest exotic baryon to be a $I = 0$, $J^P = \frac{1}{2}^-$ state with a mass of $\approx$ 1700 MeV.
Although there exist a variety of **quark models** beside the bag model, according to JAFFE [50] none of them seems to fully support a narrow and light pentaquark. Particularly the positive parity obtained by the χQSM in conjunction with its small width is problematic. In different publications, reviewed in [51], it is argued that the properties of the Θ^+ in the χQSM are in qualitative agreement with constituent quark models described by an effective GOLDSTONE boson exchange or an effective color-magnetic exchange. However, no concrete properties of the Θ^+ were derived from basic principles and it was stated that if the Θ^+ exists, the quark model treatment of, at least positive parity baryons has to be revisited.

The **diquark (correlated quark) model**, to which the mentioned review by JAFFE [50] was dedicated, seems to support the Θ^+ as a matter of principle but differs in details compared to the χQSM predictions. Since the diquark model exhibits concrete predictions for pentaquarks, basic ideas and consequences concerning exotics shall be summed up. The diquark was introduced in section 1.1.1 as intermediate step in the construction of baryons. The energetically most favorable realization of a diquark is a scalar anti-triplet in color- and flavor-space, known as "good" diquark $\mathbb{Q}$. Thus the good diquarks are made of ud, us, ds and rg, rb, gb combinations in flavor- and color-space respectively (cf. figure 1.3). JAFFE argues, that the most favorable pentaquark states in a diquark picture consequently are $\mathbb{Q}\mathbb{Q}\bar{q}$ configurations. In flavor-space this combination reads $\bar{\mathbf{3}}_\mathrm{f} \otimes \bar{\mathbf{3}}_\mathrm{f} \otimes \bar{\mathbf{3}}_\mathrm{f} = \mathbf{1}_\mathrm{f} \oplus \mathbf{8}_\mathrm{f}^{(2)} \oplus \overline{\mathbf{10}}_\mathrm{f}$, analog to the construction of baryons. Taking the spin of the $\bar{q}$ and both $\mathbb{Q}$s into account and require confinement, as well as FERMI-DIRAC statistics for the whole object, the pentaquark candidates are a s-wave $J^P = \frac{1}{2}^-$ singlet and octet and p-wave $J^P = \frac{1}{2}^+, \frac{3}{2}^+$ octets and anti-decuplets. Hence the diquark picture gives a natural explanation – considering only good diquarks – why the Θ^+ should be isoscalar, i.e. why higher dimensional representations $\mathbf{27}, \mathbf{35}$ arising in other quark models and the χQSM should vanish. The s-wave nonet is expected to be lost in the meson-nucleon continuum if the states are heavier than the corresponding fall-apart thresholds. In the diquark model $\mathbb{Q}\mathbb{Q}\bar{q}$ exotics come in spin-orbit pairs with $J^P = \frac{1}{2}^+$ and $\frac{3}{2}^+$. The width of the ROPER resonance $\Gamma_{N(1440)} \approx 300$ MeV [27], which is a candidate for the N of the octet with $uudd\bar{u}$ or $uudd\bar{d}$ content, suggests mixing between common qqq baryons and cryptoexotic pentaquarks. In summary, the Θ^+s in the diquark model are members of anti-decuplets with $J^P = \frac{1}{2}^+$ and $\frac{3}{2}^+$.

These two anti-decuplets are accompanied by nearby exotic octets, which are not predicted in the soliton approach [37]. Additionally it is necessary to excite the Θ^+ to a p-wave resonance, which qualitatively contradicts the predicted mass and width, but these properties are yet not impossible to obtain.

Another early calculation of the Θ^+ mass within the framework of the already mentioned **SU(3) Skyrme model** was done by Praszałowicz in [37]. There solutions to the effective baryonic Hamiltonian in the chiral limit plus a second order perturbation in the strange quark mass m_s were fitted in a model independent way in which the classical soliton mass and the soliton moments of inertia I_1, I_2 are free parameters. It was obtained that the mass of the anti-decuplet members is crucially influenced by the estimate of the strange moment of inertia I_2, on which the splitting between exotic ($\overline{\mathbf{10}}, \mathbf{27}$ etc.) and non exotic multiplets depend. The Θ^+ has eventually been predicted as a light $M_{\Theta^+} \approx 1530$ MeV and narrow $\Gamma_{\Theta^+} \lesssim 15$ MeV particle in **χQSM** calculations in 1997 [46]. In this model, multiplets are degenerate eigenstates of an $SU(3)$-rotational Hamiltonian, quantized by filling discrete energy levels with valence quarks. Mass splittings within the multiplets are obtained by perturbing the Hamiltonian with respect to the strange quark mass in leading order $\mathcal{O}(N_c)$ and subleading order $\mathcal{O}(N_c^0)$ [52]. The latter giving rise to additional coefficients linear in m_s, which were not present in the calculations of Praszałowicz [37], but can be fixed phenomenologically by the experimentally determined mass splittings of the qqq baryon octet and decuplet and the πN sigma term $\sigma_{\pi N} = m \left\langle N|\bar{u}u + \bar{d}d|N\right\rangle$. Again the strange moment of inertia I_2 remains unknown and was fixed by identifying the $N_{\overline{\mathbf{10}}}$ with the $J^P = \frac{1}{2}^+$ $N(1710)$ resonance, which also allows to calculate the decay modes and widths of the $\overline{\mathbf{10}}$ members. Diakonov, Petrov and Polyakov state that predictions for I_2 are rather dispersive and with a value calculated earlier in the χQSM [52] a Θ^+ below the KN decay threshold would be obtained. The fixing of free parameters in the model is controversial and subject to numerous re-evaluations, partially summarized recently in [53]. A notable re-examination within the χQSM have been performed by Weigel in 1998, yielding $\Gamma_{\Theta^+} \sim 100$ MeV [54]. Beside these quantitative discussions, there exists conceptional criticism against χQSM models, namely the failure of the model in the case of 1-flavor and N_c colors, the negligence of higher order terms in the Lagrangian, the collective coordinate quantization (cf. [55]) and the perturbative treatment of $SU(3)_f$ symmetry breaking [56].

Pentaquarks have also been studied in **lattice gauge theory** [57] with (initially) controversial results. Lattice calculations after the first experimental discoveries (cf. sec. 2.2) reported evidence for states in the KN-channel with $J^P = \frac{1}{2}^-$ [58–60] and $J^P = \frac{1}{2}^+$ [61]. These analyses have been overruled by subsequent studies which found no evidence for bound exotic states with $J^P = \frac{1}{2}^\pm$, but there seems to be evidence for a $J^P = \frac{3}{2}^+$ resonance [62]. The situation of pentaquarks in lattice QCD has been reviewed e.g. in [63, 64].
The history of the Θ^+ in **QCD sum rules** [65] is somewhat similar to that of lattice QCD studies [64,66]. First calculations were dedicated to reproduce the mass of the Θ^+ found by experiments; re-evaluation and the inclusion of the claimed discoveries of the Ξ^{--} [67] and the Θ_c [68] pentaquarks revealed problems in the initial calculations. Again, the most striking problem for this model is the narrow decay width of the Θ^+. This was also pointed out by recent positive results with QCD sum rules, where a $J^P = \frac{3}{2}^+$ Θ^+ candidate was obtained [69].
There exists a huge variety of phenomenological studies on the Θ^+ in addition to the mentioned models, and the number of publications on pentaquarks should have risen above 1000 by now. An unambiguous experimental measurement of the Θ^+ and its properties would "*offer us a golden opportunity to sharpen and expand our understanding of QCD itself*" [70].

2.2 Experimental Situation

First evidence for $S = +1$ baryons, named Z resonances at that time, were reviewed in the 1976 version of the "Review of particle properties" by the PDG [71]. In their 1986 version, where six one-star Z resonances in KN- and excited KN-channels were listed, the PDG puts the subject to rest: "*However, the results permit no definite conclusion – the same story heard for 15 years. The standards of proof must simply be much more severe here than in a channel in which many resonances are already known to exist. The general prejudice against baryons not made of three quarks and the lack of any experimental activity in this area make it likely that it will be another 15 years before the issue is decided.*" [72].
17 years later, triggered by the paper of Diakonov, Petrov and Polyakov[1], the LEPS collaboration at SPring-8 in Japan found first evidence for a narrow pentaquark in the $(nK^+)K^-X$ final state of the reaction of $1.5 - 2.4$ GeV photons with ^{12}C nuclei [74]. After communicating the evidence, several experimentalists began to search for the Θ^+ in their recent and also archived data. This brief overview will concentrate on positive reports in searches for the Θ^+ and directly contradicting measurements. Thus, searches in channels where evidence never was claimed are omitted. They are summarized e.g. in [75] and references therein. A summary plot of nine positive measurements is shown in figure 2.1. The here mentioned experiments are summarized in table 2.1.

The LEPS collaboration was able to reproduce their initial result with similar setup and ~ 8 times higher statistics in the reaction $\gamma d \to (nK^+)K^-X$ [85]. They used a newly developed minimum momentum spectator approximation (MMSA) to obtain the Fermi-motion-corrected mass distribution. They claim that the two measurements are compatible to each other, although stating that the significance of the first one was highly overestimated. In their first publication their peak was located at 1540 ± 10 MeV with a significance of $S/\sqrt{B} = 4.6^{+1.2}_{-1.0}\,\sigma$, while their peak shifted to $1524 \pm 2 \pm 3$ MeV and their significance increased to $\Delta(-2\ln L) = 5.1\,\sigma$ in the 2009 analysis. In their third article [86], the LEPS collaboration analyzed data from runs of 2006-2007, again with similar setup and ~ 2.6 times higher statistics than the previous measurement. A peak is still present in their data, but no statistical analysis is performed. Judging by eye and the given scale, the spectra of [85] and [86] are compatible.

First confirmation of the LEPS finding came from the DIANA collaboration at the ITEP in Moscow, Russia [77]. A Θ^+ signal in the pK^0_S-channel was found in data collected with the DIANA bubble chamber, which was filled with liquid Xenon and exposed to a 850 MeV K^+ beam. The claimed signal became clearer after the application of cuts on the emission angles of proton and kaon and by requiring that p and K^0_S were back-to-back in the plane transverse to the beam direction. They reported a statistical significance of $S/\sqrt{B} = 4.4\,\sigma$ and a Θ^+ mass of 1539 ± 2 MeV. In 2006 Belle, at KEK in Japan, reported upper limits on the Θ^+ width[2] and on the ratio of the Θ^+ to $\Lambda(1520)$ inclusive production cross section in K^+ secondary interactions in the material (mostly Si) of the Belle detector. Their reported upper limit at 90 % confidence level on the Θ^+ to $\Lambda(1520)$ ratio is $\frac{\sigma(KN \to \Theta^+ X)}{\sigma(\bar{K}N \to \Lambda(1520)X)} < 0.025$. The DIANA collaboration was able to support their initial claim with more statistics in 2006 and updated selection in 2009 [88, 89]. In a recent preprint, the DIANA collaboration found further evidence by increasing statistics of the sample, new selection criteria, better statistical treatment and a Monte Carlo study that verifies that the observed enhancement is not a spurious structure created by the imposed selection criteria [90]. The statistical significance of the signal is estimated as $\sqrt{2\Delta \ln L} = 6.3\,\sigma$, the mass and widths are measured to be 1538 ± 2 MeV and 360 ± 110 keV (c.f. [106]) respectively.

[1] At the QNP2000 conference Diakonov actually suggested LEPS and CLAS collaborators to search for the Θ^+ [73].
[2] The ratio of the Θ^+ yield to the charge exchange reaction yield can be expressed in terms of the Θ^+ width [106].

The first collaboration to revise their initial observation was CLAS, located at the JLab facility in Virginia, USA. Using an energy tagged photon beam, produced by 2.474 and 3.115 GeV electrons incident on a bremsstrahlung radiator, CLAS reported a $5.2 \pm 0.6\,\sigma$ excess in the exclusive $(nK^+)K^-p$ photoproduction off deuterium [78]. They were not able to reproduce their measurement with 30 times higher statistics [91, 92]. For the Θ^+ photoproduction off deuterium in the exclusive $(nK^+)K^-p$ and $(nK^+)\Lambda$ channels, CLAS reported upper limits at 95 % confidence level on the integrated cross section of $\sigma_{\text{tot}} < 0.3$ nb and $\sigma_{\text{tot}} < 25$ nb respectively. The CLAS data seem to contradict the recent LEPS measurement. In the two latest publications on the subject from LEPS [85, 86], the authors claim, that the CLAS measurements do not contradict their observation if the signal has a strong angular dependence, since the LEPS acceptance is in the forward region, while CLAS has acceptance in the wide angle regions.

In an analysis of archived data taken by neutrino and anti-neutrino scattering off nuclei with the WA21, WA25, WA59 (CERN), E180, and E632 (Fermilab) bubble chambers, ITEP physicists observed a Θ^+ peak in the pK^0_S-channel at 1533 ± 5 MeV with a significance of $S/\sqrt{B} = 6.7\,\sigma$. A similar analysis has been done with the NOMAD detector at CERN, using νA data. After having found a $4.3\,\sigma$ signal in a subsample, presented at the NEUTRINO04 conference [107], an improved analysis with the full data set has been done. In that analysis no evidence for the Θ^+ has been found and x_{F} dependent upper limits on the production rate per neutrino interaction have been reported [93].

The next positive result came from the SAPHIR collaboration at the ELSA experiment in Bonn, Germany [80]. There, the Θ^+ was produced in photoproduction off a liquid hydrogen target with a tagged photon beam, produced by 2.8 GeV electrons impinging on copper plate, and detected in the exclusive $(nK^+)K^0_S$-channel. Kinematic cuts that suppress the background were applied. The signal was located at a mass of $1540 \pm 4 \pm 2$ MeV with a statistical significance of $S/\Delta S = 4.8\,\sigma$. The evidence was contradicted by photoproduction measurements with the CLAS detector in the exclusive reactions $\gamma p \rightarrow (nK^+)K^0$ and $\gamma p \rightarrow (nK^+/pK^0)K^0$ with about 50 times higher statistics [95, 96]. About 70 pb^{-1} of data was accumulated with a 1.6 to 3.8 GeV tagged photon beam incident on a liquid hydrogen target. A Θ^+ signal was found in neither nK^+ nor pK^0_S channels and an upper limit on the total cross section in the combined channel analysis of 0.8 nb at 95 % confidence level was calculated. Also a limit on the Θ^+ to $\Lambda(1520)$ production ratio was set at 0.22 % (95 % C.L.), compatible to the Belle limit. The signal was tested with cuts comparable to those of the SAPHIR group, where no peak was seen as well. In 2012, parts of the collaboration published a reanalysis of that data, claiming to have found a peak in the interference of a ϕ meson and the KN-system at 1543 ± 2 MeV with $Z = 5.3\,\sigma$ in a distinct region of the kinematic phase space [97]. The peak was found in the K^0_S missing mass of $\gamma p \rightarrow (pK^0_L)K^0_S$, restricting the $K^0_L K^0_S$ system to the ϕ-meson peak, cutting on the mandelstam variable $-t_\Theta < 0.45$ GeV^2 and on M(pK^0_S)< 1.56 GeV. The authors claimed that the peak, being restricted to small $-t_\Theta$ values, reconcile the contradicting results from CLAS and LEPS. The majority of the CLAS collaboration decided not to release such an analysis due to the lack of justification for the kinematic cuts used therein [98]. There are rumors that the analysis at CLAS is still ongoing and that a peak is also seen outside the ϕ interference region.

Additional evidence came from the HERMES experiment in quasi-real photoproduction off deuterium [81]. An $|S| = 1$ resonance was found in the inclusive pK^0_S-channel at $1528.0 \pm 2.6 \pm 2.1$ MeV with a statistical significance of $S/\Delta S = 3.7\,\sigma$. The production cross section ratio of the resonance to the $\Lambda(1520)$ signal was found to lie between 1.6 and 3.5. In a similar approach to that of the Belle analysis, the BABAR collaboration at the SLAC National Accelerator Laboratory in Menlo Park, USA found no sign of a Θ^+ in reactions of beam-halo electrons and positrons with the beampipe material (mostly beryllium) [99].

Further observation of the Θ^+ in the inclusive pK^0_S-channel was claimed by the SVD collaboration in proton-nucleus collisions at $\sqrt{s} = 11.5$ GeV [84]. The data was taken on carbon, silicon and lead targets with the SVD-2 experiment at the IHEP accelerator in Protvino, Russia. The peak was detected at a mass of 1526±3±3 MeV with a significance of $S/\sqrt{B} = 5.6\,\sigma$. A kinematic cut at the momentum of the pK^0_S system in the center of mass system of proton and target nucleon ($\cos(\alpha) \geq 0$) and a $\mathbf{p}_{K^0_S} \leq \mathbf{p}_p$ cut were applied. Similar measurements were done by the SPHINX, HERA-B and HyperCP collaborations at IHEP, HERA and Fermilab respectively [102–104]. No evident structure was observed in these experiments and upper limits on production cross sections relative to $\Lambda(1520)$ or the pK^0_S continuum were derived. An updated analysis of the SVD-2 data is presented in [105,109], where a peak at 1523±2±3 MeV with a statistical significance of $S/\sqrt{S+B} = 8.0\,\sigma$ is seen. The update mainly comprises an improved tracking algorithm, splitting of the K^0_S sample for different regions of the detector and further systematic studies.

The COSY-TOF collaboration at COSY in Jülich, Germany was the second collaboration to revise their initial result. In their first publication, they claimed evidence for a narrow resonance at 1530 ± 5 MeV in the pK^0_S system of the exclusive reaction $pp \rightarrow (pK^0_S)\Sigma^+$ with a statistical significance of $S/\sqrt{S+B} = 4.7\,\sigma$ [82]. A kinematic cut was used to separate $pp \rightarrow (pK^0_S)\Sigma^+$ from $pp \rightarrow pK^+\Lambda$ reactions. In a subsequent measurement, about 12 times higher statistics in the final selection was obtained and an upper limit of 0.15 μb at 95% confidence level was calculated [100].

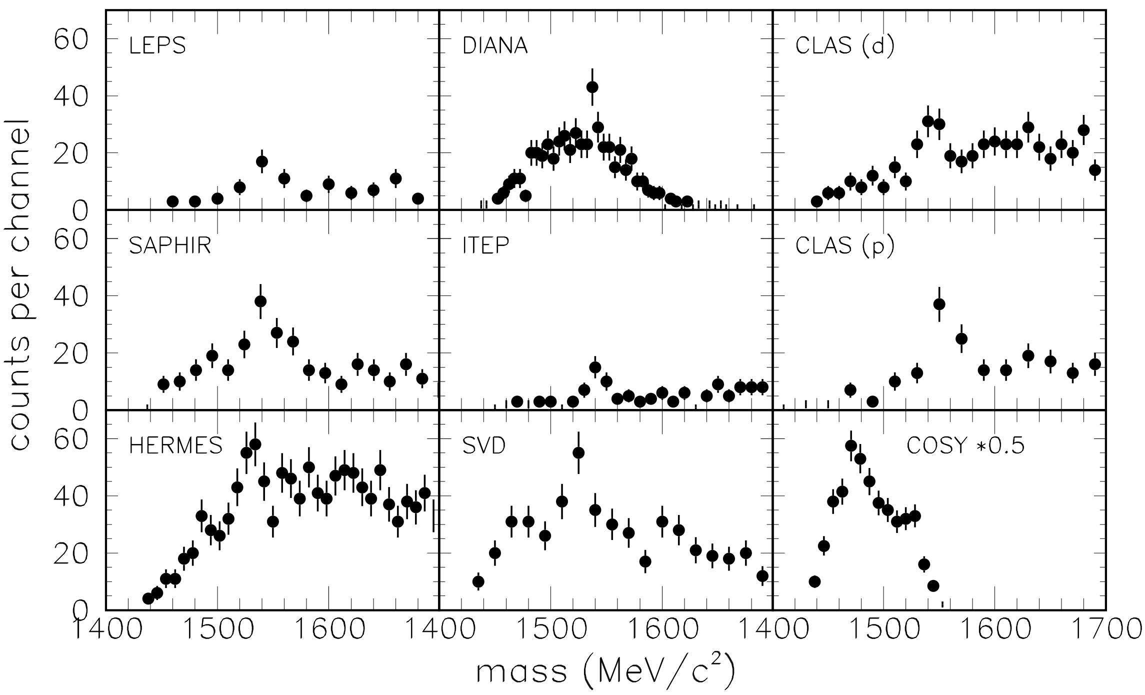

Figure 2.1: Summarized spectra of positive results in searches for the Θ^+. Taken from [76]

The ZEUS experiment, located at the HERA storage ring in Hamburg, Germany measured a resonance in the inclusive $pK^0_S + \bar{p}K^0_S$-channel in deep inelastic ep scattering at $\sqrt{s} = 300\text{-}318$ GeV [83]. The signal was visible at an exchanged photon-virtuality $Q^2 > 20$ GeV^2, where the peak was located at a mass of $1521.5 \pm 1.5^{+2.8}_{-1.7}$ GeV with a statistical significance of $S/\Delta S = 3.9\text{-}4.7\,\sigma$. The significance depended on the shape of the background, i.e. if a second structure at ~ 1465 MeV was fitted simultaneously or not. The H1 experiment using the same proton and lepton beam reported mass dependent upper limits for the inclusive cross section $\sigma(ep \rightarrow \Theta^+ X) \times BR(\Theta^+ \rightarrow pK^0_S)$ [101]. An upper limit of ~ 70 nb was set at 95% confidence level for the peak seen at the ZEUS experiment, mimicking their selection criteria. It should be noted, that a good detector resolution for the K^0_S reconstruction, i.e. a narrow width of the fitted Gaussian, is important in the search for a narrow signal in the pK^0_S channel. The resolution of the K^0_S signal at H1 was twice as high as the ZEUS K^0_S signal resolution, being subject to a more detailed study in [108].

Original measurement			**Repeated measurement**			
Group	**Reaction**	**Z**	**Group**	**Reaction**	**Stat.**	**Result**
LEPS [74]	$\gamma C \rightarrow (nK^+)K^- X$	$\sim 4\sigma$	LEPS [85]	$\gamma d \rightarrow (nK^+)K^- X$	$\times 8$	$Z \sim 5\sigma$
			LEPS [86]	$\gamma d \rightarrow (nK^+)K^- X$	$\times 20$	Θ^+ seen
DIANA [77]	$K^+\mathrm{Xe} \rightarrow (pK^0)\mathrm{Xe}'$	$\sim 4\sigma$	Belle [87]	$K^+\mathrm{Si} \rightarrow (pK^0)X$	$\times 10$	$\Gamma_{\Theta^+} < 1$ MeV
			DIANA [88]	$K^+\mathrm{Xe} \rightarrow (pK^0)\mathrm{Xe}'$	$\times 2$	$Z \sim 5\sigma$
			DIANA [89]	$K^+\mathrm{Xe} \rightarrow (pK^0)\mathrm{Xe}'$	$\times 2.2$	$Z \sim 6\sigma$
			DIANA [90]	$K^+\mathrm{Xe} \rightarrow (pK^0)\mathrm{Xe}'$	$\times 2.5$	$Z \sim 6\sigma$
CLAS [78]	$\gamma d \rightarrow (nK^+)K^- p$	$\sim 5\sigma$	CLAS [91]	$\gamma d \rightarrow (nK^+)K^- p$	$\times 30$	$\sigma_{\mathrm{tot}} < 0.3$ nb
			CLAS [92]	$\gamma d \rightarrow (nK^+)\Lambda$	$\times 30$	$\sigma_{\mathrm{tot}} < 25$ nb
ITEP [79]	$\nu A \rightarrow (pK^0)X$	$\sim 7\sigma$	NOMAD [93]	$\nu A \rightarrow (pK^0)X$	$\times 12$	$< 2.13 \cdot 10^{-3}$/evt
SAPHIR [80]	$\gamma p \rightarrow (nK^+)K^0$	$\sim 5\sigma$	CLAS [94]	$\gamma p \rightarrow (nK^+)\pi^+ K^-$	$\times 5$	$Z \sim 8\sigma$
			CLAS [95]	$\gamma p \rightarrow (nK^+)K^0$	$\times 50$	$\sigma_{\mathrm{tot}} < 0.8$ nb
			CLAS [96]	$\gamma p \rightarrow (nK^+/pK^0)K^0$	$\times 50$	$\sigma_{\mathrm{tot}} < 0.7$ nb
			CLAS [97]	$\gamma p \rightarrow (pK^0)K^0$	$\times 50$	$Z \sim 5\sigma$[1]
HERMES [81]	$e^+ d \rightarrow (pK^0)X$	$\sim 4\sigma$	BaBar [99]	$e^+\mathrm{Be} \rightarrow (pK^0)X$	$\times 190$	no Θ^+ seen
COSY [82]	$pp \rightarrow (pK^0)\Sigma^+$	$\sim 5\sigma$	COSY [100]	$pp \rightarrow (pK^0)\Sigma^+$	$\times 12$	$\sigma_{\mathrm{tot}} < 0.15\,\mu$b
ZEUS [83]	$ep \rightarrow (p/\bar{p}K^0)e'X$	$\sim 4\sigma$	H1 [101]	$ep \rightarrow (p/\bar{p}K^0)e'X$	$\times 0.6$	$\sigma_{\mathrm{tot}} < 90$ pb
SVD [84]	$pA \rightarrow (pK^0)X$	$\sim 6\sigma$	SPHINX [102]	$p\mathrm{C} \rightarrow (pK^0)K^0\mathrm{C}$	$\times 12$	$\frac{\sigma(\Theta^+\bar{K}^0)}{\sigma(\Lambda(1520)K^+)} < 0.02$
			HERA-B [103]	$pA \rightarrow (pK^0)X$	$\times 4$	$\frac{\sigma(\Theta^+)}{\sigma(\Lambda(1520))} < 0.12$
			HyperCP [104]	$p/\pi^+/K^+W \rightarrow (pK^0)X$	$\times 40$	$\frac{\sigma(\Theta^+)}{\sigma(pK^0_S\,_{\mathrm{bkg}})} < 0.003$
			SVD [105]	$pA \rightarrow (pK^0)X$	$\times 1.5$	$Z \sim 6\text{–}9\sigma$

Table 2.1: Summary of positive results in searches for the Θ^+ and repeated experiments from the same group or from another group with a similar measurement. If a group revised their initial finding, no more experiments of the same type are listed. If the situation is controversial, all similar experiments are listed. The measurements are chronologically ordered by submission to the publisher. Due to inconsistencies in the calculation of the significance Z, only a rounded value is given. Details are described in the text.

The question arises whether a real signal was measured or if the bumps seen in some experiments are subject to statistical fluctuations or fake, due to cuts in the kinematic phase space or reflections or interference of other processes. The PDG wrote in their latest statement on the Θ^+ in 2008: "*There are two or three recent experiments that find weak evidence for signals near the nominal masses, but there is simply no point in tabulating them in view of the overwhelming evidence that the claimed pentaquarks do not exist. The only advance in particle physics thought worthy of mention in the American Institute of*

[1] The kinematic cuts used in this analysis are not accepted by the majority of the CLAS collaboration [98].

Physics "Physics News in 2003" was a false alarm. The whole story–the discoveries themselves, the tidal wave of papers by theorists and phenomenologists that followed, and the eventual "undiscovery" –is a curious episode in the history of science." [75].
The recently reported signals were only observed in a limited region of the phase space and their properties seem to be exceptional. A phenomenological approach explaining the situation by the assumption that multiquark hadrons are mainly produced from short-term hadron fluctuations or hadron remnants in a hard process is presented in reference [110]. The therein derived kinematic restrictions are stringent, but explain the conflict qualitatively. The only ongoing experiment, claiming evidence for a signal associated with the Θ^+ is LEPS, which is going to be upgraded to LEPS II and will start to take data in 2014. This data, and maybe searches at other experiments, will hopefully shed more light on the subject.

3 The HERMES Experiment at HERA

The HERMES experiment (HERA MEasurement of Spin) was designed to study the nucleon spin structure by inclusive and semi-inclusive deep inelastic scattering of polarized leptons from undiluted polarized nuclear gas targets. The experiment was running from 1995 until 2007 at the east hall of the HERA storage ring (Hadron-Elektron-RingAnlage), depicted in figure 3.1, at DESY (Deutsches Elektonen SYnchrotron) in Hamburg, Germany. Essential progresses in the field of spin physics were the utilization of a highly polarized longitudinal lepton beam in a storage ring, and the storage cell technique, allowing high polarizations at high densities [111]. HERMES was also able to access semi-inclusive measurements, where hadrons are detected in coincidence with the scattered lepton. Earlier experiments were only able to measure polarization asymmetries from inclusive scattering where solely the scattered lepton is detected. Semi-inclusive processes in which the hadron type is identified by the elaborate particle identification system of HERMES also allow for studies on the flavor-dependent spin structure functions. In addition to runs with polarized targets, data from unpolarized targets were taken to provide higher statistics for non spin related studies.
This section briefly reviews the setup of the experiment; the focus lies on relevant components for this analysis. A full technical review of HERMES is found in [112].

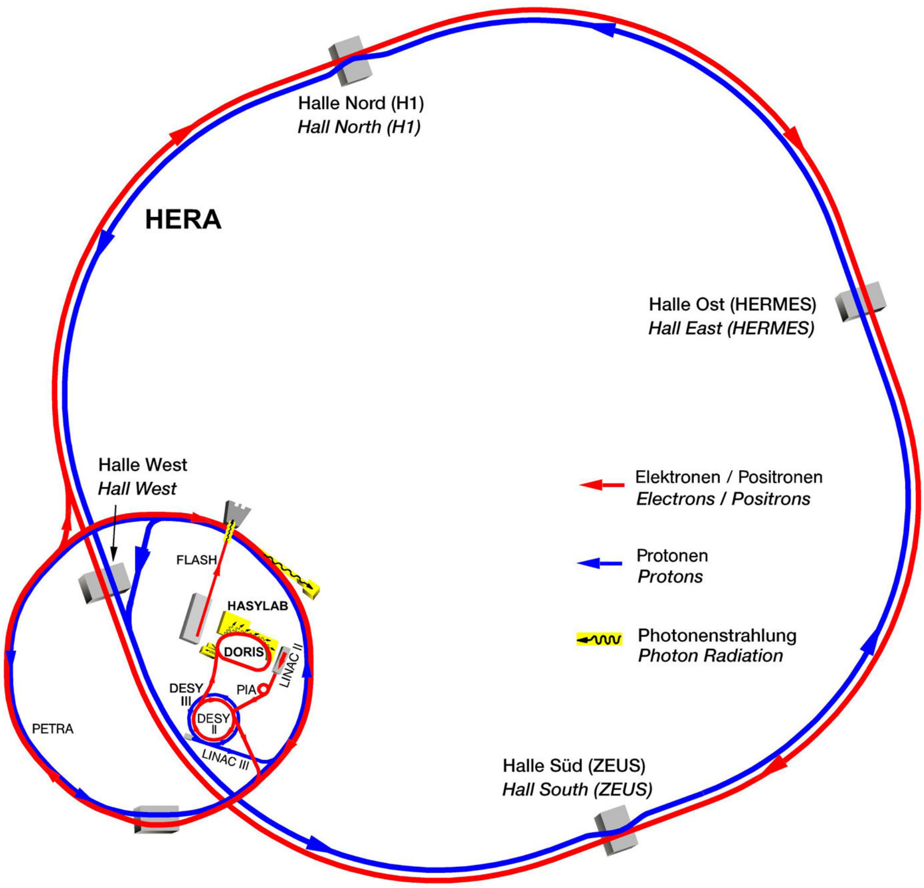

Figure 3.1: A schematic view of the HERA storage ring with the pre-accelerators LINAC II (pre-acceleration up to 450 MeV), DESY II (7.5 GeV) and PETRA (14 GeV). Electrons/positrons in HERA were accelerated up to 27.6 GeV, protons up to 920 GeV.

3.1 Experiment Setup

3.1.1 The Hadron Electron Ring Accelerator HERA

The HERA tunnel is located 15 to 30 m underground and has a circumference of 6336 meters. Electrons or positrons and protons were stored in two independent rings and brought to collision at four interaction regions, where the experiments H1, ZEUS, HERMES and HERA-B were located. H1 and ZEUS were ep collider experiments at $\sqrt{s} = 300$ or 318 GeV, designed for a broad physics program including studies of the proton structure at low x_{Bjorken}, tests of standard model physics, searches for physics beyond the standard model, diffractive physics etc. HERA-B was designed to study $\mathcal{CP}$ violation in B meson decays in the collisions of 920 GeV protons with the nuclei of target wires, positioned in the halo of the HERA proton beam.

HERMES utilized only the lepton storage ring, initially filled with electron/positron currents of about 40 mA in 180-190 bunches separated by 96 ns [113]. The beam current decreased during a fill due to collisions and other effects, until after about 10 hours of running the HERMES target was operated with unpolarized gas of higher density. The beam was dumped after about another hour. The beam was transversely self-polarized due to the Sokolov-Ternov effect, an asymmetry in the emission of spin-flip synchrotron radiation for $e^{\pm}$ at relativistic energies in a magnetic field. The saturating limit of polarization by the Sokolov-Ternov effect is 92.4 %. HERA was able to reach typical equilibrium beam-polarizations of ∼50 % in a rise time of 40 minutes, which, given that rise time, comes close to the theoretical expectations of Sokolov and Ternov. Since HERMES required a longitudinally polarized beam, mainly to measure the spin structure functions $g_1(x_{\text{Bjorken}})$ and $g_2(x_{\text{Bjorken}})$, the transversely polarized lepton beam was rotated by spin rotators [114]. Between 2000 and 2002, HERA underwent a luminosity upgrade and additional spin rotator pairs for H1 and ZEUS were installed.

3.1.2 The HERMES Target and Spectrometer

The HERMES target system utilized the innovative storage cell technique to reach high polarization (75-85 %) of the target gas and a two orders of magnitude higher density than commonly used polarized jet targets [115, 116]. The target cell [117] was an elliptical open ended tube within the storage ring, where the target gas from the Atomic Beam Source (ABS) [118], i.e. polarized deuterium or hydrogen, was injected from a pipe perpendicular to the beam. The polarization and the atomic fraction of the gas were monitored by a Breit-Rabi Polarimeter (BRP) [119] and a Target Gas Analyzer (TGA) [120] respectively. Various unpolarized gases of higher density were provided by the Unpolarized Gas Feed System (UGFS).

The HERMES spectrometer, schematically depicted in figure 3.2, is a forward angle instrument of conventional design. It consisted of two identical halves which were separated by a flux shielding plate in the mid plane of the magnet, eliminating deflection of the HERA lepton and proton beams passing through the spectrometer. The coordinate system used at HERMES has the z-axis along the beam line, the y-axis – also the direction of the magnetic field of the spectrometer magnet – upwards and the x-axis points towards the outside of the ring. Multiple tracking detectors were installed before, after and within the gap of the 1.3 Tm dipole magnet. An extensive particle identification system was located behind the magnet. The gap between the pole faces of the magnet enclose the geometrical acceptance of ±(40-140) mrad in the vertical direction and ±170 mrad in the horizontal direction.

Another ±100 mrad starting half-way through the magnet due to deflection in the magnetic field were provided horizontally. The experiment was mounted on a platform together with a trailer for electronics and the gas systems, which could be moved on rails.
Due to relatively high event rates, interesting events which should be recorded by the Data AcQuisition (DAQ) system had to be triggered [121]. The main physics trigger at HERMES was designed to detect deep-inelastic scattering events by looking for scattered leptons in the fast detector components, and involved the hodoscopes H0[1],H1 and H2 and the calorimeter. This trigger fired, if the hodoscopes registered signals in the expected chronological order, i.e. H0 first, then H1 and H2, and if the deposited energy in the calorimeter was above a certain threshold, increasing the likelihood that the particle was a lepton. This threshold was usually set to 1.4 GeV, or 3.5 GeV for high density runs. Other triggers, e.g. a photoproduction trigger, which looked for at least one signal in H0, H1 and the back chamber (BC) in every detector half, were usually prescaled by a factor n, meaning, that the n^{th} event firing that trigger is recorded by the DAQ. Since the main physics trigger rejects many interesting events for the Θ^+ search, a special pentaquark trigger was installed in 2004, looking for at least two tracks in one detector half and another track in the opposite half. Unfortunately, the trigger had severe acceptance problems and the data could not be used for the analysis (c.f. sec. 4.1). The major part of the data used in this analysis consists of events where the main physics trigger fired, but since no requirement on the triggers were set in the later analysis, there is also contribution from other triggers.

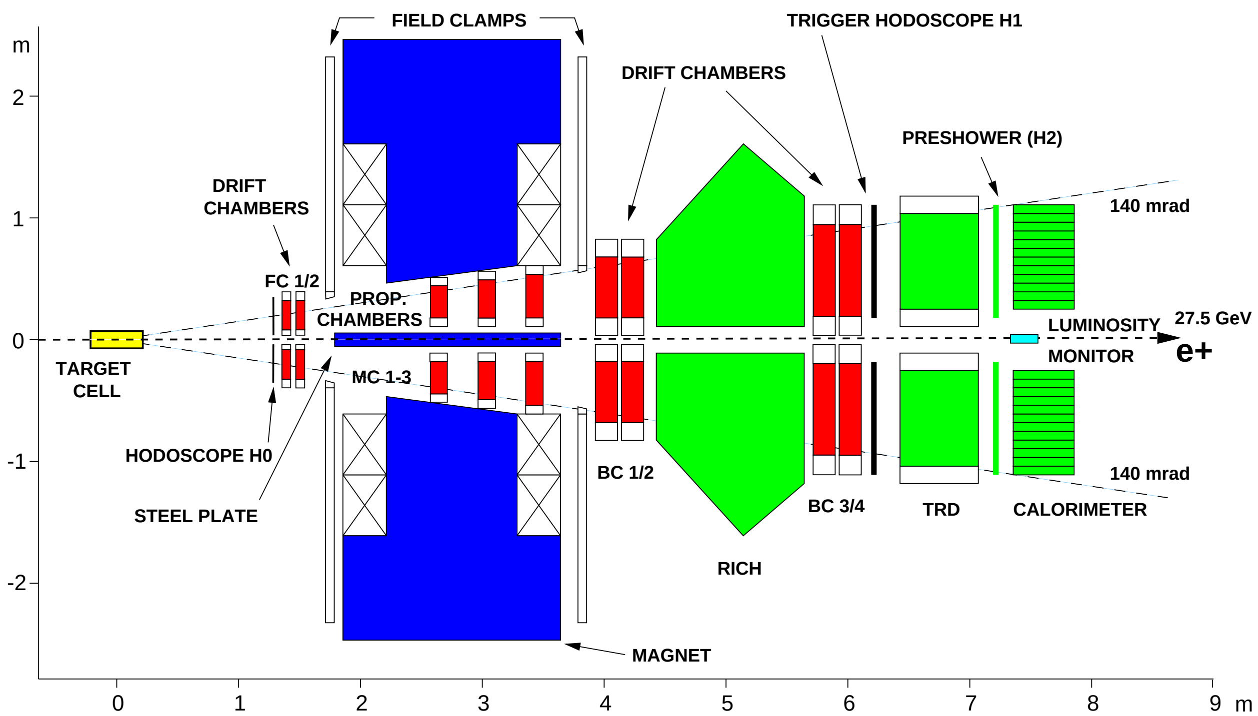

Figure 3.2: A schematic view of the HERMES spectrometer with the main relevant components for this analysis. Tracking devices are colored red, PID detectors green and the magnet/shielding blue.

[1] H0 was installed in 1996, mainly to reject residual interactions of the HERA proton beam.

3.2 Track Reconstruction

The tracking system was required to determine vertices, measure scattering angles, total momentum and to identify hits in the PID detectors associated with each track. Tracking information were provided by two different drift chamber detectors, namely the Front [122] (FC 1/2) and Back Chambers [124] (BC 1-4), and multi wire proportional chambers, the Magnet Chambers [123] (MC 1-3). The momentum resolution is 0.7-1.25 % over the kinematic range and the resolution in the scattering angle is below 0.6 mrad everywhere.

3.2.1 Hardware

The FC and BC tracking detectors were horizontal (in x-direction) drift chambers with alternating anode and cathode wires between two cathode foils, and consisted of six planes each. The cathode foils and wires were at high (few kV) negative potential, while the anode wires were at ground potential. Because of the large horizontal width of the rear chambers, a vertical (X planes) and a tilted $\pm 30°$ (U and V planes) alignment from the vertical of the wires has been chosen. To resolve left-right ambiguities X', U' and V' planes were staggered with respect to their partners by half the wire spacing. The drift chambers use a gas mixture of Ar (90%), CO_2 (5%) and CF_4 (5%), while the MCs use a different proportion of the same gas mixture, Ar (65%), CO_2 (30%) and CF_4 (5%).
The FCs were set up to measure the scattering angle and vertex position. In conjunction with the front tracking, the BCs were able to measure the magnetic deflection for momentum information and were also used to identify the tracks leaving hits in the PID detectors. The MCs were designed to ensure that multi-track ambiguities could be resolved, but were in this regard redundant due to a relatively low number of tracks per event. Nevertheless, the MCs were useful in the reconstruction of short tracks, i.e. tracks that were deflected too much to reach the BCs. The FCs were set up in a $UU'XX'VV'$ module configuration and had a cell width of 7 mm, reaching a resolution of 225 μm. The MCs were UXV modules with a cell width of 2 mm and a resolution of 700 μm. The module configuration of the back chambers was identical to the FC configuration and the cell width was 15 mm allowing for a resolution of 275 μm and 300 μm for the BC 1/2 and BC 3/4 detectors respectively.

3.2.2 Software

HERMES ReConstruction (HRC) [125]
Particle tracks were reconstructed as straight lines in the front and back chambers for U,V and X planes separately. HRC used a tree-search algorithm for fast track finding. The algorithm iteratively increases the artificial resolution of a plane and compares stored hit patterns with combined patterns of planes in the given orientation. Only physically possible tracks are kept and allowed patterns for the next iteration are generated. Note that the tree-search algorithm with about 11 iterations was considerably faster than a track fitting routine. The track projection in the planes were then combined to front and back partial tracks and combined with the hits in the MCs to produce the full track. The momentum of the track is reconstructed by reading a lookup-table which contains the momentum of the track as a function of the relevant track parameter from the front and back partial tracks.
The data-flow is organized as follows: The DAQ writes raw data returned from the detectors into EPIO (Experimental Physics Input Output package) format, which is decoded by the HERMES Decoder (HDC) into pre-calibrated data in the DAD [126] format which are used by HRC to reconstruct tracks.

HRC is succeeded by the input of slow control data[1], PID data and other data. The data is then organized in tables and written into μDST (micro Data Summary Tape) files.

HERMES Tracking Code (HTC) [127]
The HERMES Tracking Code was written to account for the passage through materials and magnetic fields (multiple scattering). It also took the beam position and deflection of tracks by the target/recoil magnet into account, which were used for a transversely polarized target or the recoil detector [128] respectively. The space points of HRC were used and re-parametrized using the KALMAN filter [129]. One important feature, especially for the Θ^+ analysis, is that scattering angles and momenta were provided for each vertex-hypothesis accordingly, i.e. corrected scattering angles and momenta were assigned to every track combination and beam-track combination resulting in a better resolution in inclusive reconstruction of particles. HTC also provides tracking quality parameters, vertex probabilities and covariance matrices from the track fitting routine. This analysis will use the vertex probability, which is the probability that is returned by a χ^2 fit.

3.3 Particle Identification

The Particle IDentification (PID) system at HERMES comprised the four different detectors listed below, which were able to discriminate hadrons from leptons. Additionally pions, kaons and protons could be separated with the RICH detector which was installed in 1998.

3.3.1 Hardware

Ring Imaging CHERENKOV detector (RICH) [130]
The HERMES RICH used a novel dual radiator design, allowing for hadron separation in the entire kinematic range of the experiment (c.f. figure 3.3(a)). One radiator was C_4F_{10} gas with a refraction index of $n = 1.00137$, the other consisted of aerogel tiles with a refraction index of $n = 1.0304$ mounted behind the entrance window(c.f. figure 3.3(b)). The tiles were 1.1 cm thick and stacked in five layers. The CHERENKOV photons from the aerogel and gas radiators were focused by a mirror array of curvature of 220 cm onto a plane of 1934 PhotoMultiplier Tubes (PMTs) per detector half.

Transition Radiation Detector (TRD) [131]
The TRD was able to reject hadrons by a factor of 300 at 90% $e^\pm$ detection efficiency at energies above 5 GeV. It consisted of six modules per half, each containing a polyethylene foil radiator and a MWPC using a gas mixture of Xe (90%) and CH_4 (10%) to detect the transition radiation X-rays.

Preshower Detector (H2)
The preshower detector provided additional information for lepton hadron separation and was able to suppress hadrons by a factor of 10 with 95% detection efficiency for $e^\pm$. It consisted of lead with a thickness of two radiation lengths ($\sim$1.2 cm) and 42 vertical scintillator modules per detector half, of which one was about 1 cm thick and had an active area of 9.3 cm $\times$ 91 cm. The lead initiated electromagnetic showers of $e^\pm$ that deposit typically more energy in the scintillator than minimum ionizing particles.

[1] data from measurements that are read every few minutes, e.g. pressure gauges, high voltage settings, etc.

Calorimeter [132]
The calorimeter measured the energy of electrons/positrons and photons, and suppressed hadrons by a factor of 10 in the trigger and 100 offline. The calorimeter consisted of 42 × 10 blocks of radiation resistant lead glass per detector half. One block was 9 cm × 9 cm in area, 50 cm (∼ 18 radiation lengths) thick and viewed from the back by a PMT. The measured energy resolution was $\sigma(E)/E[\%] = 5.1 \pm 1.1/\sqrt{E\,[\mathrm{GeV}]} + (1.5 \pm 0.5)$, the energy response to electons/positrons was linear within 1 % over a 1-30 GeV energy range, the spatial resolution of the impact point was about 0.7 cm and the pion rejection factor was $\approx 2500 \pm 1200$ integrated over energy in combination with the preshower detector.

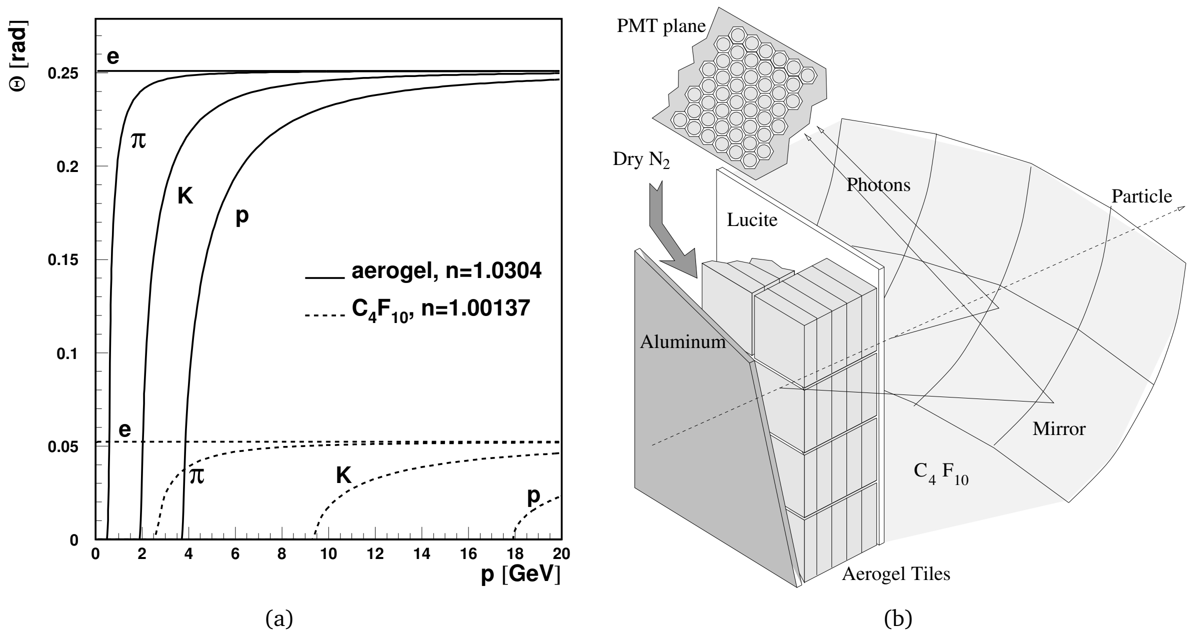

Figure 3.3: (a) Theoretical dependence of the Cherenkov angle and the particle momentum for electrons/positrons, pions, kaons and protons in C_4F_{10} gas and aerogel radiators. (b) A schematic view of the geometry and radiator configuration of the HERMES RICH. Taken from [130]

3.3.2 Software

Lepton-Hadron Separation
The offline lepton-hadron separation algorithm is based on Bayesian statistic, calculating the conditional probability

$$P(H_{l(h)}|R,p,\theta) = \frac{P(H_{l(h)}|p,\theta)P(R|H_{l(h)},p)}{\sum_{i=l,h} P(H_i|p,\theta)P(R|H_i,p)} \tag{3.1}$$

that the track is a hadron or lepton given the response of the considered detector R, the track momentum p and its polar angle θ. The Bayesian prior of each detector $P(R|H_{l(h)},p)$ was extracted from tracks where the particle type was known with high confidence. In first approximation the lepton and hadron fluxes are uniform

$$P(H_l|p,\theta) = P(H_h|p,\theta) \Longrightarrow \log\frac{P(H_l|R,p,\theta)}{P(H_h|R,p,\theta)} = \log\frac{P(R|H_l,p)}{P(R|H_h,p)} := \mathrm{PID}_d\ . \tag{3.2}$$

PID_d is taken as likelihood for the lepton hadron separation for a single detector. In the HERMES naming scheme the PID distributions of the RICH, the preshower detector and the calorimeter are added to the quantity PID_3, while $\mathrm{PID}_{\mathrm{TRD}}$ is defined as PID_5. The particle fluxes $P(H_{l(h)}|p,\theta)$ were computed iteratively by comparing PID_d to data and varying the fluxes iteratively. The total quantity for lepton hadron separation, PID, is then given by

$$PID = \mathrm{PID}_3 + \mathrm{PID}_5 - \log\Phi = \mathrm{PID}_3 + \mathrm{PID}_5 - \log\frac{P(H_h|p,\theta)}{P(H_l|p,\theta)}\,, \tag{3.3}$$

with the flux-factor Φ.

Hadron Identification

Different types of charged hadrons could be separated with algorithms that use data from the RICH detector. Several types of algorithms were developed at HERMES of which the Inverse Ray Tracing (IRT) [134], the Direct Ray Tracing (DRT) [133] and the event level (EVT) [135] methods are used in this analysis.

- *IRT* – The IRT algorithm computes Cherenkov angles $\langle\theta\rangle$ from hits in the RICH photo-detector plane and the available track information. The angle has to be calculated for both radiators, since the point of emission of the corresponding photon is unknown. A Gaussian likelihood

$$L^{(h,r)}(\langle\theta^{(h,r)}\rangle) = \exp\left[-\frac{\left(\theta_{\mathrm{th}}^{(h,r)} - \langle\theta^{(h,r)}\rangle\right)^2}{2\left(\sigma_{\langle\theta\rangle}^{(h,r)}\right)^2}\right] \tag{3.4}$$

  for each radiator r and particle type hypothesis $h = \{\pi, K, p\}$ (`iType`$=\{3,4,5\}$) given the track information is calculated and normalized. $\theta_{\mathrm{th}}^{(h,r)} = \arccos[(\beta^{(h)} n^r)^{-1}]$ is the theoretical Cherenkov angle for a particle with velocity β and a radiator with refraction index n. The average angle resolution $\sigma_{\langle\theta\rangle}^{(h,r)}$ is set to 3.6 mrad for aerogel and 2.5 mrad for the gas radiator from experimental data with $\beta \approx 1$ electrons.
  The algorithm assigns a value of 0.5 to the likelihood if no PMTs fired and the momentum of the track was below the Cherenkov radiation threshold $p_{\mathrm{min}}^{(h,r)} = M^{(h)}/\sqrt{(n^{(r)})^2 - 1}$ with M being the mass of the hypothesized particle. If the momentum of the hypothesized particle was below the threshold and Cherenkov photons were detected, a minimum likelihood was calculated, which smoothly connects with the likelihood behavior in well defined regions. The same minimum likelihood was calculated for the case no photons were detected, but the momentum of the particle was above threshold.
  The hypothesis that maximized the product of gas and aerogel likelihood is chosen as particle type and stored in the μDST tables. Beside the PID assignment, IRT also provides the likelihoods, $\langle\theta\rangle$ and its RMS for every hypothesis and radiator. The decimal logarithm of the likelihood ratio of the most likely hypothesis to the second most likely hypothesis is defined as rQp value and also stored in the μDST tables.

- *DRT* – The DRT algorithm uses the HERMES Monte Carlo engine to simulate $N_{\mathrm{MC}}^{(t,h,r)}$ =360 photons for each particle hypothesis h and radiator r, given the momentum of track t. The likelihood of the particle type hypothesis h given the track information t is

$$L^{(h,t)} = \prod_i \left[P_{\mathrm{PMT}}^{(h,t)}(i) C_{\mathrm{PMT}}(i) + \overline{P}_{\mathrm{PMT}}^{(h,t)}(i) \left(1 - C_{\mathrm{PMT}}(i)\right) \right] \tag{3.5}$$

  with the recorded hit pattern $C_{\mathrm{PMT}}(i)$ and its probability to fire the i-th PMT $P_{\mathrm{PMT}}^{(h,t)}(i)$ according to Monte Carlo. This probability is calculated as

$$P_{\mathrm{PMT}}^{(h,t)}(i) = 1 - \exp\left[-\sum_r \left(\frac{N_{\mathrm{MC}}^{(t,h,r)}(i)}{N_{\mathrm{MC}}^{(t,h,r)}} \cdot n^{(t,h,r)} \right) - B(i) \right] \ , \tag{3.6}$$

  and its complement $\overline{P}_{\mathrm{PMT}}^{(h,t)}(i) = 1 - P_{\mathrm{PMT}}^{(h,t)}(i)$. The 360 MC photons are scaled by $n^{(t,h,r)}$ to a realistic expected value of photons and $B(i) = 10^{-4}$ is the assumed probability of a randomly firing PMT due to electronic noise. The likelihoods for every hypothesis, the rQp value analog to the IRT definition and the PID assignment are stored in the μDST tables.

- *EVT* – The EVT algorithm uses the likelihood definition and MC simulation from DRT and regards the whole event rather than a single track. Thus EVT is called as soon as there are two to five tracks in the same detector half; else DRT is called. EVT adds the simulated hit patterns from DRT and evaluates the likelihood of every track-hypothesis combination, named Combined Particle Type Hypothesis (CPTH). To extract the most likely combination of tracks, a t-dimensional CPTH tensor with h entries per dimension, where t is the number of tracks in one detector half and h is the number of considered hypotheses, is calculated and the most likely combination of particle types are assigned to the tracks. Electrons and positrons now also have to be taken into account, since they contribute to the misinterpretation of hit patterns. If the most likely CPTH contains an electron/positron track, the particle type is set to 3 (a pion), relying on the lepton-hadron separation of other detector components, which is far better than the ep separation with the RICH. The rQp value is calculated as the ratio of the most likely CPTH to the next most likely CPTH that has the considered track identified as a different particle type. EVT writes the particle type, the rQp value and a sum of the CPTH tensor entries for a track with given hypothesis to the μDST tables.

4 Analysis of the pK_S^0-channel

This chapter is dedicated to the description of the analysis chain and event selection criteria/cuts, and to the results of the studies on the pK_S^0-channel at HERMES including systematic and statistical considerations. The pre-selection of events for the inclusive p and K_S^0 candidates and the reconstruction of invariant masses is addressed in the first section of this chapter. The second section concentrates on the selection criteria for K_S^0 candidates, decaying into an oppositely charged pair of pions in the HERMES spectrometer. The section is further divided into systematic studies, where possible cuts are examined, and into the optimization of the K_S^0 yield, where the cuts were optimized with respect to their naive significance $Z = \frac{S}{\sqrt{S+B}}$. The philosophy of optimizing the K_S^0 yield is to maximize the statistic without introducing too much background, enhancing the expressiveness of the final result. This philosophy is referred to as Z^* henceforth. Another, similar ansatz, named P^*, optimizes the naive significance for a given purity $P = \frac{S}{S+B}$ of the K_S^0 signal, in order to provide a systematic check of the final result for the Θ^+. The main advantage of these two approaches, beside providing a sample with optimized statistic, is their objectivity, referred to as blind analysis [136]. Such a blind analysis automatically protects against any subjective bias which could be introduced by the analyzer.
The selection of Θ^+ candidates is subject to the following section, which is again divided into systematic studies of the selection criteria, the optimization of the proton candidates, the statistical analysis and the discussion of systematic uncertainties.
The analysis was carried out with the software ROOT, an object orientated analysis framework based on `C` and `C++`, developed by CERN to analyze and handle huge amounts of data efficiently [137]. For the fitting procedure and the statistical analysis the ROOT-packages RooFit [138] and RooStats [139] were used.

4.1 Data Quality and Pre-Selection of Events

The data used for this analysis was taken during the years 1998-2000(HERA I) and 2002-2007 (HERA II) on deuterium and hydrogen targets. The main properties of this data is summarized in table 4.1. If not explicitly mentioned otherwise, deuterium data is used in the following.
The 1995-1997 data was not taken into account, since the RICH detector was not installed then. The 2004-2005 deuterium data was excluded because the pentaquark trigger, which was only in operation during this time, caused acceptance problems in multi-track events [140]. The next step was the selection of runs, which have not been marked as "bad" in a (digital) logbook; a run is corresponding to about 3-10 minutes of data taking, resulting in approximately 500 MB of raw data. Runs in which a high density target was used were taken out of the analysis, since the calorimeter threshold for the main physics trigger was set to 3.5 GeV. The data was taken out in order to maintain the compatibility between the published analysis of HERA I data and this analysis, as well as the compatibility between deuterium and hydrogen. The underlying reason were different production rates of K_S^0s [140] as well as known strange baryons, such as $\Sigma(1385)$ and Ξ^-. An event had to consist of at least three and at most six long tracks, i.e. tracks passing both front- and back-chambers. The cut for the maximum number of tracks was introduced to keep the number of track-combinations low and to exclude unusually high pile-up. With this cut less than 0.1 % of the total statistics is lost. At least one of the three tracks, taken as proton candidate, had to be identified as hadron ($-100 <$ PID3+PID5 < 0) and had to have a HTC momentum greater than 4 GeV to assure proton identification with the RICH detector.

Year	Production code	Target	N_{DIS}
1998	98e1	D	1,552,212
1999	99d1	D	2,007,157
2000	00e1	D	9,643,969
2006	06f1	D	7,957,780
2007	07d1	D	7,277,342
2002-2003	02d1,03d1	H	2,457,553
2004	04d2	H	3,433,011
2005	05d2	H	7,060,898
2006	06f1	H	23,361,450
2007	07d1	H	18,763,946
Total		D	28,438,460
Total		H	54,876,858

Table 4.1: Properties of data sets used in the analysis. The number of deep inelastic scattering events N_{DIS} is approximately proportional to the integrated luminosity of the experiment. Taken from [143]

The parameters to be used of the events fulfilling the above mentioned cuts were written from the HERMES internal μDST tables to `.root` files by an previously existing and several times cross-checked `FORTRAN` code. The μDST tables already contain a complete set of physical parameters requested by this analysis, such as vertex positions, absolute momenta, scattering angles from the track fitting, as well as PID information, vertex probabilities and event information. Due to the year dependence of the cut on the primary vertex position[1], the many `.root` files from the μDST tables were combined into distinct `.root` files, separated by year and target type. At this stage data quality cuts were applied on burst level basis; a burst corresponds to ~ 10 seconds of data taking. Bursts which had problems with the PID detectors were taken out. The HERMES internal hexadecimal data quality mask required for this cut is `0x02780000`. In addition, tracks with momenta greater than 15 GeV have been cut.
The next step comprised the reconstruction of the particles to analyze. Their invariant masses, certain angles, transverse and longitudinal momenta were calculated using the ROOT classes `TLorentzVector` and `TVector3`, which allows for easy handling of the corresponding variables. Due to combinatorial reasons different cuts had to be applied in the reconstruction of Θ^+ candidates and $\Sigma(1385)/\Xi^-$ candidates. In the Θ^+ decay configuration (fig. 4.1) the proton candidate, i.e. the track identified as hadron and with momentum greater than 4 GeV, is treated as if it stems from the interaction point. The interaction point is calculated as the crossing point of proton track candidate and beam V_{pB}. In the $\Sigma(1385)/\Xi^-$ decay configuration, the proton candidate originates from a displaced secondary vertex. Momenta and scattering angles will slightly differ between these configurations because the HTC tracking algorithm corrects these variables according to the hypothesized track origin. The cuts applied at this point are charge-, in target interaction- and fiducial volume cuts. The latter ensures that the tracked particles passed the detector within its acceptance region. In order to calculate the fiducial volume cuts, the scattering angle and vertices of the tracks had to be known, so that the cuts could only be applied at this or a later stage of the analysis chain. The in target interaction cut is year dependent, because the target cell was shifted and shortened with the installation of the recoil detector. All cuts and their values are summarized in appendix A.

[1] The z coordinate of the primary vertex was required to be within the target cell, which was moved and shortened for the recoil detector period in 06-07.

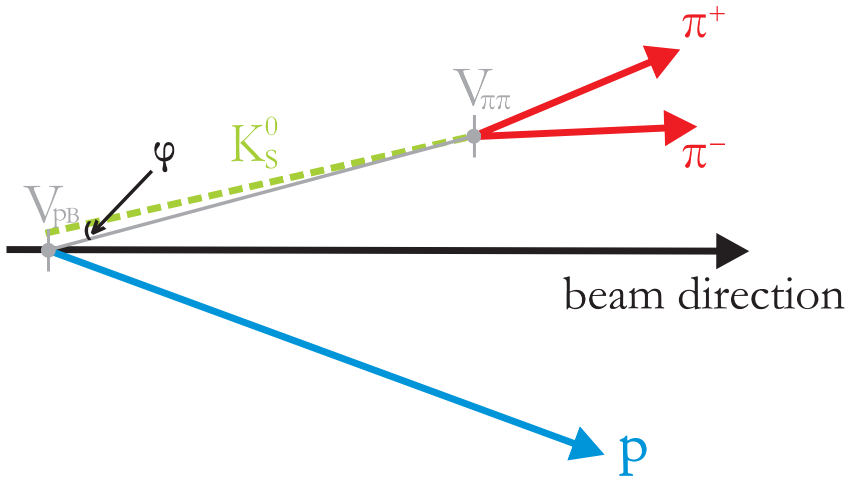

Figure 4.1: Schematic picture of the Θ^+ decay. Colored lines represent momenta of particles. The K_S^0 momentum is reconstructed from the two pion momenta. The coplanarity angle φ is calculated between the K_S^0 momentum and the gray line linking the vertices V_{pB} and $V_{\pi\pi}$.

4.2 Selection of K_S^0 Candidates

This section reviews cuts affecting the K_S^0 reconstruction, subject to an earlier HERMES analysis [141] and introduces new selection criteria. If there was no prior systematic reason to apply a certain cut, the naive significance $Z = \frac{S}{\sqrt{S+B}}$ of the K_S^0 signal-region was tested by application of that cut, or certain cut-values, and compared to the obtained naive significance of the non-cutted K_S^0 spectrum. All subsequent studies were done with deuterium data, in order to retain compatibility with the HERMES publication on the pentaquark [81] and because a dependence on the target gas was observed (c.f. paragraph 4.3.1.1). The obtained selection criteria were later applied one-to-one to the hydrogen datasets.
The flow of work was organized as follows: First the feasibility of old and new cuts was studied by testing the naive significance at fixed cuts from previous work. The fixed cuts were similar to the ones presented in [141]. Next came the optimization of cut values by a scan in the parameter-space, discussed in section 4.2.2. After the scan the previously excluded cuts were tested again at fixed cut values obtained by the optimization. The results of this second check, justifying the exclusion of cuts after the optimization, are presented in the following section. The benchmark, to which the systematic checks are compared is shown in figure 4.2, corresponding to the final K_S^0 selection after optimization. The K_S^0 spectra were fitted with the unbinned Extended Maximum Likelihood (EML) method, using two Gaussian Probability Density Functions (PDFs) with a common mean as signal and an exponential function as background model. In figure 4.2 the sum of the fitted PDFs is indicated by the solid blue curve and the exponential (background) PDF is displayed by the dashed blue curve. The quantities S and B for the estimation of the naive significance $Z = \frac{S}{\sqrt{S+B}}$ were calculated, independently for each fit, in the signal region bounded by two times the by normalization weighted average σ of the standard deviations σ_1, σ_2 of the two Gaussian PDFs

$$2\sigma = 2\frac{N_1\sigma_1 + N_2\sigma_2}{N_1 + N_2} \ . \tag{4.1}$$

In the following figures the signal region is within the blue vertical lines, whereas the sidebands are marked yellow.

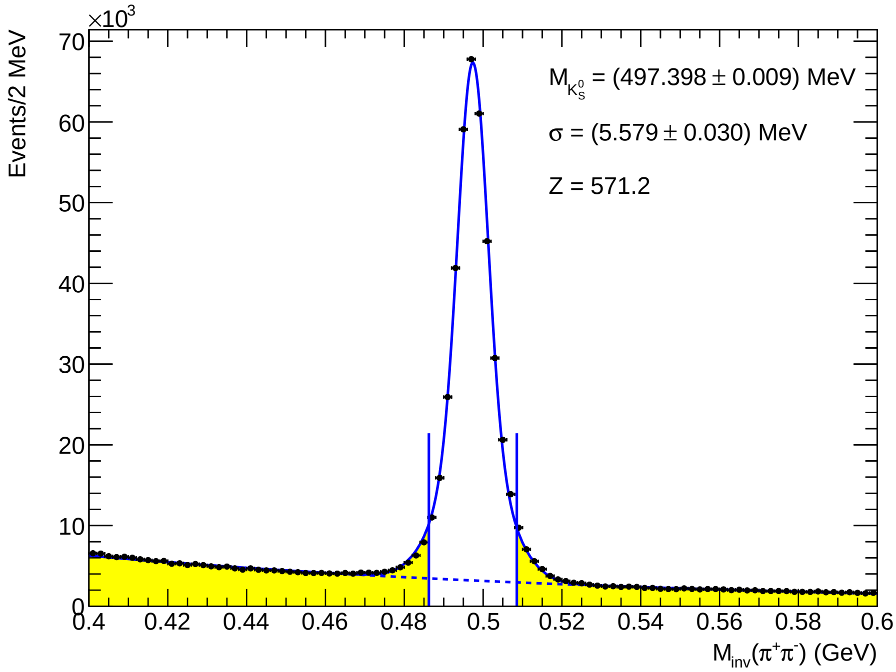

Figure 4.2: Invariant mass spectrum of two oppositely charged pions after optimization showing a clear K_S^0 signal peak. The fit parametrization is described in the text. The indicated σ is the by normalization weighted average of the standard deviations of the single Gaussian distributions.

4.2.1 Systematic Studies

Former analyses at HERMES on this subject used either RICH-PID [81] or lepton-hadron separation without PID requirement for the pion candidates [141]. The comparison between the left panel of figure 4.3 and the optimized K_S^0 spectrum (fig. 4.2), where no hadron-lepton separation is used, shows a slightly deviating significance. Indeed, the gain in signal events by omitting the hadron-lepton separation ($\sim$ 0.6 %) is rather marginal, but the increasing significance shows that some pions have been identified as leptons by the detector. This is not surprising, since the lepton-hadron misidentification is known to be at the 0.5 % level at HERMES. The selection of RICH-identified pions on the other hand comes with a substantial decrease in significance and a loss of $\sim$ 25 % K_S^0 signal events.
It is also known that leptons in quasi-real photoproduction at HERMES predominantly originate from pair production processes and have small forward angles with relatively low momenta. Due to relatively low Q^2 values of these photoproduction process, scattered leptons which consequently have high energies, are not detected. Thus the momentum of the mother particle is mainly due to the hadron, which is combined with the lepton and used for reconstruction. Therefore the transverse momentum p_T of the hadron with respect to the mother particle in conjunction with a lepton will be small. With this in mind, a cut on p_T was studied and such a cut did increase Z. Figure 4.4(a) shows the Armenteros-Podolanski plot [142] before the application of K_S^0-specific cuts. In this plot the asymmetry of longitudinal momenta of the decay products with respect to the mother particle $\alpha = \frac{p_L^+ - p_L^-}{p_L^+ + p_L^-}$ is plotted against the transverse momentum of either decay particle[1].

[1]The transverse momenta of the two daughter particles are the same in a two body decay due to momentum conservation.

A close look to figure 4.4(a) (this might only be possible in the online version of this document where zooming is available) reveals a sharp peak concentrated in two bins at p_T values smaller than 1 MeV and $|\alpha| < 0.0075$. All other bins have at most a one order of magnitude lower number of entries. These two bins are most likely populated with ghost tracks.

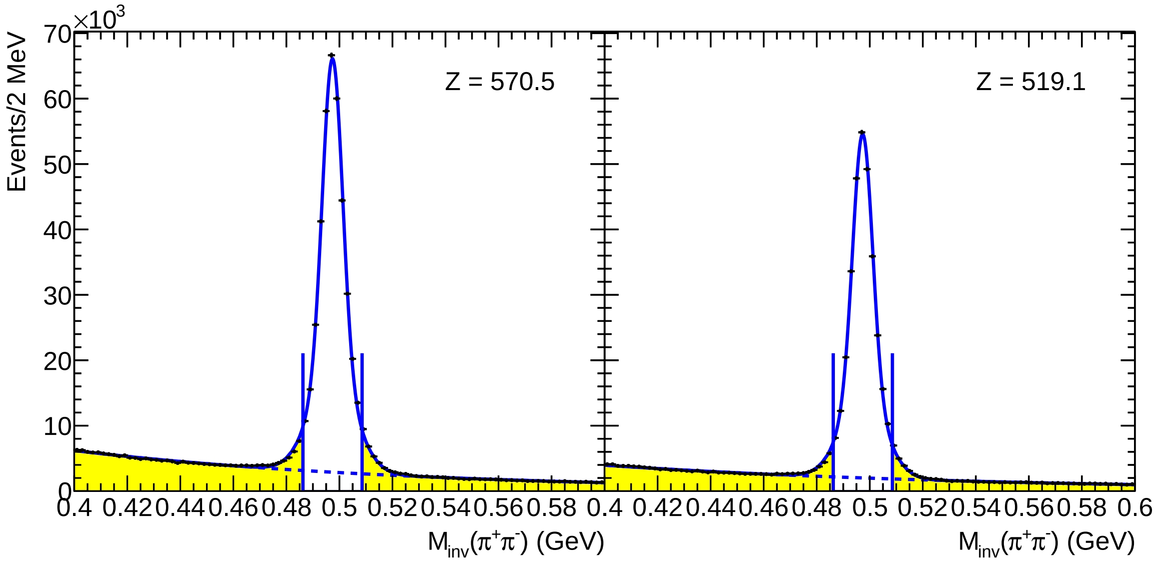

Figure 4.3: K^0_S spectra with hadron-lepton separation (left panel) and with PID for both pion track candidates (right panel).

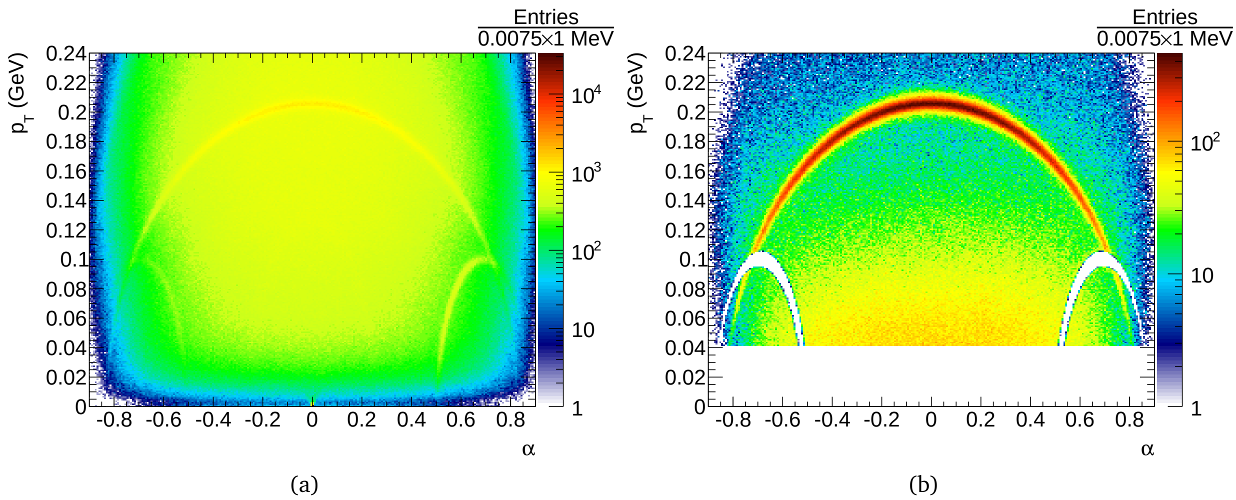

Figure 4.4: ARMENTEROS-PODOLANSKI plots for the data sample before (a) and after cut-optimization (b).

Since no PID for both tracks is required, it is obvious that these tracks can also originate from other two body decays of neutral particles such as $\Lambda \to p\pi^-$ or $\phi \to K^+K^-$. The ARMENTEROS-PODOLANSKI plot exhibits three major arcs, corresponding to K^0_Ss, forming the big arc, and $\overline{\Lambda}/\Lambda$s, which form the smaller arcs on the left and right side respectively.

$\overline{\Lambda}$ and Λ are separated by kinematics in the plot, because the (anti-)proton is always the leading particle, i.e. the particle with the larger longitudinal momentum. It is also seen, that the arcs of K^0_Ss and $\overline{\Lambda}/\Lambda$s intersect. This means that the K^0_S peak is contaminated by $\overline{\Lambda}/\Lambda$ baryons. Since these baryons are a known source of unwanted background, a cut in the $p\pi$ invariant mass spectrum within 2σ of the $\overline{\Lambda}/\Lambda$ peak is set. The corresponding values of the $p\pi$ invariant mass for this cut were obtained by a fit to the combined $\overline{\Lambda} + \Lambda$ spectrum with the same PDF which was used to fit the K^0_S spectrum. The effect of this cut is shown in figure 4.4(b). The decay of the ϕ meson to K^+K^- is not visible in either of the two ARMENTEROS-PODOLANSKI plots. In fig. 4.4(a) the background is too high and in fig. 4.4(b) the cuts are not suitable for ϕ mesons.

This means that the displacement of the secondary vertex is expected to be significantly less than the optimized cut for the K^0_S, because the ϕ lifetime is several orders of magnitude shorter than the K^0_S lifetime. Additionally a contamination of the K^0_S peak with ϕ mesons can be excluded due to kinematics. The mass of the ϕ meson is close to the K^+K^- threshold and therefore p_T and α of the kaons is considerably smaller than that of the pions in the case of the K^0_S decay, resulting in a smaller arc which does not intersect the arc of the K^0_Ss.

The remaining cuts were studied in a straightforward manner. First the correlation between the cut parameter $\mathcal{X}$ and the invariant mass of the pion candidates was plotted. For the pion momentum this is done in figure 4.5(a). The correlation plots give a first hint if a cut on $\mathcal{X}$ is feasible and if so, which region of the cut-values can be considered for optimization. In figure 4.5(a) the K^0_S peak is distributed almost isotropically over the whole momentum range, suggesting to omit the cut on pion momenta. In former studies, an event was cut if one of the pion momenta was less than 1 GeV to ensure lepton-hadron separation with the TRD for the pion candidates. After the correlation plot, the flow of work described in the beginning of this section was pursued. Figure 4.5(b) shows the control scan of the cut on either pion momentum. In this context a control scan is the scan of an for the optimization omitted parameter $\mathcal{X}'$, which is performed after the optimal set of cuts have been found. Figure 4.5(b) shows that the best value of Z was obtained when no cut on $p_{\pi^\pm}$ was set.

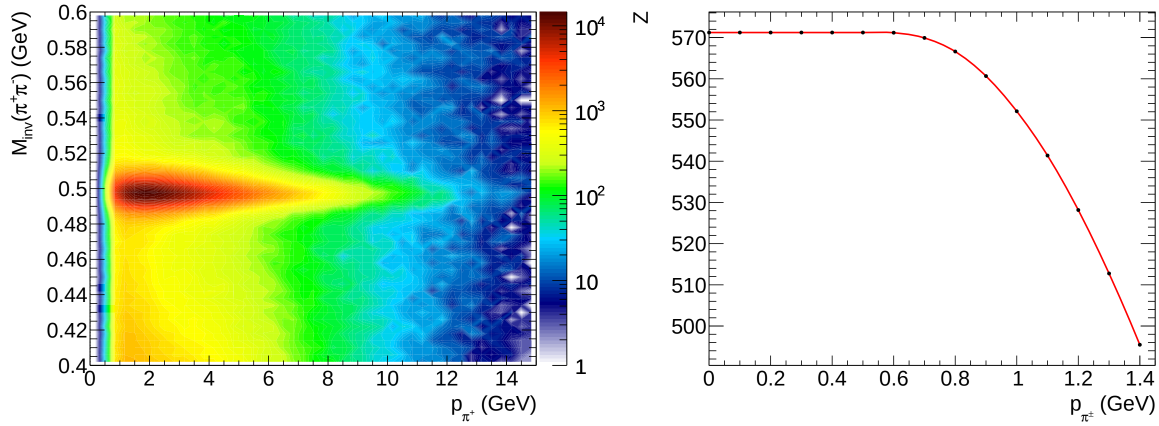

(a) (b)

Figure 4.5: (a) p_{π^+}-$M_{\text{inv}}(\pi^+\pi^-)$ correlation over the whole momentum range. (b) 1-D scan profile of the $p_{\pi^\pm}$ cut in a constrained region of the pion momenta. Both plots show data where the optimized cuts were applied.

4.2.2 Optimization of the K^0_S Yield

The remaining cuts after the systematic studies for the optimization were:

- The transverse momentum of the pions p_T with respect to $\mathbf{p}_{K^0_\mathrm{S}}$
- The coplanarity angle $\varphi = \frac{180}{\pi} \arccos\left(\left|\frac{(\mathbf{V}_{\pi\pi}-\mathbf{V}_{p\mathrm{B}})\cdot\mathbf{p}_{K^0_\mathrm{S}}}{|\mathbf{V}_{\pi\pi}-\mathbf{V}_{p\mathrm{B}}|\ |\mathbf{p}_{K^0_\mathrm{S}}|}\right|\right)$
- The distance between primary and secondary vertex in beam direction $\left(\mathbf{V}_{\pi\pi}-\mathbf{V}_{p\mathrm{B}}\right)_z$
- The negative decimal logarithm of the probability of two tracks forming a secondary vertex, obtained by track fitting with the χ^2-method $-\log\left(\mathrm{prob}(\mathbf{V}_{\pi\pi})\right)$

The correlation plots for φ, $\left(\mathbf{V}_{\pi\pi}-\mathbf{V}_{p\mathrm{B}}\right)_z$ and $-\log\left(\mathrm{prob}(\mathbf{V}_{\pi\pi})\right)$ with $M_\mathrm{inv}(\pi^+\pi^-)$ are shown in figures 4.6(a), 4.7(a) and 4.8(a) respectively. The correlation plots illustrate that the optimized cut selects a region where the K^0_S peak dissolves from the background. An explicit p_T-$M_\mathrm{inv}(\pi^+\pi^-)$ correlation plot would not reveal new insight. It can be derived from figure 4.4, where the $\pi^+\pi^-$ invariant mass corresponds to a curvilinear coordinate transformation along the prominent K^0_S arc. The invariant mass decreases with perpendicular movement against this curvilinear coordinate towards lower values of p_T and α, and increases by moving in the opposite direction.

The naive significance Z was scanned in a four-dimensional space spanned by the above listed parameters. The scan was performed by iteratively setting up grids with variable size. The first scans were performed in three dimensions, where a cut on the vertex probability $-\log\left(\mathrm{prob}(\mathbf{V}_{\pi\pi})\right)$ has been neglected. This parameter was initially examined down to a minimal value of $\mathrm{prob}(\mathbf{V}_{\pi\pi}) = 10^{-6}$ following the suggestion of the internal HERMES documentation [127]. The vertex probability has been added as fourth parameter to the grid after the one dimensional control scan was performed in the logarithmic scale down to the lowest possible value of $\mathrm{prob}(\mathbf{V}_{\pi\pi}) \approx 10^{-30}$.

The first three dimensional scans were performed using 8 grid points per dimension, resulting in a loop over 512 individual fits to the K^0_S spectrum per scan. The naive significance Z, the purity P and the grid-coordinates, as well as the plots of the spectra and fit-quality plots have been stored in suiting formats. A major problem for the first scan with a wide parameter range was to assure convergence of each fit. This was done by anticipating start values and constraints of the fit parameters in certain scan-space regions. Additionaly a narrower fit range was chosen ($[0.46, 0.54]$ GeV) because the exponential function was not able to describe the background for a cut at high p_T, which led to a decreasing background in the low invariant mass region. The convergence of the fits has been checked automatically. The conditions were a low χ^2 value of the fit, returned after plotting the binned data and the normalized PDF. Also the final value of each fit-parameter should not reach close to its constraint. In such a case the output was marked accordingly as non-convergent and those fits were redone.

The results of each scan were visualized by two-dimensional scan profile plots; examples are shown in figures 4.6(b), 4.7(b) and 4.8(b). Subsequent scans were arranged as a zoom into the peaking region of these plots. The iteration of scans (or the zooming) was performed until the profile plots did not exhibit a smooth structure any more, albeit the fits converged. A smooth structure in that sense is a profile with exactly one local maximum. A non-smooth profile can be understood in terms of statistical errors of S and B, which become visible.

The scan profile from the first scan in figure 4.6(b) shows a zoomed region of p_T and φ to clarify the maximum in $\tilde{Z}$ at $p_\mathrm{T} \sim 40$ MeV. The variable $\tilde{Z}$ is an auxiliary measure. It is defined by $\tilde{Z} = Z - \min(Z)$, where $\min(Z)$ is the minimum of Z in the plot range.

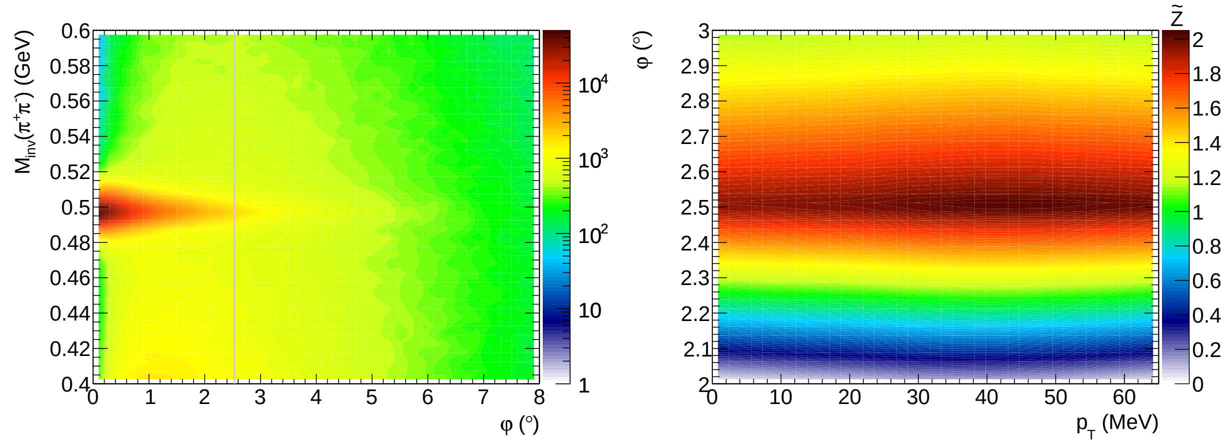

(a) (b)

Figure 4.6: (a) φ-$M_{\text{inv}}(\pi^+\pi^-)$ correlation. The optimized cut value is indicated by the gray line. (b) 2-D scan profile of the p_T and φ cuts, where $\left(\mathbf{V}_{\pi\pi} - \mathbf{V}_{p\text{B}}\right)_z > 4$ cm and no $-\log\left(\text{prob}(\mathbf{V}_{\pi\pi})\right)$ cut were set.

The scan profile in the full range of the first scan is shown in figure 4.7(b) for $\left(\mathbf{V}_{\pi\pi} - \mathbf{V}_{p\text{B}}\right)_z$ and φ. The high values of $\tilde{Z}$ in this plot indicate a strong dependence of Z on $\left(\mathbf{V}_{\pi\pi} - \mathbf{V}_{p\text{B}}\right)_z$ and φ. Note that the maximum of $\tilde{Z}$ in figure 4.7(b) is more than 50 times as high as in figure 4.6(b) and more than 1000 times as high as in figure 4.8(b). The scan profile of $\left(\mathbf{V}_{\pi\pi} - \mathbf{V}_{p\text{B}}\right)_z$ and $-\log\left(\text{prob}(\mathbf{V}_{\pi\pi})\right)$ (fig. 4.8(b)) shows the situation after the K^0_S yield was already optimized in tree dimensions. Therefore the $\left(\mathbf{V}_{\pi\pi} - \mathbf{V}_{p\text{B}}\right)_z$ range is very narrow and the coplanarity and transverse momentum cuts are close to their optimized value.

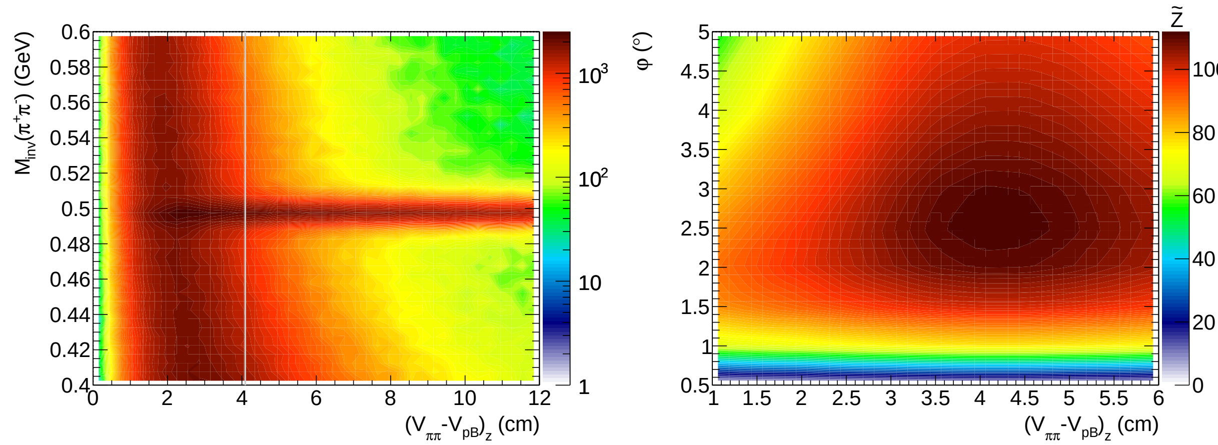

(a) (b)

Figure 4.7: (a) $\left(\mathbf{V}_{\pi\pi} - \mathbf{V}_{p\text{B}}\right)_z$-$M_{\text{inv}}(\pi^+\pi^-)$ correlation. The optimized cut value is indicated by the gray line. (b) 2-D scan profile of the $\left(\mathbf{V}_{\pi\pi} - \mathbf{V}_{p\text{B}}\right)_z$ and φ cuts, where $p_\text{T} > 40$ MeV and no $-\log\left(\text{prob}(\mathbf{V}_{\pi\pi})\right)$ cut were set.

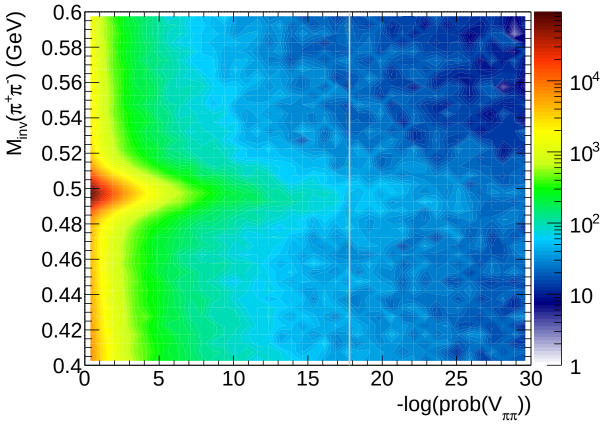

(a)

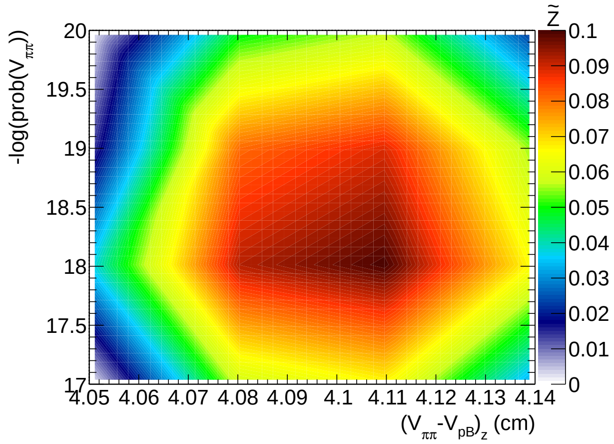

(b)

Figure 4.8: (a) $-\log\left(\mathrm{prob}(\mathbf{V}_{\pi\pi})\right)$-$M_{\mathrm{inv}}(\pi^+\pi^-)$ correlation. The optimized cut value is indicated by the gray line. (b) 2-D scan profile of the $\left(\mathbf{V}_{\pi\pi}-\mathbf{V}_{p\mathrm{B}}\right)_z$ and $-\log\left(\mathrm{prob}(\mathbf{V}_{\pi\pi})\right)$ cuts, where $p_{\mathrm{T}} > 43$ MeV and $\varphi < 2.54°$ were required.

After the maximum in the naive significance was found, a Z-optimized sample for a given purity $P = 97$ % of the K^0_{S} signal was searched. This sample should mimic the selection criteria of [141], where a 97 % pure K^0_{S} was obtained. The selection provides a systematic check of the final result for the Θ^+. The process of this optimization at a given purity is referred to as purity scan in the following. A discrete purity level spans a hyper-surface in the scan space. Every parameter maximizes the naive significance in a certain area of that space and can thus change the purity as well, since Z and P are correlated (both depend on S and B only).
The work flow of the purity scan is straightforward: The first step was to extrapolate the results of the optimization-scan, in order to find an area of the scan space in which the purity is approximately 97 % and where Z is greatest. The principles of the scan in that area did not differ from the optimization-scan. The dimension of the scan space was reduced by omitting the optimization in p_{T} to simplify the succeeding steps. In the optimization scan it was found that the naive significance for $p_{\mathrm{T}} \gtrsim 60$ MeV and also the pion momentum p_π, which was included in the first scans, decreases strongly in conjunction with a slowly increasing purity. Hence the cut on p_{T} had been fixed to its Z-optimized value $p_{\mathrm{T}} < 41$ MeV and a cut on the pion momentum has also been omitted in the purity scans. The results of the first purity scan are shown in figure 4.9, where four of the eight scanned points in $-\log\left(\mathrm{prob}(\mathbf{V}_{\pi\pi})\right)$ are depicted.
The purity contour was obtained by converting a `TGraph2D` object (a 2 dimensional graph in ROOT) into a `TH2` object (a 2 dimensional histogram) and extracting the bins whose purity were closest to 97 %. These points were then fitted in the corresponding parameter plane to get a smooth curve. In figure 4.9 only a section of the naive significance in arbitrary units is shown, to provide a better visualization. The optimized sample for a given purity is at the point where the purity contour traverses a local maximum of the naive significance. In figure 4.9 this corresponds to the panel where $-\log\left(\mathrm{prob}(\mathbf{V}_{\pi\pi})\right) < 8$ at $\left(\mathbf{V}_{\pi\pi}-\mathbf{V}_{p\mathrm{B}}\right)_z \gtrsim 6.6$ cm and $\varphi \lesssim 1.6°$. This first scan was followed by another scan around the obtained values and a last manual scan, approximately along the purity contour. In summary two different K^0_{S} samples were obtained by finding a global maximum of Z in the cut-parameter-space for the Z^* philosophy and a local maximum at a given purity of 97 % for the P^* philosophy. It was found that Z and P are sensitive to $\left(\mathbf{V}_{\pi\pi}-\mathbf{V}_{p\mathrm{B}}\right)_z$ and very sensitive to φ. The dependence of Z on p_{T} and $-\log\left(\mathrm{prob}(\mathbf{V}_{\pi\pi})\right)$ in the region of their optimized values is small.

From this experience the uncertainties of the obtained cut values can be approximated as $\mathcal{O}(1\ \%)$ for $\left(\mathbf{V}_{\pi\pi} - \mathbf{V}_{p\mathrm{B}}\right)_z$, $\mathcal{O}(0.1\ \%)$ for φ and $\mathcal{O}(10\ \%)$ for p_T and $-\log\left(\mathrm{prob}(\mathbf{V}_{\pi\pi})\right)$.

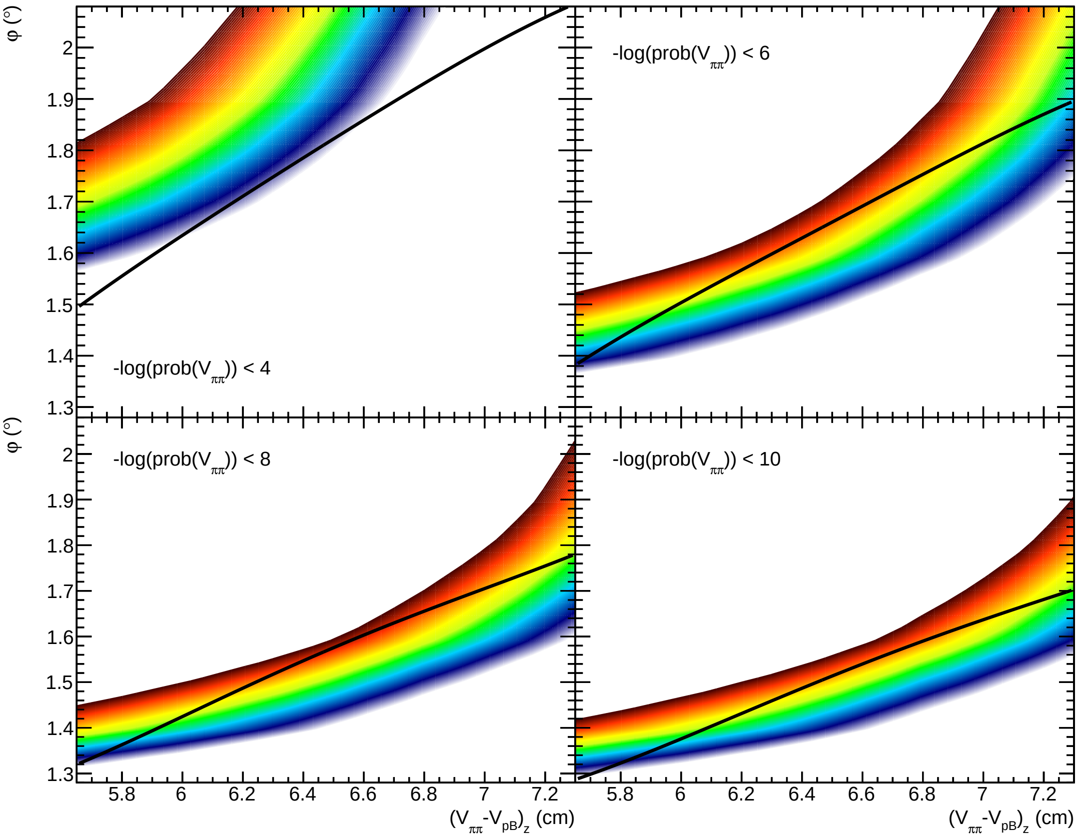

Figure 4.9: Purity scan profile of the $\left(\mathbf{V}_{\pi\pi} - \mathbf{V}_{p\mathrm{B}}\right)_z$ and φ cuts at four different $-\log\left(\mathrm{prob}(\mathbf{V}_{\pi\pi})\right)$ cut values. The fitted 97 % purity contour is shown as solid black line. The naive significance Z is depicted by the colored band in arbitrary units. All four panels show the same section of Z.

4.3 Selection of Θ^+ Candidates

This section reviews cuts affecting the proton selection and systematic studies which help to understand certain cuts and the final results. The two philosophies Z^* and P^* are pursued in subsequent studies. Z^* now optimizes yields of known particles in a straight forward manner and translates the obtained cuts directly to the pK^0_S selection. P^* follows a more careful selection with the drawback of a possible bias to the final result. The P^* philosophy mainly suffers from a missing physical Monte Carlo model for the HERMES environment, associated with the fact that the properties of the Θ^+ – if existent – are not known. On the other hand there are arguments that translation of cuts from known particles to the pK^0_S selection is a oversimplified approximation and could produce fake peaks due to carelessly chosen cuts. Nevertheless, these two approaches provide a benchmark for systematic uncertainties whose quantification is extremely challenging and beyond the scope of this work. Systematic uncertainties are discussed after the statistical analysis of the resulting spectra, which is carried out in section 4.3.2.

4.3.1 Systematic Studies

An extensive amount of systematic studies on the Θ^+ has been carried out since the foundation of the exotics group in 2003. Profitable studies – in the sense of contributing to cuts or the comprehension of the results – are presented in the following.

4.3.1.1 Preceding Systematic Studies

Dependence on the Target Gas
The HERMES target was operated with different types of gases. All gases heavier than deuterium ran in high density mode and are excluded due to reasons given in section 4.1. A dependence of the pK^0_S spectra on the target gas has been observed [144]. Since the bump associated with the Θ^+ only appeared on deuterium, the systematic studies done in this work are carried out with deuterium data and the results from those studies are used analogously on hydrogen.

Combination of HERA I and HERA II Data
The consistency of Θ^+ yields from HERA I and HERA II data on deuterium was tested using a χ^2 function, minimized with the least squares method, as test statistic for three different hypotheses [145]. The outcome of this test was, that the yield from the combined data set is statistically consistent with the sum of yields from its constituents. Therefore HERA I and HERA II data are combined for the analysis.

Separate Study of $\mathbf{pK^0_S}$ and $\mathbf{\bar{p}K^0_S}$
In most moderate and high energy spectroscopy publications, the spectrum obtained from the charge conjugative channel (if existent) is added to the actual spectrum. The HERMES publication on the Θ^+ only showed the pK^0_S-channel [81]. After the publication, most of the analysis was done by adding pK^0_S and $\bar{p}K^0_S$. In spite of the particle/antiparticle cross section ratio obtained from other known particles compared to the Θ^+ bump at HERMES and the complicated (unknown) production mechanism of the hypothetical $\overline{\Theta}^-$, the addition of the $\bar{p}K^0_S$ to the pK^0_S-channel is disputable. Subsequently, the systematic studies using the Z^* logic will be carried out by adding pK^0_S and $\bar{p}K^0_S$ events, while studies with the P^* logic will use the pK^0_S-channel only. The statistical analysis is done for both combinations.

Tagging of Additional Particles
Simple considerations concerning the production of the Θ^+, such as baryon number conservation and the conservation of strangeness suggest the abundance of additional particles in the process. In the Θ^+ photoproduction off protons the dominant process should be $\gamma^{(*)}p \to \Theta^+\overline{K}^0$, where the $\overline{K}^0$ could be detected if it was a $K^0_S \to \pi^+\pi^-$. The Θ^+ photoproduction off a neutron should have an additional K^- in the final state $\gamma^{(*)}n \to \Theta^+K^-$. In the photoproduction off deuterium, an energetically favorable process compared to the productions off protons and neutrons is $\gamma^{(*)}d \to \Theta^+\Lambda$. Tagging of a K^- in an exclusive reaction off the neutron, i.e. on the deuterium target, would be the cleanest possible way to detect the Θ^+ at HERMES and additionally measure its strangeness. If a fourth particle is tagged, it has been observed that a signal is still visible, but the statistic decreased significantly [146, 147].

Isospin of the Θ^+
According to group theoretical considerations presented in section 1.1.1 the anti-decuplet of exotic baryons should be accompanied by a 27-plet and a 35-plet. In these representations the Θ pentaquark is an isotriplet and an isoquintet [33]. A search for the isotriplet partner of the Θ^+, the Θ^{++} has been done in [81], where an upper limit on the cross section was calculated.

4.3.1.2 Optimization of PID Parameters for p Candidates and Event Topologies I

The selection of proton candidates in this analysis mainly depends on the available RICH-PID information and the proton-beam vertex probability addressed in the next paragraph. Over the years several PID algorithms were developed at HERMES whose properties are discussed in section 3.3.2.
An optimization of the available PID algorithms with respect to the particular selection of protons in conjunction with a K^0_S became necessary because the final pK^0_S spectra were quantitatively sensitive to the used PID method. The likelihoods calculated in these algorithms are lacking an important condition in the case of pK^0_S reconstruction. This means that likelihoods for the proton track candidate change under the condition that the other two tracks are pions with a very high probability. The likelihoods are expected to depend on the event topology, i.e. if the proton candidate is accompanied by one, two or more (pion) tracks or if it passed alone through the detector half.
The available methods[1] and parameters at the μDST level were tested by optimizing the $\Lambda + \overline{\Lambda}$ yield with respect to Z. Due to the data structure, where every track combination of an event was written as a new entry in the `.root` file, and the prior cuts on the proton candidate, a different pre-selection compared to section 4.1 had to be done. Both samples initially contain the same events, but the calculation of four-momenta differs because the HTC algorithm corrects angles and momenta according to the track vertices. Hence the four-momentum of the π^+ candidate in the Θ^+ decay configuration, where the track originates from a secondary (displaced) vertex $\mathbf{V}_{\pi\pi}$, differs from the four-momentum of the π^+ candidate in the $\Sigma(1385)$ decay configuration, where the track-beam crossing vertex $\mathbf{V}_{\pi\mathrm{B}}$ is calculated. The configurations are shown in figure 4.10. Again, before and after the optimization scans, parameters in consideration were scanned in one dimension and omitted if a cut on them did not maximize Z. The remaining parameters for optimization were $\left(\mathbf{V}_{p\pi} - \mathbf{V}_{\pi\mathrm{B}}\right)_z$, φ and the PID parameters. The optimization itself was carried out in three steps. First the cut values of $\left(\mathbf{V}_{p\pi} - \mathbf{V}_{\pi\mathrm{B}}\right)_z$ and φ were optimized while the proton selection of the considered PID method was fixed. E.g. if the IRT method is tested, a proton (particle type 5 according to the μDST entry) was selected with the IRT method and the naive significance of Λs was scanned in $\left(\mathbf{V}_{p\pi} - \mathbf{V}_{\pi\mathrm{B}}\right)_z$ and φ.

[1] The development of a new and optimized PID algorithm at the slow control level for this purpose was not feasible in consideration of manpower and the unknown gain.

This step is called pre-optimization or preOpt. One reason for the pre-optimization was that the IRT and DRT methods each had more than one PID parameter available for a scan, resulting in several scans for each method. On the other hand the scans would have been higher dimensional, thus more time-consuming.
The second step was the optimization of the available PID parameters for the proton selection. Used parameters are listed in table 4.2. Cuts on the rQp$_{\pi,K}$ values, provided by the DRT, EVT and IRT methods, were done by selecting particle ID 3 or 4, for pion and kaon respectively, and treating tracks with low rQp, i.e. bad identification quality, as proton candidates. The selection of a particle ID is mandatory since the rQp value is coupled to the particle type for any method (cf. sec. 3.3.2). The correlation of rQp$_{\pi,K}$ and the invariant mass of $p\pi^- + \bar{p}\pi^+$ for the EVT method is shown in figure 4.11, where a $\Lambda + \bar{\Lambda}$ peak emerges at low rQp$_K$ values but no clear structure is seen in the rQp$_\pi$ plot.

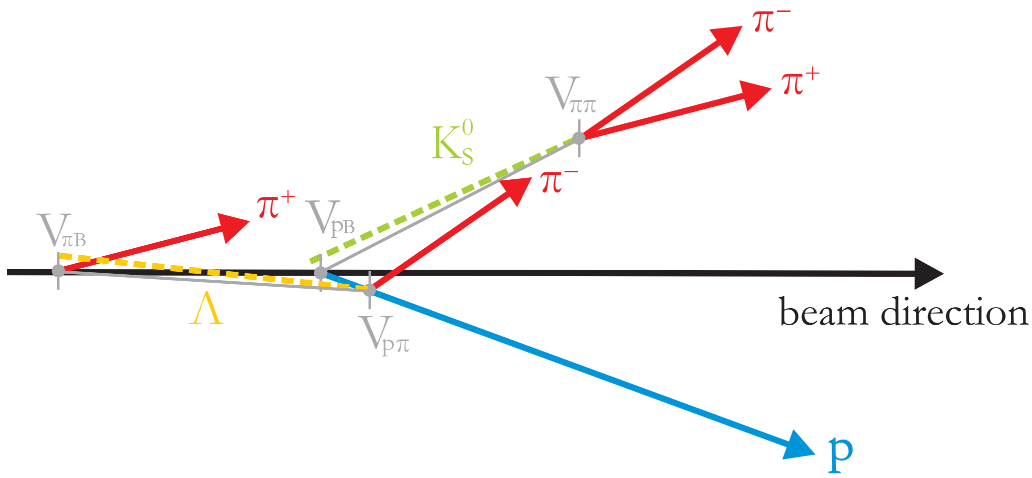

Figure 4.10: Schematic picture of the Θ^+ decay configuration with an intermediate K^0_S and the $\Sigma(1385)$ decay configuration with an intermediate Λ.

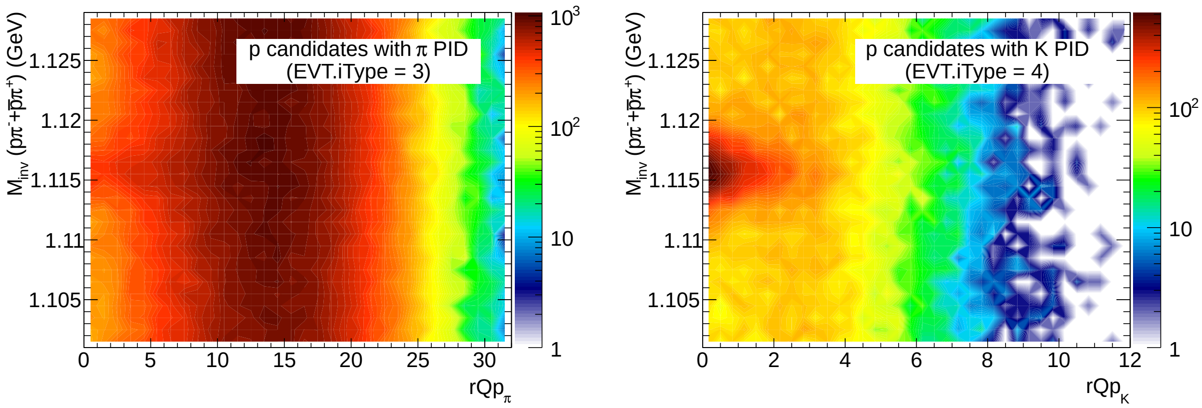

(a)

(b)

Figure 4.11: (a) rQp$_\pi$- and (b) rQp$_K$-$M_{\text{inv}}(p\pi^- + \bar{p}\pi^+)$ correlations. A clear $\Lambda + \bar{\Lambda}$ peak is seen at rQp$_K \lesssim 2$.

rQp cuts were studied in both directions simultaneously, meaning that pions and kaons (RICH-PID=3 and 4) with low identification quality were added to the proton candidates as described, and that protons (RICH-PID=5) could be cut by having low rQp values. The latter did not increase Z in any case and is therefore not mentioned in table 4.2.
In addition to the rQp values, likelihood values for every RICH-PID hypothesis are accessible by the DRT and IRT methods. The IRT method also provides likelihoods for the gas and aerogel radiators separately. The distribution of likelihood ratios for DRT and IRT from aerogel are shown in figure 4.12. Unfortunately only "row-sums" of the charged particle type hypothesis tensor (CPTH tensor) were written to the μDSTs for the EVT method [135]. The entries of the CPTH tensor are likelihoods for each track and hypothesis combination from one event in one detector half. The row-sums sum up likelihoods for each track given a particle hypothesis and have therefore no physical meaning. The likelihoods/row-sums for a track given a hypothesis (RICH-PID = 1,...,5) are obtained by calling `rProb[i]` in the μDSTs, with `i` being the RICH-PID.

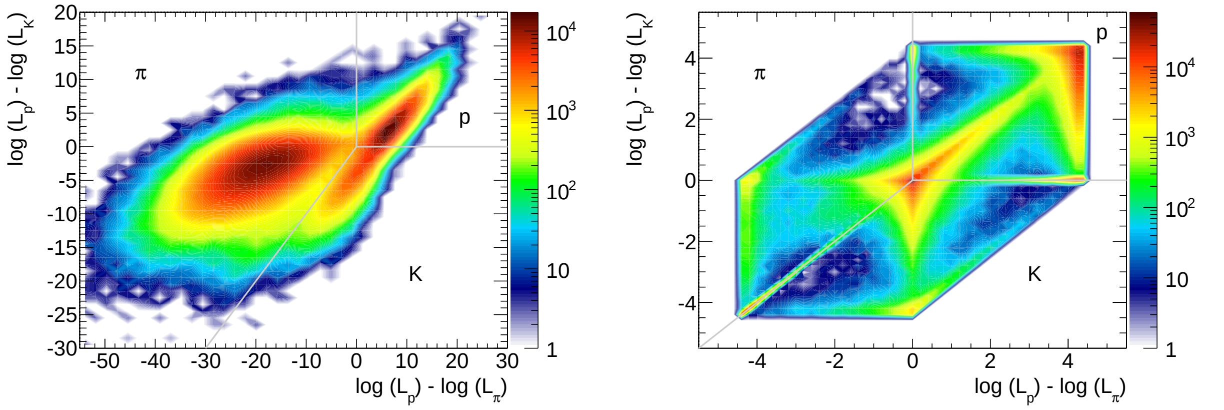

(a) (b)

Figure 4.12: Distribution of likelihood ratios for the DRT method (a) and IRT method (b). The IRT plot shows the likelihood ratios from aerogel only, while the DRT likelihoods contain information of both radiators. The plots are divided by gray lines into distinct regions of particle type assignment according to the particle ID definitions of these methods. The distributions were obtained with the pre-optimized Λ samples.

Cuts in the likelihood ratio spaces were performed along the horizontal and vertical gray lines in figure 4.12. The results of the PID optimization scans are summarized in table 4.2. Note that the naive significance could be increased for every original method accordingly. The maximal naive significance was obtained with the OROR method, a logical `OR` of the methods: `DRT.iType = 5` or `EVT.iType = 5` or `IRT.iType = 5`. These results do not indicate that the PID methods are inefficient or poorly optimized, but it shows that there is a certain inevitable misidentification and that these events can be taken into account if a gain in statistics is important. The cuts on rQp and the likelihood ratios, as well as the OROR method are not normalizable in general. For example if the goal would be maximizing Z for a ϕ meson reconstruction, tracks which were identified as protons or pions would presumably be added to the kaon sample. This means that a track, which is identified as a proton - and therefore treated as such in the case of Λ reconstruction - with low rQp or low log (L_p/L_K) value would presumably be taken as kaon for the ϕ analysis. Hence ambiguities arise which will affect e.g. cross section measurements.

preOpt	$\left(\mathbf{V}_{p\pi} - \mathbf{V}_{\pi B}\right)_z$ [cm]	φ [°]	Z	P [%]	N_Λ
DRT	> 2.15	< 7.05	299.2	88.32	108169
EVT	> 3.00	< 7.00	297.3	89.18	105754
IRT	> 3.00	< 6.75	272.9	88.51	89785
OROR	> 3.00	< 6.95	313.9	87.88	119625
rQp	rQp_π	rQp_K	Z	P [%]	N_Λ
DRT	< 2	< 2.4	311.1	84.15	122855
EVT	-	< 1.8	305.5	87.00	114544
IRT	-	< 3.4	288.8	85.31	104423
LLRs	$\log(L_p/L_\pi)$	$\log(L_p/L_K)$	Z	P [%]	N_Λ
DRT	> -3.6	> -3.0	313.5	85.13	123312
$\mathrm{IRT}_{\mathrm{gas}}$	> -5.0	> -5.0	309.2	85.11	119953
$\mathrm{IRT}_{\mathrm{aero}}$	> -4.4	> -3.5			

Table 4.2: Cuts optimizing Z obtained by the PID scans described in the text. N_Λ is the total number of Λ signal events from the fit, i.e. not only those restricted in the signal region which are used to calculate P and Z. Green values indicate the best overall results of the scans.

The last step in the optimization was to test different event topologies. The reason for this test is that pions, which produce more CHERENKOV-light in the radiators, could bias the proton identification if they hit the same region of the detector. A first systematic check is shown in figure 4.13, where it is immediately seen that the acceptance of the HERMES detector mainly allows for a reconstruction of $\Lambda(\overline{\Lambda})$ if protons and pions traversed the same detector half. The selection to obtain the right panel of figure 4.13 does not limit the (anti-)proton candidates to be alone in one detector half. They could thus be accompanied by additional tracks which do not originate from the considered Λ decay.

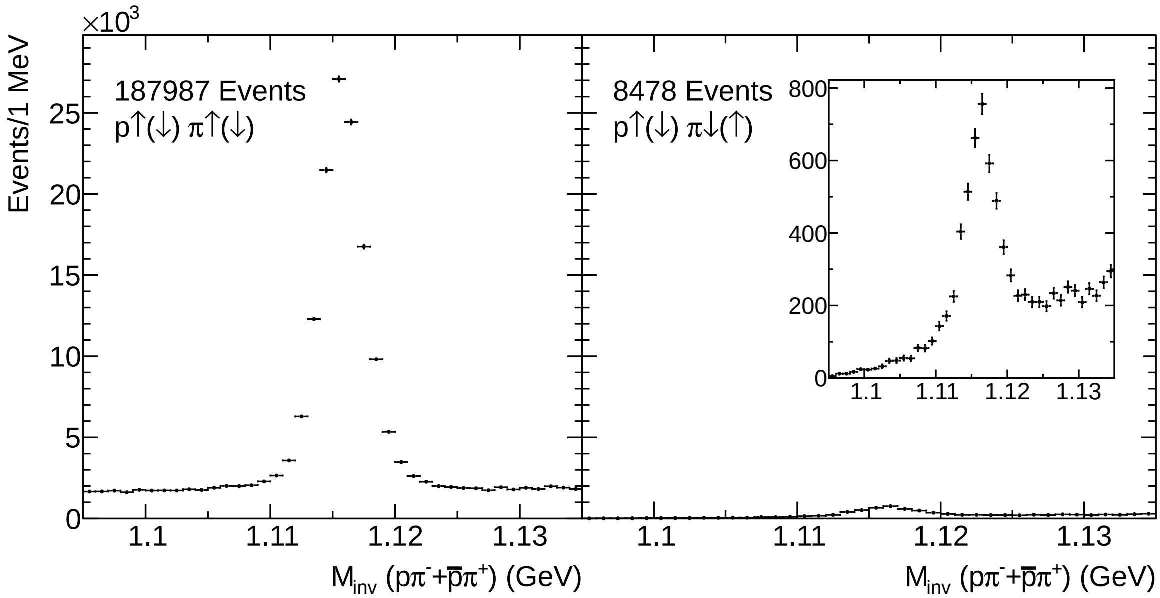

Figure 4.13: Λ spectra with different event topologies with the OROR method. The left panel shows the configuration where the p $(\bar{p})$ and the π^- (π^+) were detected in the same half of the detector. In the right panel the contrary configuration is shown, where the two tracks were detected in opposite detector halves. The inset shows the spectrum with zoomed-in ordinate.

The resulting topology dependence for Λ decays was not anticipated but can be understood in terms of the detector acceptance. Especially the $\sim$ 20 times lower statistic comparing the left to the right panel of fig. 4.13 and the change of the background shape are remarkable. Due to the result of this systematic study, a topology-dependent optimization of the proton identification has been dismissed. The question for the Θ^+ topology dependence arises naturally and is shown in figure 4.14.

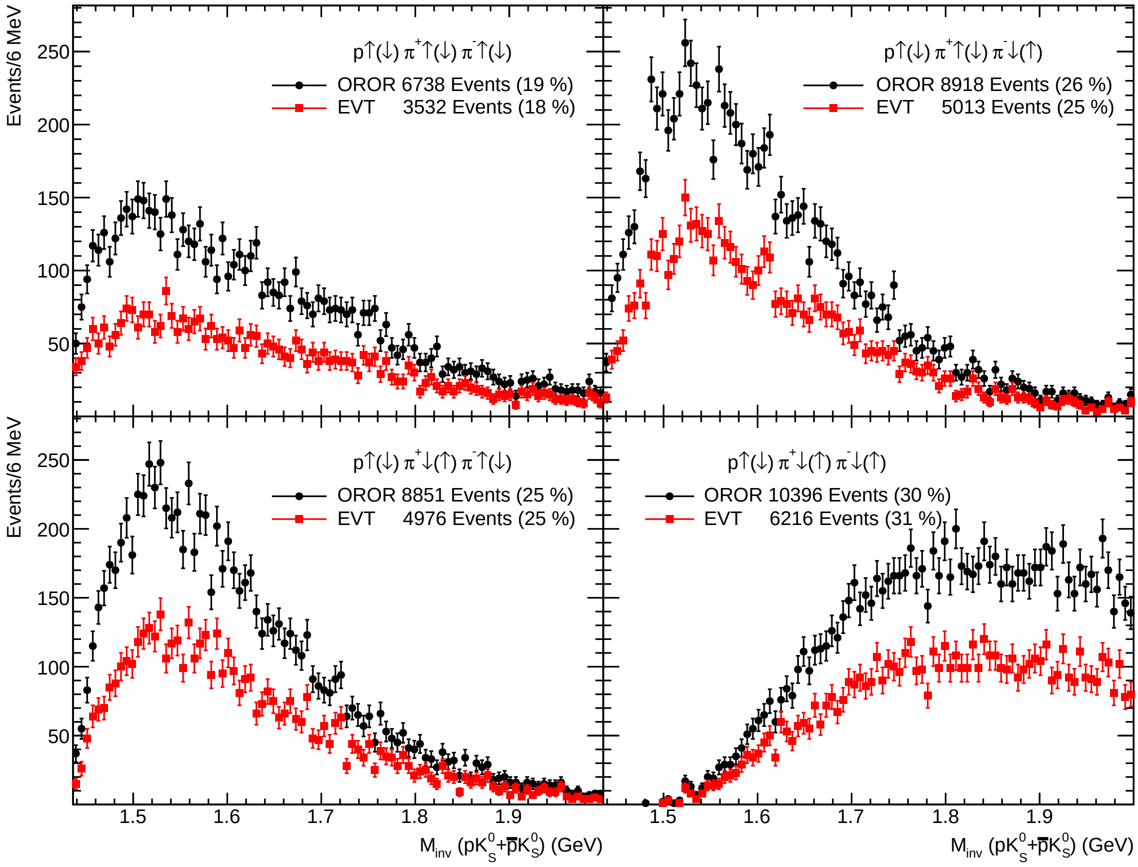

Figure 4.14: The $pK^0_S + \bar{p}K^0_S$ invariant mass for different event topologies with the OROR and EVT methods. The arrows next to the particle symbols indicate through which detector half the reconstructed track passed. E.g. the upper left panel shows events where all three tracks needed for the reconstruction passed through the same detector half (upper or lower). The number in parenthesis is the fraction of total entries in that panel. The Z^* selection for the K^0_S and the subsequent cuts following this philosophy, have been applied.

Figure 4.14 contains two important messages. One is that the Θ^+ signal in all topology configurations is unfortunately located at the maximum or close the onset of the background. The possibility of producing a fake signal by adding four different background shapes produced by the acceptance of the detector has been tested by fitting all four spectra separately and adding their probability distribution functions. No fake bumps or discontinuities have been obtained. The second important message concerns the PID methods. Table 4.2 has shown that the Λ signal yield increased $\sim$ 13 % with the OROR method compared to EVT. For the proton identification in the $pK^0_S + \bar{p}K^0_S$-channel the increase in total statistics with the OROR method is $\sim$ 77 %, ranging from $\sim$ 90 % in the upper left panel to $\sim$ 67 % in the lower right panel. Comparing OROR to the IRT method, the increase in statistics is $\sim$ 41 % for the $pK^0_S + \bar{p}K^0_S$-channel and $\sim$ 33 % for the $p\pi^- + \bar{p}\pi^+$-channel.

OROR yields $\sim$ 134 % and $\sim$ 11 % statistics compared to the DRT method in the $pK^0_S + \bar{p}K^0_S$-channel and in the $p\pi^- + \bar{p}\pi^+$-channel respectively. The ineffectiveness of the DRT and EVT methods in this particular channel has not been understood. A possible explanation might me, that the MC simulation or the likelihoods which are the same for both DRT and EVT were tuned for protons from a Λ-decay, e.g. by cuts to a certain kinematic phase space. Protons from other regions of the phase space would then be treated differently, which could subsequently lead to the observed inefficiency.
A study of protons being the only track[1] in one detector half has been carried out as well, yielding qualitatively the same result.

4.3.1.3 The Proton-Beam Vertex Probability

The proton-beam vertex probability prob($\mathbf{V}_{pB}$) is the probability from a χ^2 fit in the tracking routine of the crossing of the proton track candidate with the beam. This is taken as the probability that the proton candidate stems from the interaction point. A Θ^+ decays in less than 10^{-21} s, corresponding to $c\tau \approx 0.3$ pm, if $\Gamma_\Theta \approx 0.6$ MeV. Therefore the production and decay vertices are not distinguishable for the detector. The proton-beam vertex probability has been tested in a different way for the Z^* and P^* samples. In this work, the negative decimal logarithm of the proton-beam vertex probability $-\log\left(\text{prob}(\mathbf{V}_{pB})\right)$ is used.
In the case of the Z^* sample $-\log\left(\text{prob}(\mathbf{V}_{pB})\right)$ is compared to $-\log\left(\text{prob}(\mathbf{V}_{\pi B})\right)$ in a scan of Z by the reconstruction of charged $K^*(892) \to \pi K^0_S$ mesons. Figure 4.15(a) shows a fit to the $\pi^+K^0_S + \pi^-K^0_S$ invariant mass where the $K^*(892)$ signal region was taken within the vertical lines to calculate Z. The signal region is defined by $\left[M_{K^*} - \frac{\Gamma_{K^*}}{\sqrt{2\ln 2}}, M_{K^*} + \frac{\Gamma_{K^*}}{\sqrt{2\ln 2}}\right]$ with M_{K^*} being the $K^*(892)$ mass determined by the fit. The interval corresponds to a 2σ window when the relationship between the full width at half maximum and the standard deviation $\sigma = \frac{\Gamma}{2\sqrt{2\ln 2}}$ is used.

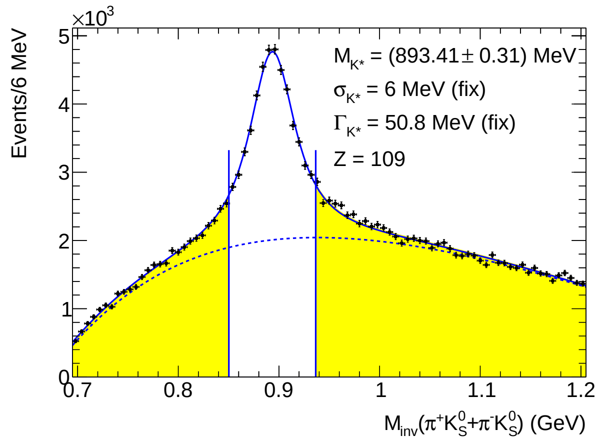

(a)

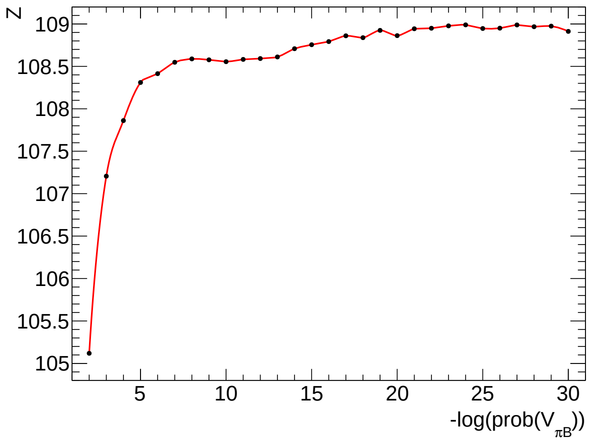

(b)

Figure 4.15: (a) Fit to the $\pi^+K^0_S + \pi^-K^0_S$ invariant mass. The fit parametrization is described in the text.
(b) Fit Results of the in $-\log\left(\text{prob}(\mathbf{V}_{\pi B})\right)$ scanned naive significance for $K^*(892)$s from the Z^* sample with the OROR method applied to the selection of the third pion (i.e. the π from the beam).

[1]The protons in the lower right panel of figure 4.14 could be accompanied by an additional track.

The fit function is defined by

$$f(M_{\text{inv}};\nu) = N_{\text{Bkg}} \left\{ \left[\left(1 - e^{-\frac{M_{\text{inv}}-m_0}{c}}\right) \left(\frac{M_{\text{inv}}}{m_0}\right)^a + b\left(\frac{M_{\text{inv}}}{m_0} - 1\right) \right] H(M_{\text{inv}} - m_0) \right\}$$
$$+ N_{K^*} \left\{ \int \frac{1}{\sqrt{2\pi\sigma_{K^*}^2}} e^{-\frac{\left(\tilde{M}-M_{K^*}\right)^2}{2\sigma_{K^*}^2}} \cdot \frac{1}{2\pi} \frac{\Gamma_{K^*}}{\left(M_{\text{inv}} - \tilde{M} - M_{K^*}\right)^2 + \frac{1}{4}\Gamma_{K^*}^2} \, \mathrm{d}\tilde{M} \right\} , \tag{4.2}$$

where $H(\bullet)$ is the HEAVISIDE-function and ν the set of free parameters. The model is thus composed of the $D^* - D^0$ background function, implemented in RooFit, and a Voigtian distribution for the $K^*(892)$ signal. The background function is a modified WEIBULL-distribution, modified to parametrize the $D^* - D^0$ background empirically. The Voigtian is a BREIT-WIGNER-distribution convoluted with a Gaussian, describing the natural line shape of the $K^*(892)$ signal, smeared with the Gaussian detector resolution. The fits were carried out as unbinned EML fits, where the width was fixed to the PDG value $\Gamma_{K^*} = 50.8$ MeV and the detector resolution was fixed to 6 MeV.
Since figure 4.15(b) shows no evident maximum, a cut on $-\log\left(\text{prob}(\mathbf{V}_{p\text{B}})\right)$ is dismissed from the Θ^+ reconstruction with the Z^* logic. The kinks in the scan profile can be understood by the complexity of the fit and its statistical uncertainty as well as binning effects in $-\log\left(\text{prob}(\mathbf{V}_{\pi\text{B}})\right)$. This scan has simultaneously been performed with the EVT plus Z^* K_S^0 sample, yielding the same result.

In June 2013 the HERMES group at Beijing found that a cut on $-\log\left(\text{prob}(\mathbf{V}_{p\text{B}})\right)$ reduces the background contamination from (partly reconstructible) Λ decays [148]. Since the P^* logic aims for a more careful analysis, the removal of the $-\log\left(\text{prob}(\mathbf{V}_{p\text{B}})\right)$ cut has to be studied in more detail. The idea is to compare Λs from the $\Sigma(1385)$ P^* sample (c.f. paragraph 4.3.3 and appendix A) in the signal and sideband region to relatively pure $\Lambda(1520)$s from the signal region shown in figure 4.16(a). The majority of Λs decay at a displaced vertex, and the distribution of the proton-beam vertex probability for protons from the Λ decay should thus be concentrated at lower values. The $\Lambda(1520)$ decays under the strong interaction to pK^- and therefore provides a sample where the proton-beam vertex probability should be concentrated at high values. The Λ sidebands ([1095, 1105] MeV and [1125, 1135] MeV) are thought of as background with no clear signature ranging between the two other distributions. Cuts for the $\Lambda(1520)$ sample are summarized in appendix A and were chosen in a subjective manner aiming for high signal purity. The $\Lambda(1520)$ fit function and signal region are chosen in the same manner described above for the $K^*(892)$. The result of this study is shown in figure 4.16(b), where the distribution of $-\log\left(\text{prob}(\mathbf{V}_{p\text{B}})\right)$ behaves as expected for the three samples and where a cut of $-\log\left(\text{prob}(\mathbf{V}_{p\text{B}})\right) < 1.2$ was derived for the P^* sample. The cut was chosen as the value below which the samples (particularly the Λ signal region and the $\Lambda(1520)$) are separable.
Despite the fixed cut value of $-\log\left(\text{prob}(\mathbf{V}_{p\text{B}})\right) < 1.2$ for the P^* sample – e.g. 0.8 or 1.7 could arguably be used instead – the "right" method (Z^* or P^*) to use for this cut is disputable. The main argument of using a tight cut on $-\log\left(\text{prob}(\mathbf{V}_{p\text{B}})\right)$ in [148] was the background contamination from (partly reconstructible) Λ decays. In addition to the effectiveness of the cut, the question arises what the impact of protons from Λ decays have on the pK_S^0 spectrum. If they do not produce fake peaks in the signal region of the hypothetical Θ^+ and if the structure in the pK_S^0-channel is real, both Z^* and P^* should yield statistically the same result. I.e. the observed number of Θ^+ candidates scaled with the total entries in the Z^* and P^* samples are approximately the same.

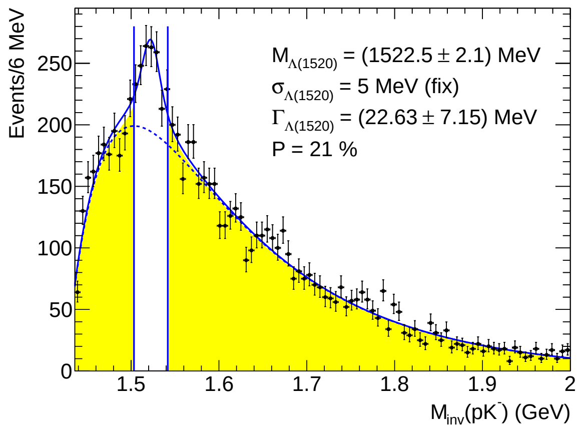

(a)

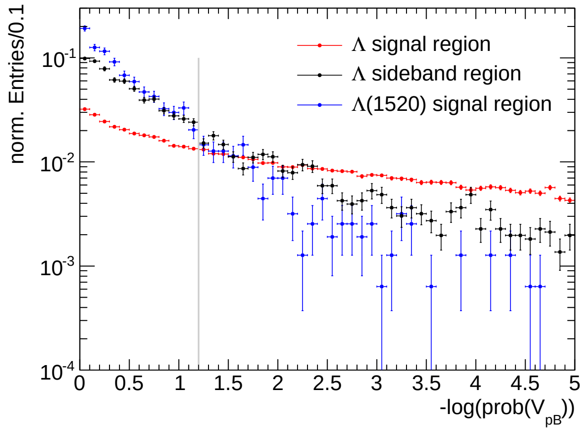

(b)

Figure 4.16: (a) Fit to the pK^- invariant mass. The fit parametrization is described in the text. (b) Normalized distributions of $-\log\left(\text{prob}(\mathbf{V}_{pB})\right)$ for the Λ signal and sideband region and the $\Lambda(1520)$ signal region. The cut for the Θ^+ P^* selection is marked by the gray line.

4.3.1.4 Background Contamination from Other Decays

This paragraph gives more insight to the possible contamination of the pK^0_S spectrum from Λ decays where the proton candidate is involved, and $K^*(892)$ decays where a pion was misidentified as proton. A different Λ-veto has already been discussed in section 4.2.1. There, the Λ was reconstructed from π candidates where no PID information was required. Here the situation is different and can be understood easiest by a look on figure 4.10. Since there is a certain amount of background in the final K^0_S selection, it is clear that some pion candidates do not originate from a K^0_S decay. If these pions come from a Λ decay instead, a peak in the $p\pi$ invariant mass, where p is the proton candidate for the Θ^+ selection, should be seen (c.f. fig. 4.17(a)). If this peak is visible, an additional Λ veto has to be applied in the selection chain. It is then important to check if the reflection from these Λs produces fake bumps or discontinuities in the pK^0_S spectrum (c.f. fig. 4.17(b)). Figure 4.17(a) shows a Λ contamination in the Z^* sample and no contamination in the P^* sample. As a consequence, an additional Λ veto, removing the 762 events in the upper panel of figure 4.17(b) is applied in the Z^* selection.

The reflection from Λs in the upper panel of figure 4.17(b) exhibits a rather smooth background structure with steeper slopes than those observed for the $pK^0_S + \bar{p}K^0_S$ (c.f. 4.14) or pK^- (c.f. 4.16(a)) backgrounds. The maximum of that distribution in pK-channels is at $\approx$ 1470 MeV and becomes visible if certain kinematic cuts are applied. The trickiest part here certainly is to anticipate or extrapolate, what the effect of proton candidates from not reconstructible Λ decays on the final pK^0_S spectrum would be. Not reconstructible means in this case, that the pion track from the Λ decay was not detected. If undetected pions from a different kinematic region, i.e. not from the K^0_S signal region, form Λs with the Θ^+ p candidates, the reflection in the pK^0_S invariant mass will be broadened. This is due to the kinematic correlation of $M_{\text{inv}}(pK^0_S)$ and $M_{\text{inv}}(\pi^+\pi^-)$. Hence the formation of a narrow peak at ~1520 MeV due to the kinematic reflection of Λs is excluded.

The second possible contamination comes from pions which were misidentified as protons from the OROR or EVT method. A contamination is checked if the mass hypothesis for the proton candidate is reversed and set to the pion mass. All other cuts remain the same. Figure B.1 in the appendix shows no worrisome contamination from $K^*(892)$s, therefore no such cut will be applied subsequently.

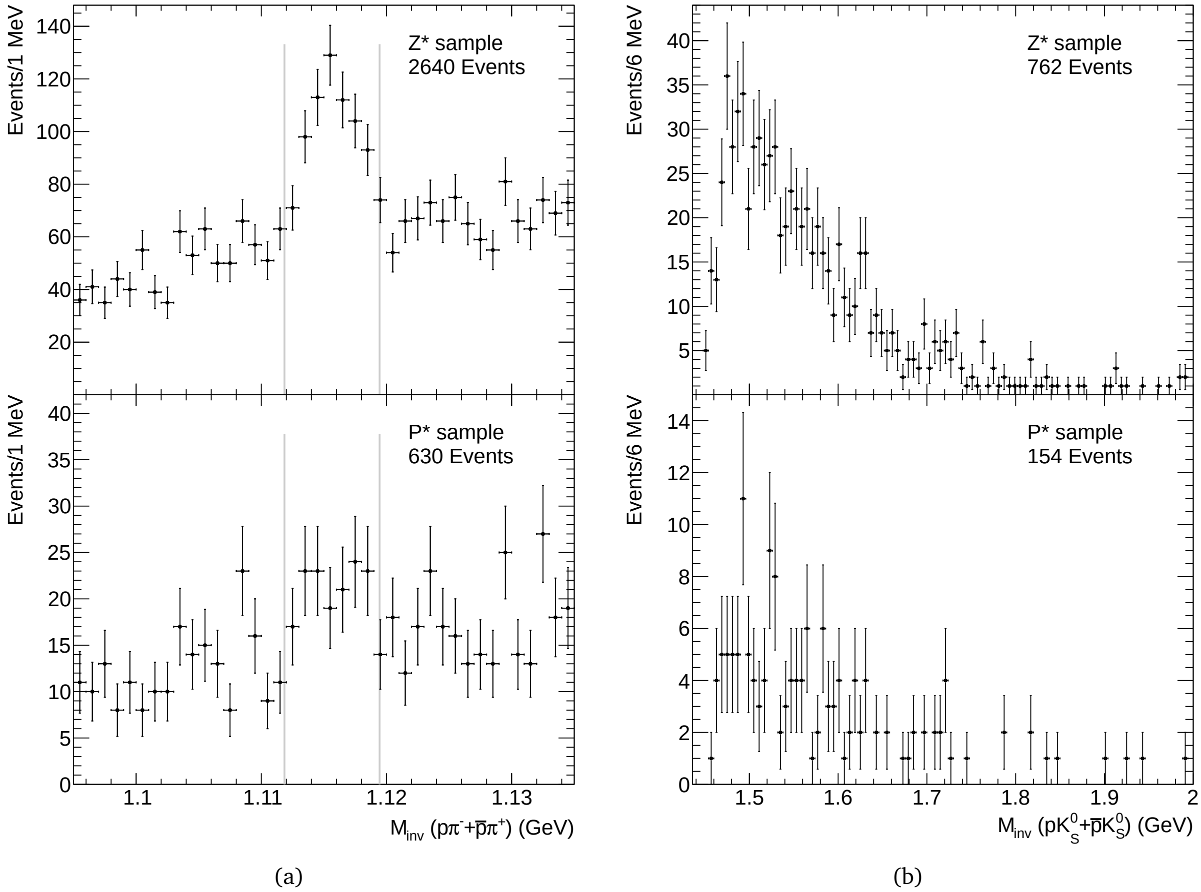

Figure 4.17: (a) $p\pi^- + \bar{p}\pi^+$ invariant mass distributions from from combinatorial background for the Z^* and P^* samples. (b) Reflections in the $pK^0_S + \bar{p}K^0_S$-channel of events within the Λ signal region, illustrated by the gray line. All final cuts except the second Λ veto in the Z^* case have been applied.

4.3.1.5 Angular Correlations and Event Topologies II

In June 2013 the HERMES group at Beijing claimed a correlation between the intensity of the hypothetical Θ^+ peak and an angle θ [149]. θ is the angle between the momentum of the pK^0_S system and the beam direction (taken as $\mathbf{e}_z$ for simplicity) in the lab frame. This dependence is not reproducible with modified Z^* cuts and was initially considered as Λ reflection [150]. In [148] the hypothesis that the dependence is a Λ reflection was proven wrong and the θ dependence could be reproduced with the P^* selection. Nevertheless, questions why the signal yield does not systematically increase with smaller angles[1] and why the correlation is not seen in the Z^* sample remain. This paragraph provides additional perspectives in the study of this correlation.
The study of the pK^- invariant mass for finding a suiting cut on $-\log\left(\mathrm{prob}(\mathbf{V}_{p\mathrm{B}})\right)$ for the P^* selection (c.f. 4.3.1.3) revealed that the reconstruction of $\Lambda(1520)$s strongly depends on the event topology, discussed in paragraph 4.3.1.2 for the $p\pi$- and pK^0_S-channels.

[1]A by-eye interpolation of the $\theta < 1.5°$ spectra shown in [148,149], supported by the $M_{\mathrm{inv}}(pK^0_S)$-θ correlation plots in [150].

The pK^- spectrum shown in figure 4.16(a) is subject to a event topology cut, selecting protons and kaons which were reconstructed in the same detector half. The right panel of figure 4.18 shows the contrary selection. A distinct correlation between θ and the event topology for the $\Lambda(1520)$ is observed by comparing left and right panel of figure 4.18. But the intensity of the $\Lambda(1520)$ does not depend on θ, once the topology is fixed. This explains the correlation of the $\Lambda(1520)$ intensity and θ claimed in [148] as an acceptance effect due to the spectrometer geometry.

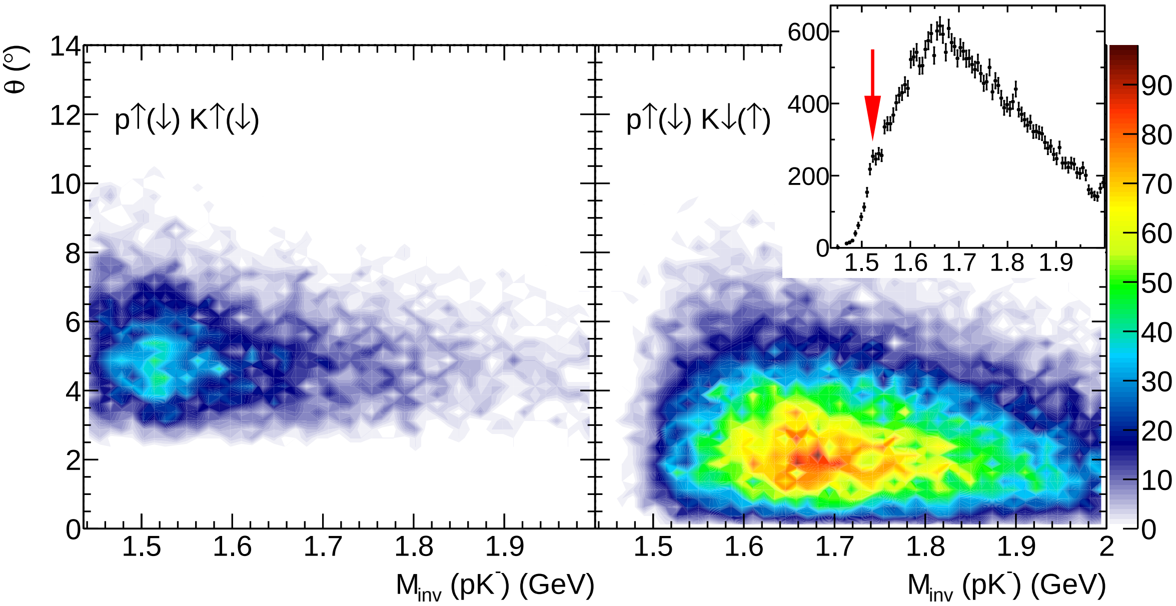

Figure 4.18: $M_{\text{inv}}(pK^-) - \theta$ correlation plots with different event topologies. The arrows next to the particle symbols indicate through which detector half the reconstructed track passed. The inset in the right panel shows the pK^- invariant mass for this topology. A red arrow points to the mass obtained by the fit the pK^- from the left panel (fig. 4.16(a)).

The correlation of $M_{\text{inv}}(pK^0_S)$, subject to the P^* selection, and θ is plotted in 4.19. Again no evident dependence of $M_{\text{inv}}(pK^0_S)$ on θ is observed, once the topology is fixed. Other angular correlations in the lab frame, namely the angle between $\mathbf{p}_p$ or $\mathbf{p}_{K^0_S}$ and $\mathbf{p}_{pK^0_S}$, and the opening angle between p and K^0_S have been tested with similar results.

It became evident that signal yields rather depend on their event topology – and therefore acceptance effects – than on angles in the lab frame. On the other hand, if the observed bump in the pK^0_S-channel is real, it should not be worrisome if the signal only appears in certain topology configurations, because it was shown that the intensities of known resonances like the Λ and $\Lambda(1520)$ depend on their event topology, given the acceptance of the HERMES spectrometer. It is now tempting, but dangerous to some extent, to find a particular topology where a signal is most prominent. The decay of the hypothetical Θ^+ is, as those of Λ and $\Lambda(1520)$, a two-body decay. Hence, translating the observed topology dependence to the decay of the Θ^+, the p and K^0_S tracks should pass through the same detector half. But the intermediate K^0_S, decaying into two charged pions, complicates the situation. The topology has now been subdivided into eight regions to account for the direction of the K^0_S momentum. These topologies are shown in figure 4.20(a). Two of these regions are by pairs equivalent and symmetric to the origin, e.g. the upper left (↓↑↑) and the lower right (↑↓↓). These regions correspond to some extend to the division of topologies in paragraph 4.3.1.2. In the middle regions the ↑↑↓ (↓↓↑) and ↑↓↑ (↓↑↓) configurations mix and are rearranged by a division into regions where the leading pion (in y-direction) and the proton hit the same detector half, and where the leading pion is separated from the proton and the other pion. There is some overlap of the classifications in the area close to the dashed gray line. The arrows can therefore be seen as indication that the region is mainly populated by this configuration, but not exclusively.

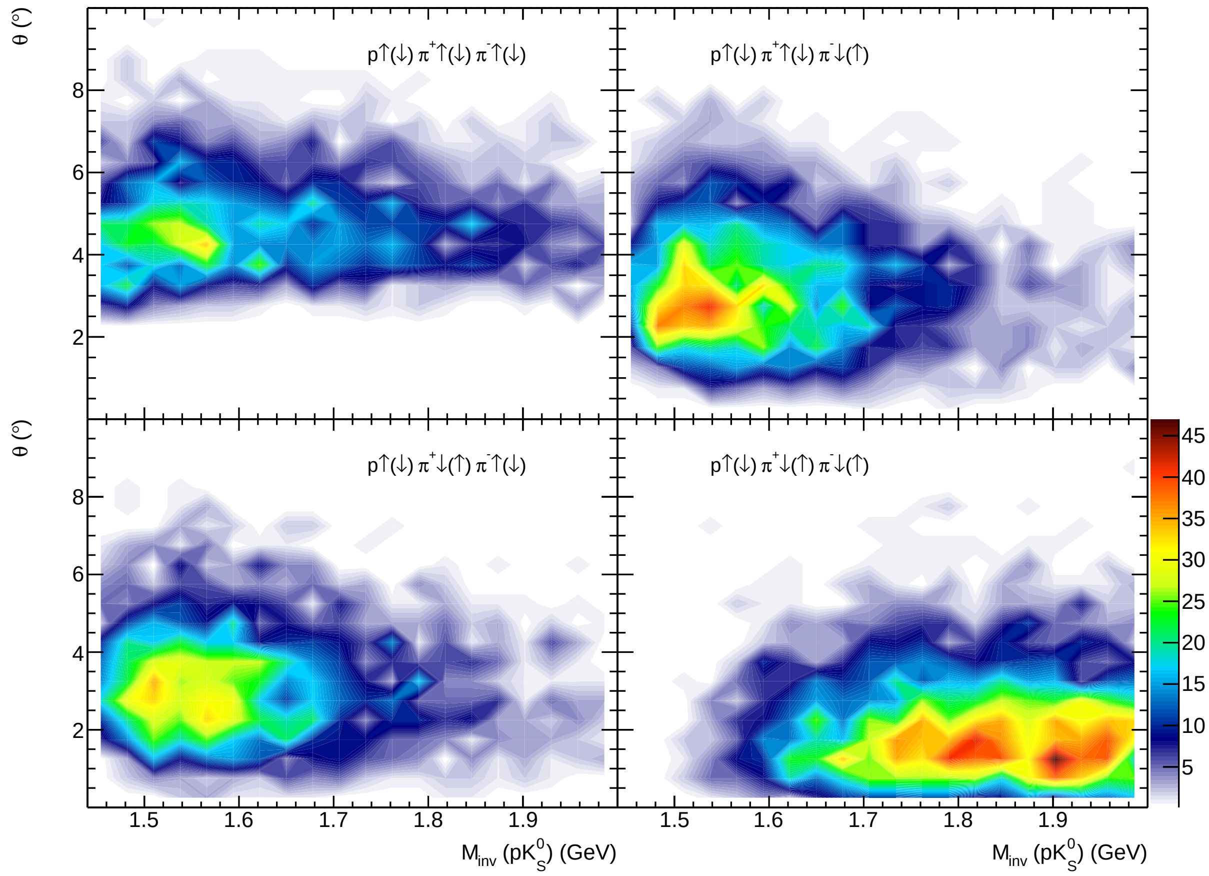

Figure 4.19: $M_{\text{inv}}(pK^0_S) - \theta$ correlation plots with different event topologies obtained with the P^* logic. The arrows next to the particle symbols indicate through which detector half the reconstructed track passed.

A narrow peak in the pK^0_S invariant mass is observed for the configuration where the leading particle of the K^0_S decay passed through a different half of the detector than both other tracks, marked by the arrows in red. Figure 4.20(b) was obtained by a cut on the $p_{K^0_S,y}$ value (0.23 GeV) , and not by selecting the corresponding configuration. The peak has been tested by loosen and tighten the essential cuts for the final selection, such as the proton PID, the proton-beam vertex probability, contamination of Λs and the coplanarity angle. It was observed that the signal to background ratio systematically dropped by choosing tighter cuts on these parameters, suggesting that the signal is real.
Several checks whether the peak is real have been carried out, but nothing pointing towards an systematic artifact has been found. A similar signal could not be observed in hydrogen data. A Monte Carlo study testing the kinematic properties of a narrow peak at 1520 MeV has been done. 50 runs, corresponding to 5.65 million (signal) events, were simulated with the HERMES-MC engine (decayMC with Ξ(1530) parameters from PYTHIA). The outcome of this study is plotted in figure 4.21(a). It is

seen that the area in the $p_{p,y}$-$p_{K^0_S,y}$ plane is limited due to the kinematics of a hypothetical signal. This limitation can be approximated by a first order polynomial above (below) which a signal would be located if the proton was detected in the upper (lower) part of the detector. Figure 4.21(a) also shows that most of the signal events should be located in the region where the peak was seen in figure 4.20(b). Nevertheless, the MC-study also shows that a selection of topologies is a masked cut on the kinematic itself, and thus disputable. In addition, the MC sample provided relatively narrow distributions, e.g. in the opening angle between p and K^0_S momenta and other kinematic variables. A cut on those quantities would reduce the background as well, but it is known that a selection of kinematic properties is susceptible to the production of fake signal peaks. Similar problems have been disputed by members of the CLAS collaboration in 2011/12. A part of the group found a narrow peak, associated with the Θ^+, in a distinct region of the kinematic phase space [97]. In a comment on that observation [98], the other part of the collaboration questioned the motivation for the kinematic cuts used in the analysis.

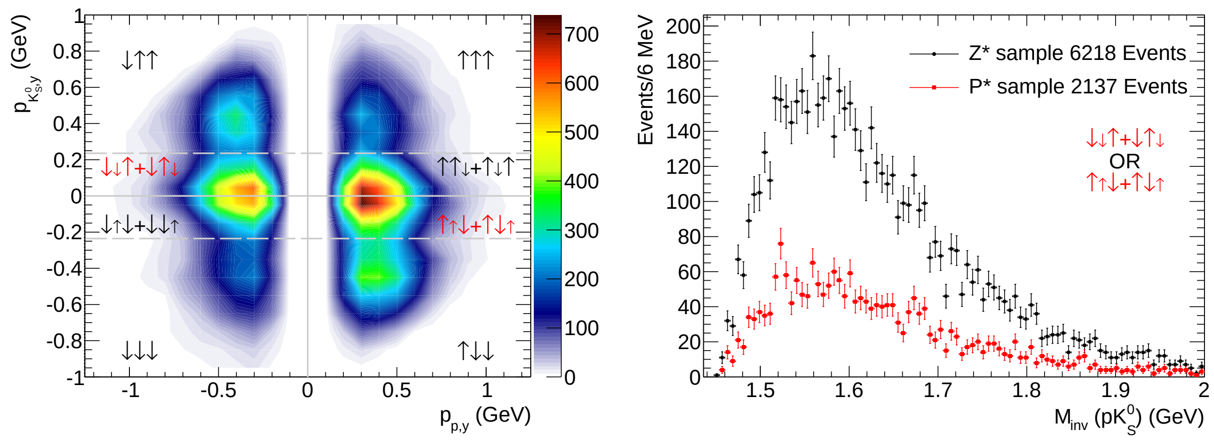

(a) (b)

Figure 4.20: (a) Correlation between momenta of p and K^0_S in y-direction. New event topologies, taking the direction of the K^0_S momentum into account are indicated by the arrows and separated by the gray lines. The first arrow marks the direction of the proton, the second of the π^+ and the third marks the direction of the π^-. Smaller arrows indicate which of the pions had lower momentum in y-direction. The plot was created with the Z^* sample. (b) $M_{\text{inv}}(pK^0_S)$ spectrum for the Z^* and P^* sample on deuterium for the topology where the leading particle of the K^0_S decay passed through a different half of the detector than both other tracks.

In addition, the MC sample also gives insight to the hypothesized correlation between θ and the Θ^+ yield from the kinematic point of view. Figure 4.21(b) shows the comparison between the MC simulation with P^* cuts and the P^* data, where only minor differences are observed. If the claimed dependence, where the Θ^+ yield increases with lower θ would be real, then this would hint towards exceptional properties of the particle rather than a kinematic property. In addition, the production mechanism is not regarded by MC. To account for baryon number- and strangeness- conservation, at least an additional Λ must be produced. Therefore less energy for the Θ^+ is available in the center of mass system, shifting the MC data to higher θ angles.

In conclusion, neither a θ cut nor a event topology cut should be used since both select regions of the kinematic phase space which are susceptible to artificial suppression of the background. However, the signal obtained with those selections is robust against $-\log\left(\text{prob}(\mathbf{V}_{pB})\right)$ and φ cuts.

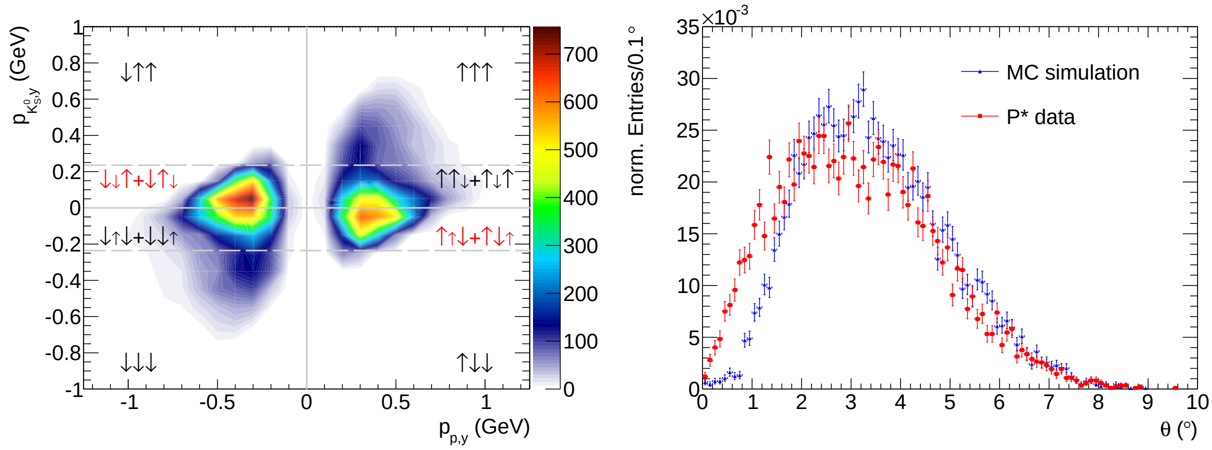

(a) (b)

Figure 4.21: (a) Correlation between momenta of p and K^0_S in y-direction. Lines and arrows as in fig. 4.20(a). The plot was created with the Monte Carlo sample described in the text, using Z^* cuts. (b) Normalized θ distribution of signal events from MC and data, using P^* cuts.

4.3.2 Statistical Analysis and Discussion of Systematic Uncertainties

The statistical analysis of the final pK^0_S spectra has been prepared in [151]. In addition to the methods presented there, the hypothesis test inversion using the asymptotic formulae for likelihood-based tests [152] and the CL$_s$ technique [153] are employed to quantify the sensitivity of the experiment statistically and to calculate upper limits on the number of signal events N_Θ - the parameter of interest in this analysis.

Two different empirical background models are used in the analysis, because the signal yield depends on the parametrization of the background. In addition, the models provide another systematic check. The reason why empirical models are used is, that there was no ready-to-use physical Monte Carlo model available, which involved KN scattering for the HERMES environment. The used models are the $D^* - D^0$ background (c.f. eq. (4.2)) in the $M_{\text{inv}}(pK^0_S)$ range from 1436 to 2000 MeV and a 3$^{\text{rd}}$ order CHEBYSHEV polynomial in the range from 1460 to 1592 MeV, used in [141]. The signal was parametrized as a Gaussian with a fixed resolution of 6 MeV, corresponding approximately to the detector resolution in that mass range of the pK^0_S-channel [144]. The convergence of the fits was checked automatically and manually by assuring that no parameter approached its limits, and by examining the correlation matrix as well as residual and pull distributions from the fit. In the case of hydrogen, the signal position parameter was limited to the obtained mass from the fit to the deuterium spectra plus two times the asymmetric error from the `MINOS` routine of ROOT. Hence for hydrogen, the signal position was allowed to approach its limitation. The number of signal events was restricted to be positive for the fitting and the calculation of p values. To account for downward background fluctuations, the restriction on the number of signal events was abrogated for the calculation of CL$_s$ limits and the Bayesian technique described later. The fits to the final Z^* $M_{\text{inv}}(pK^0_S + \bar{p}K^0_S)$ and P^* $M_{\text{inv}}(pK^0_S)$ spectra are plotted in figure 4.22 and the corresponding inverse Z^* $M_{\text{inv}}(pK^0_S)$ and P^* $M_{\text{inv}}(pK^0_S + \bar{p}K^0_S)$ spectra are shown in figure B.2 in the appendix.

The fits on deuterium data exhibit a narrow bump, whereas no peak seems to be present in hydrogen data. By visual impression the bump seems to be more pronounced in the P^* data, which is expected if the bump is real and no statistical fluctuation. If the charge conjugated channel is added, the number of signal events doubles in the Z^* case and increases by 22 % in the P^* case considering the $D^* - D^0$ fits. The latter is comparable to the particle over antiparticle ratio of the Ξ^- [154]. The doubling of N_Θ for the Z^* samples might be due to statistical fluctuations in the signal region; not only of the bump itself, but also of the region close to the bump. Other reasons for a relatively small particle over antiparticle ratio might be acceptance effects of the detector or a different rate of misidentified pions and kaons in the Z^* and P^* samples. In the analysis of the $\Lambda(1520)$ resonance, a reciprocal behavior was obtained, i.e. only a small $\overline{\Lambda}(1520)$ signal was seen. If the observed Θ^+ bump turns out to be real and its kinematical dependence follows the extracted pattern in paragraph 4.3.1.5, the different particle to antiparticle ratios could be explained in terms of detector acceptance, since the kinematic dependence of the $\Lambda(1520)(\overline{\Lambda}(1520))$ and the claimed $\Theta^+(\overline{\Theta}^-)$ are contrary. This might also apply to the $pK^0_S(\bar{p}K^0_S)$ and $pK^-(\bar{p}K^+)$ background production. These speculations could be subject to further investigations.

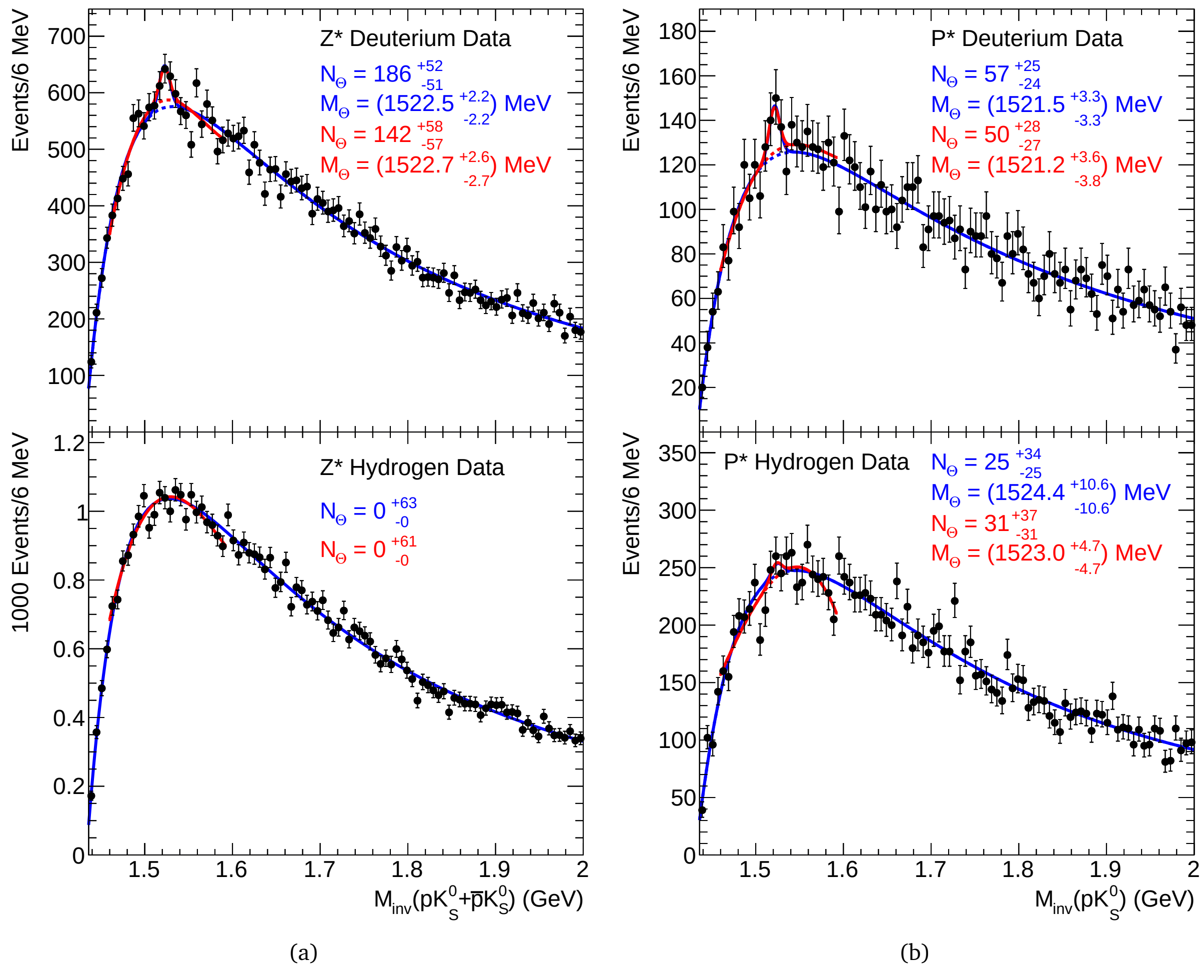

Figure 4.22: Fits to the final Z^* $M_{\text{inv}}(pK^0_S + \bar{p}K^0_S)$ (a) and P^* $M_{\text{inv}}(pK^0_S)$ spectra (b) with the RooFit `RooDstD0BG` (blue line and blue parameters) and 3rd order CHEBYSHEV polynomial (red line and red parameters) as background model. The indicated errors correspond to asymmetric 1σ intervals from the `MINOS` fitting routine.

The lower errors from MINOS are not displayed by the routine if those would fall below the restriction of 0 signal events. Therefore the lower error is manually set such, that it reaches down to 0. The disadvantages of the 3rd order CHEBYSHEV polynomial as background model in a narrow range becomes explicitly apparent in the lower panel of figure 4.22(b). There, the slope of the background left from its maximum is rather moderate. This is mainly influenced by a dip at $\sim$ 1510 MeV. On the other side of the maximum, at $\sim$ 1580 MeV, the polynomial suggests a steep fall of the background. As a result, the signal events in the bump left from the maximum of the background appear to be overestimated. In all other cases, the curvature of the CHEBYSHEV polynomial background compared to the $D^* - D^0$ background is more pronounced in the signal region. The result is a lower number of signal events. On the other hand, the $D^* - D^0$ background behaves stiff and may underestimate discontinuities of the detector acceptance, but is considered superior to the CHEBYSHEV polynomial background, since it is able to describe the whole mass range reasonably well. The significances/upper limits of the signal with both background models will be tested in the following. The results of the CHEBYSHEV polynomial background will be shown in the appendix.
The estimation of the significance of the excess on deuterium and the computation of an upper limit on the number of signal events on hydrogen is done by a scan of the local p values and $\mathrm{CL_s}$ values along the pK^0_S invariant mass similar to [155, 156]. In [151] details of the application of the calculations and their implementation in RooStats were discussed. For the scan of local p values and $\mathrm{CL_s}$ values, the asymptotic formulae for likelihood-based tests [152] were used, with

$$q_0 = \begin{cases} -2\ln\lambda(0), & \hat{\mu} \geq 0 \\ 0, & \hat{\mu} \leq 0 \end{cases} \tag{4.3}$$

as test statistic for the p value scan and

$$q_\mu = \begin{cases} -2\ln\lambda(\mu), & \hat{\mu} \leq \mu \\ 0, & \hat{\mu} > \mu \end{cases} \tag{4.4}$$

as test statistic for the $\mathrm{CL_s}$ values. $\lambda(\mu) = \frac{L(\mu,\hat{\hat{\nu}})}{L(\hat{\mu},\hat{\nu})}$ is the profile likelihood ratio [152], with the parameter of interest μ and the nuisance parameters ν. In the search for the Θ^+, these parameters are $\mu = N_\Theta$ and $\nu = \{M_\Theta, a, b, c, m_0, N_{\mathrm{Bkg}}^{(D^*-D^0)}\}$ for the $D^* - D^0$ background (c.f. eq. (4.2)) and $\nu = \{M_\Theta, a, b, c, N_{\mathrm{Bkg}}^{(\mathrm{Chebyshev})}\}$ for the CHEBYSHEV polynomial background respectively.
In the scan for local p values a hypothesis test was made for every point in the mass range 1510-1550 MeV, where a Θ^+ signal is assumed. The case of $N_\Theta = 0$ is taken as null-hypothesis and the local p value is interpreted as probability that the signal is due to a fluctuation of the background. The $\mathrm{CL_s}$ technique was introduced as appropriate method when a search is performed, with the main advantage of conservative frequentist coverage. The $\mathrm{CL_s}$ limit for one mass point is obtained by the inversion of various hypothesis tests. I.e. the test statistics of null- and alternative hypotheses are evaluated for a given value of μ. In practice, a range of N_Θ was given to the RooStats calculator which was scanned. So for every point of the scan a hypothesis test, for a value of N_Θ given the Asimov data set of the null-hypothesis, was done. In this way the expected and observed upper limits were calculated. The following figures 4.23 and 4.24 show the result of the $\mathrm{CL_s}$ and p value scans on deuterium and hydrogen targets. The corresponding inverse charge selection Z^* $M_{\mathrm{inv}}(pK^0_S)$ and P^* $M_{\mathrm{inv}}(pK^0_S + \bar{p}K^0_S)$, and the results from the scans with the CHEBYSHEV polynomial background are shown in figures B.3 - B.8 in the appendix.

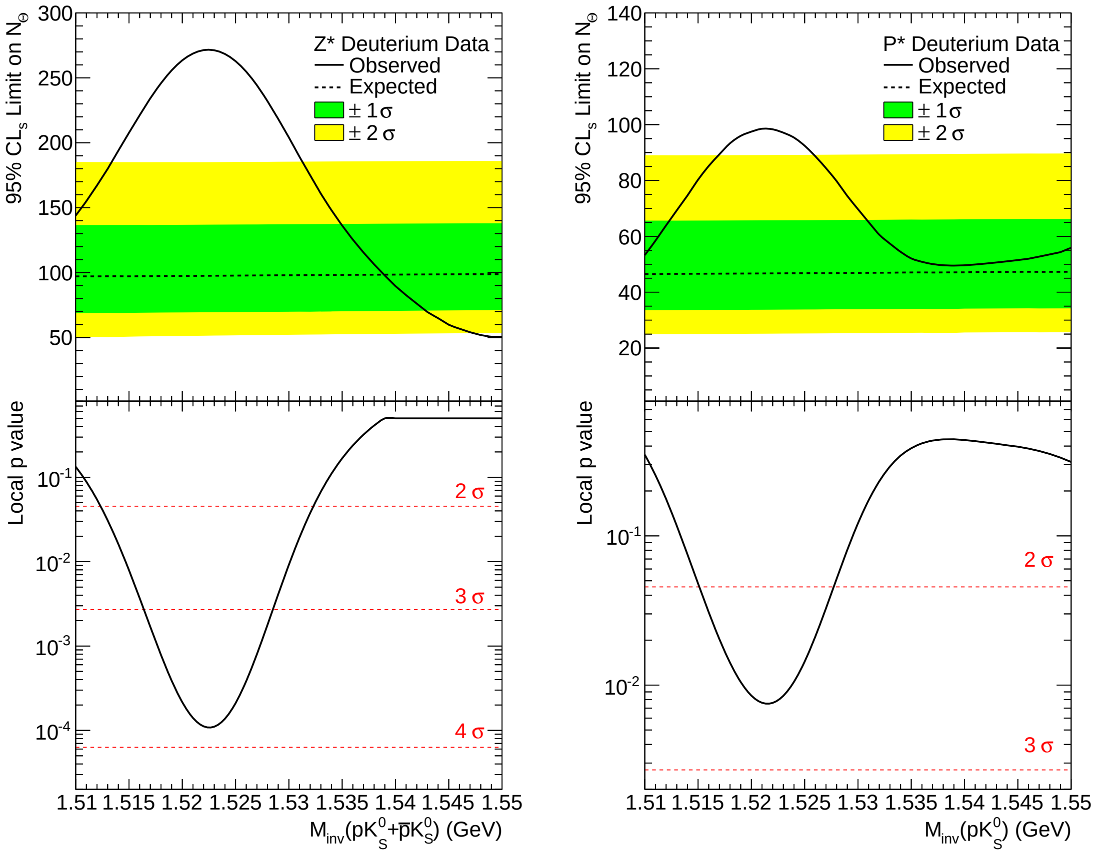

(a) (b)

Figure 4.23: The upper panels show the observed 95 % CL$_s$ limits on the number of signal events N_Θ as a function of $M_{\text{inv}}(pK^0_S)$ (solid line) and the expectation (dashed line) under the background only hypothesis ($N_\Theta = 0$) for the Z^* (a) and P^* (b) data on deuterium. The green and yellow bands show the $\pm1\sigma$ and $\pm2\sigma$ uncertainties on the background only expectation. The observed local p values are plotted in the lower panels.

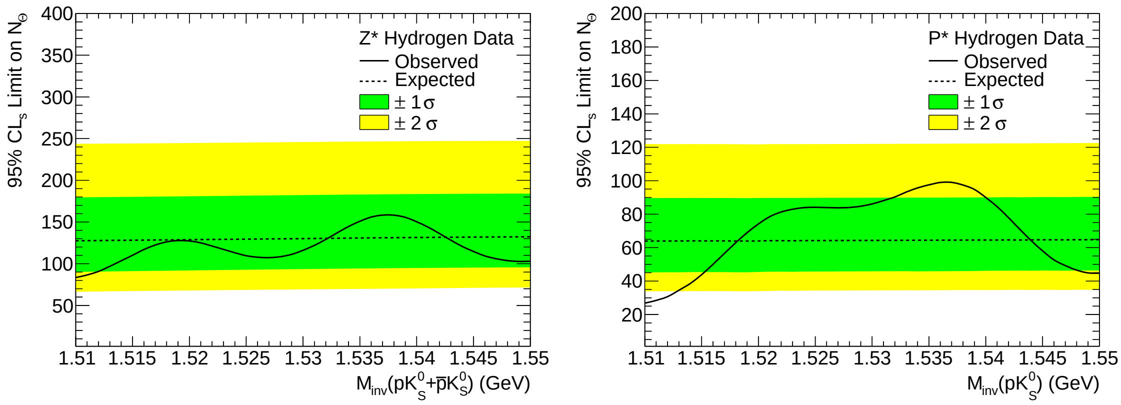

(a) (b)

Figure 4.24: Observed 95 % CL$_s$ limits on the number of signal events N_Θ as a function of $M_{\text{inv}}(pK^0_S)$ (solid line) and the expectation (dashed line) under the background only hypothesis ($N_\Theta = 0$) for the Z^* (a) and P^* (b) data on hydrogen. The green and yellow bands show the $\pm1\sigma$ and $\pm2\sigma$ uncertainties on the background only expectation.

Both deuterium data sets exhibit an excess of events at $M_{\text{inv}}(pK^0_S) \approx 1522$ MeV. Although the bump in the P^* data seemed to be more pronounced, its local significance is – because of the lower statistics – lower than that of the Z^* bump. The local and global significances from the scans on deuterium data and the upper limits on hydrogen are combined in table 4.3. An upper limit on hydrogen was calculated as the ratio

$$\mathcal{R} = \frac{e^{\pm}p \to (pK^0_S)X}{e^{\pm}d \to (pK^0_S)X} = \frac{N^p_{\Theta,\text{UL}}}{N^d_{\Theta,\text{obs}}} \frac{N^d_{pK^0_S}}{N^p_{pK^0_S}}, \tag{4.5}$$

where $N^p_{\Theta,\text{UL}}$ is the 95 % CL$_\text{s}$ limit of N_Θ on hydrogen, $N^d_{\Theta,\text{obs}}$ is the observed number of signal events on deuterium and $\frac{N^d_{pK^0_S}}{N^p_{pK^0_S}}$ is the fraction of total events in the sample from $[1.436, 2]$ GeV, which is assumed to be a valid approximation for the luminosity ratio taking a possible pK^0_S production cross section asymmetry into account. $N^p_{\Theta,\text{UL}}$ is obtained within the $2\,\sigma$ mass window from the deuterium fit. Thus the region outside that window were plotted just for illustration.

In the calculation of the CL$_\text{s}$ values, the signal was allowed to be negative. This is seen e.g. in figure 4.23(a) where the observed limit falls below the expected limit for $M_{\text{inv}}(pK^0_S) \gtrsim 1538$. It is disputable if a negative signal for an empirical background model makes sense or not. But dips would also be found in the case where a physical model (normalized to this data) is available. For the final results, only one upper limit on hydrogen, namely from the Z^* sample was observed below, but close to the expected limit. In this case, the expected upper limit is given in parenthesis in table 4.3.

In case of a significance above $2\,\sigma$, the look elsewhere effect [157] was applied. The idea behind that effect is, that the probability of finding a signal somewhere in the search region is greater than the probability if only one point in the search region is tested. In other words: if 100 distinguishable (by detector-resolution) points in the invariant mass are tested, a $2\,\sigma$ effect is expected to appear somewhere in the search region according to statistics. A rule of thumb has been empirically derived in [158], and is assumed to hold for a rather simple search like the one presented here. The global p value for significances $Z_{\text{local}} \gtrsim 2\,\sigma$ was calculated as

$$p_{\text{global}} = p_{\text{local}} \frac{Z_{\text{local}} \left(M_{\text{inv,max}} - M_{\text{inv,min}} \right)}{3\,\sigma_{\text{res}}} \tag{4.6}$$

where $M_{\text{inv,max}} - M_{\text{inv,min}}$ is the search range and σ_{res} the detector resolution. The fraction is the approximated trial factor.

		Deuterium Z_{local} (Z_{global})		Hydrogen 95 % upper limit on $\mathcal{R}$	
		$pK^0_S + \bar{p}K^0_S$	pK^0_S	$pK^0_S + \bar{p}K^0_S$	pK^0_S
Z^*	$D^* - D^0$	$3.7\,\sigma$ $(3.1\,\sigma)$	$2.2\,\sigma$ $(1.5\,\sigma)$	$0.39\,(0.39) \pm 0.11$	0.67 ± 0.32
	CHEBYSHEV	$2.5\,\sigma$ $(1.8\,\sigma)$	$1.4\,\sigma$	$0.55\,(0.60) \pm 0.22$	1.1 ± 0.8
P^*	$D^* - D^0$	$2.5\,\sigma$ $(1.9\,\sigma)$	$2.4\,\sigma$ $(1.7\,\sigma)$	0.80 ± 0.33	0.77 ± 0.34
	CHEBYSHEV	$1.7\,\sigma$	$1.9\,\sigma$	1.1 ± 0.7	1.0 ± 0.6

Table 4.3: Observed significances and upper limits on the ratio of signal events on hydrogen to deuterium $\mathcal{R}$ for all examined samples. The errors on $\mathcal{R}$ are statistical errors, coming from $N^d_{\Theta,\text{obs}}$ only.

Since no evident structure was observed in the hydrogen data, it could be used as background model. There are several ways to do this, from which two are presented in the following. The first method took the binned ratio of deuterium to hydrogen and fitted the background with a constant. The signal was again described by a Gaussian with a fixed width of 6 MeV. In this approach, systematic effects, like the observed inefficiency of proton detection in the pK^0_S-channel by the EVT and DRT methods or background models of the fit effectively cancel. This is confirmed by the fact that the ratio plot, shown in figures 4.25 and B.9, is statistically consistent with a constant outside region of the Θ^+ bump.

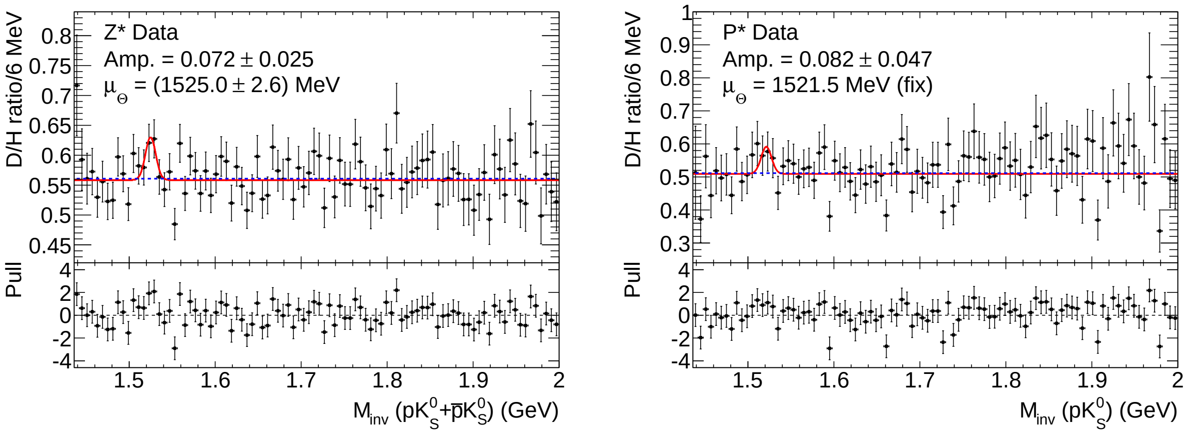

(a) (b)

Figure 4.25: Deuterium to Hydrogen ratio for the Z^* (a) and P^* (b) samples. The ratio was fitted with the sum of a Gaussian signal and a constant background (red solid line) as signal plus background model and a constant (blue dashed line) as background only model. In the lower panels the pulls from the background only fit were plotted.

The mass parameter of the P^* pK^0_S sample had to be fixed to its fit value from the $D^* - D^0$ background model fit to deuterium. Because the dip at ≈ 1515 MeV in the hydrogen spectra (c.f. fig. 4.22(b)) produced an excess in the ratio that would have been considered as the hypothesized Θ^+ by the fit. This shows, that the ratio is to some extend sensitive to statistical fluctuations of the data. If the background fit to hydrogen is considered as the true distribution in the limit of infinite statistics, then the Z^* hydrogen data fluctuates downwards in the signal region, whereas the P^* data fluctuates upwards. The outcome is an enhanced signal in the Z^* case and a small signal in the P^* data. If the hydrogen data is not regarded as background, but the ratio is considered a test of how compatible the hydrogen and deuterium data are, these problems vanish. The degree of compatibility could be expressed as a $\mathrm{CL_s}$ limit, for which the RooStats tools would be needed. Unfortunately a sophisticated statistical analysis of the fits to the deuterium to hydrogen ratio is complicated, since the RooStats macros used in this analysis usually run unbinned data sets or histograms with integer bin content. A simple approximation to obtain the corresponding $\mathrm{CL_s}$ limit is discussed for the next method. The significance of the bump on deuterium with hydrogen as a background model in the ratio plots can naively be expressed as ratio of the signal amplitude to its error. The naive significances are then $2.9\,\sigma$, $1.7\,\sigma$, $1.6\,\sigma$ and $1.3\,\sigma$ for the Z^* $pK^0_S + \bar{p}K^0_S$, P^* pK^0_S, Z^* pK^0_S and P^* $pK^0_S + \bar{p}K^0_S$ samples respectively.
The other way of testing the hydrogen data as a background model is a p value calculation from Bayesian posterior distributions, prepared in [151]. The posterior distributions were obtained by the Markov-chain-Monte-Carlo technique, using the Metropolis-Hastings algorithm [159] to perform a random walk in the space spanned by the fit parameters.

In order to get good results from that method – i.e. an acceptance rate close to the asymptotically optimal acceptance rate of 0.234 [160] – the fit parameters had to be restricted to a reasonable interval. For this work $3\,\sigma$ intervals for every nuisance parameter of the $D^* - D^0$ background was used. It was found, that the acceptance rate of the METROPOLIS-HASTINGS algorithm was sensitive to the value of the peak position. Therefore that parameter was restricted to $\pm 2\,\sigma$ for deuterium and fixed to a $[1515.5, 1531.5]$ MeV interval for hydrogen. The parameter of interest was restricted to an approximate $5\,\sigma$ window. The results of this test are depicted in figures 4.26 and B.10.

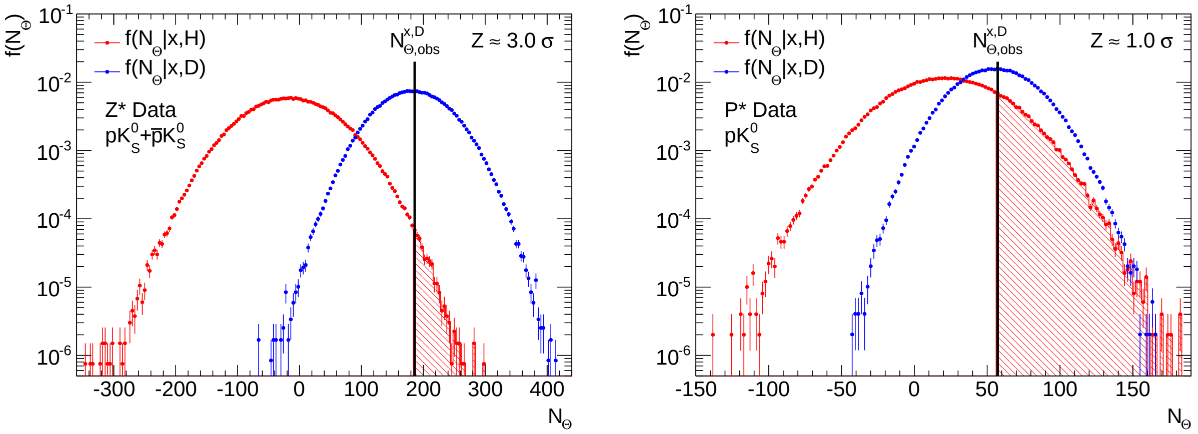

Figure 4.26: Posterior distributions of N_Θ from Z^* (a) and P^* (b) deuterium and hydrogen data. The observed value on deuterium is marked by the solid vertical line. The calculated p value corresponds to the hatched red area.

The resulting significances for the Bayesian test were $3.0\,\sigma$, $1.0\,\sigma$, $1.8\,\sigma$ and $1.0\,\sigma$ for the Z^* $pK^0_S+\bar{p}K^0_S$, P^* pK^0_S, Z^* pK^0_S and P^* $pK^0_S+\bar{p}K^0_S$ samples respectively. Hence the Bayesian analysis of the Z^* samples overshoot the naive significances of the fits to the deuterium to hydrogen ratio by $0.1\,\sigma$ for $pK^0_S+\bar{p}K^0_S$ and $0.2\,\sigma$ for pK^0_S. For the P^* samples a reciprocal behavior is observed. The Bayesian method gives much lower significances and undershoots the P^* pK^0_S samples by $0.7\,\sigma$ and the P^* $pK^0_S+\bar{p}K^0_S$ by $0.3\,\sigma$. Thus the Bayesian method is even more sensitive to the assumed downward (upward) fluctuation in the Z^* (P^*) data, which were discussed for the ratio plots.
To quantify the compatibility of the samples, rather than taking hydrogen as background model, a Bayesian equivalent to the $\mathrm{CL_s}$ limit can be computed from the obtained posterior distributions. From the definition of the limit in [153], the $\mathrm{CL_s}$ value is given by

$$\mathrm{CL}_{\mathrm{s,Bayes}} = \frac{\int_{N^{(x,D)}_{\Theta,\mathrm{obs}}}^{\infty} f\left(N_\Theta|x,H\right)\,\mathrm{d}N_\Theta}{1-\int_{-\infty}^{N^{(x,D)}_{\Theta,\mathrm{obs}}} f\left(N_\Theta|x,D\right)\,\mathrm{d}N_\Theta}\,. \tag{4.7}$$

Since $N^{(x,D)}_{\Theta,\mathrm{obs}}$ is approximately the median of the posterior $f\left(N_\Theta|x,D\right)$ and the integral in the numerator is the p value, which was used to calculate the significances, the $\mathrm{CL_s}$ value is simply $2p$. Inserting the observed p values, a minimal compatibility of 0.27 % for the Bayesian Z^* $pK^0_S+\bar{p}K^0_S$ sample and a maximal compatibility of 31 % for the Bayesian P^* $pK^0_S+\bar{p}K^0_S$ sample is found. Using the approximation for the ratio plots, a minimal compatibility of 0.4 % for the Z^* $pK^0_S+\bar{p}K^0_S$ sample and a maximal compatibility of 19 % for the Bayesian P^* $pK^0_S+\bar{p}K^0_S$ sample is found.

The statistical analysis showed that the extracted deuterium data sets are compatible among themselves. The same statement is valid for hydrogen data. A greater signal to background ratio was obtained for the P^* samples as it would be expected. The quantification of the expected increase of the purity for the P^* selection with respect to the Z^* sample would be highly speculative without proper MC techniques. Hence an approximation of the statistical uncertainty due to different selection criteria is dismissed.
The data collected off deuterium and hydrogen are incompatible to each other. The incompatibility is quantitatively not highly significant, although all studied samples show qualitatively the same behavior. This statement is weakened by taking correlations among the samples into account. It is important to note, that the 2004 published data [81] is compatible to the P^* pK^0_S selection if the different PID selection, the detector resolution, the different background shape and different cuts are taken into account. A proper quantification of systematic uncertainties is beyond the scope of this work, since a Monte Carlo model involving KN scattering at HERMES energies would have to be implemented into the HERMES MC environment. In addition, the production mechanism of a hypothetical Θ^+ is elusive and the involved couplings come with relatively large errors. The systematic uncertainties can thus only be approximated. From the measurements of the mass and width of other baryon resonances compared to the PDG values, an uncertainty of ≈ 3 MeV for the mass can be assumed. The systematic uncertainty for the signal strength is approximated by a comparison between the signal yields of the $D^* - D^0$ and Chebyshev fits. It was evaluated to be ≈ 20 % using the ratio of the standard deviation to the mean value of all four deuterium samples.
Considering that the spectra obtained from both philosophies exhibit a compatible signal, the Z^* selection should be chosen over the P^* selection. The reason is, that systematic artifacts due to selection criteria can be ruled out at high confidence with the above results in hands, and that a search requires high (and blindly optimized) statistics provided by the Z^* selection.
In summary, the global statistical significance of the deuterium data was calculated to be $3.1\,\sigma$. Accounting for the systematic uncertainties due to the background shape, the observed bump can be taken as a hint for a real resonance.

4.3.3 Search for a Non-Exotic Resonance in the $\Lambda\pi^+$-channel

The search for a resonance in the $\Lambda\pi^+$-channel is another systematic study, which needs the input of the statistical analysis of the pK^0_S-channel to determine if the observed bump on deuterium is an excited Σ resonance. The idea to test the strangeness of the signal and additional considerations were presented in [161]. There the final result was given in terms of a limit on the ratio of branching fractions

$$\mathcal{B} = \frac{\Gamma(\Theta^+ \to \Lambda\pi^+)}{\Gamma(\Theta^+ \to pK^0_S)} \Longrightarrow \mathcal{B}_{\mathrm{UL}} = \frac{N^{\Lambda\pi^+}_{\Theta,\mathrm{UL}}}{N^{pK^0_S}_{\Theta,\mathrm{obs}} \cdot \mathcal{A}} , \tag{4.8}$$

where $\mathcal{A} = \frac{A(\Theta^+\to\Lambda\pi^+)}{A(\Theta^+\to pK^0_S)}$ is the acceptance ratio from a toy model in the HERMES-MC engine used in paragraph 4.3.1.5. The search addressed only the Z^* $pK^0_S + \bar{p}K^0_S$ and P^* pK^0_S selections and their equivalents in the $\Lambda\pi^+$-channel.
The Z^* $\Lambda\pi^+$ sample was created with the optimized Λ cuts from paragraph 4.3.1.2 and by optimizing cuts on the $\Sigma(1385) \to \Lambda\pi^+$ signal yield. This was done by fixing the width and position of the $\Sigma(1385)$ was to its PDG value to ensure consistency among the yields of different selections. The final set of cuts for the Z^* sample is summarized in appendix A and the scan profile is shown in figure B.11(a). The P^* selection for Λs is similar to the P^* K^0_S selection, described in section 4.2.2.

The outcome is shown in figure B.11(b) and the P^* $\Lambda\pi^+$ cuts are summarized in appendix A. The pion beam vertex probability was set to 1.2 according to the proton beam vertex probability in pK^0_S-channel, derived in paragraph 4.3.1.3. The coplanarity angle was not considered further since the scan of the $\Sigma(1385)$ signal yield showed, that a cut on the coplanarity could not maximize the naive significance. Fits to the final Z^* $\Lambda\pi^+ + \overline{\Lambda}\pi^-$ and P^* $\Lambda\pi^+$ spectra on deuterium are shown in figure 4.27. No significant excess in the region of ~ 1520 MeV is visible. The detector resolution in fits for the optimization and also for the following $\mathrm{CL_s}$ scan was fixed to rounded values of fits to the $\Xi^- \to \Lambda\pi^-$ baryon obtained with similar selection criteria in [161].

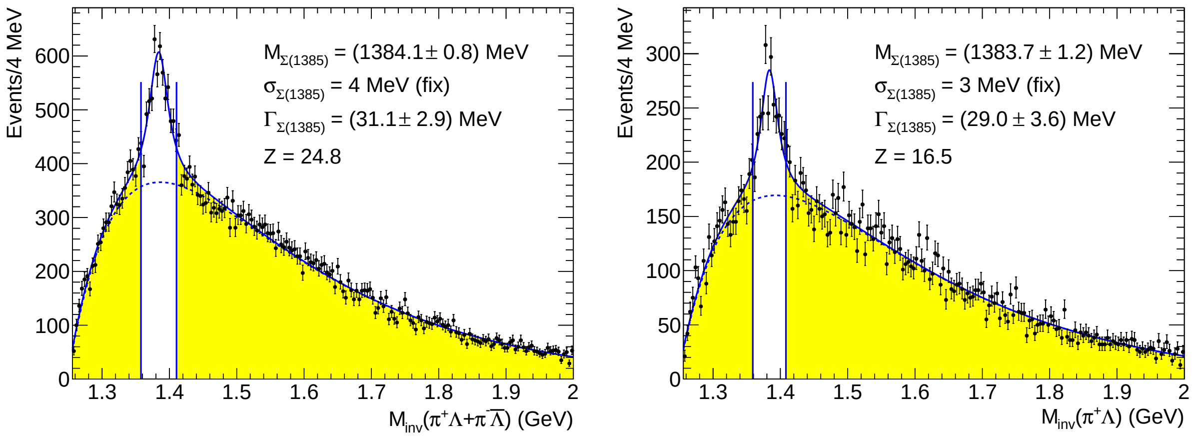

(a) (b)

Figure 4.27: Fits to the Z^* $M_{\mathrm{inv}}(\Lambda\pi^+ + \overline{\Lambda}\pi^-)$ (a) and P^* $M_{\mathrm{inv}}(\Lambda\pi^+)$ spectra (b) with the RooFit `RooDstD0BG` background model and a Voigtian signal shape (c.f. eq. (4.2)).

The calculation of the 95 % upper limit on the number of signal events $N^{\Lambda\pi^+}_{\Theta,\mathrm{UL}}$ was carried out by a scan of $\mathrm{CL_s}$ values along $M_{\mathrm{inv}}(\Lambda\pi^+)$ with the test statistic specified in equation (4.4) using the asymptotic formulae of likelihood based tests [152]. The result of that scan is plotted in figure 4.28.
The acceptance ratio $\mathcal{A} = \frac{A(\Theta^+\to\Lambda\pi^+)}{A(\Theta^+\to pK^0_S)}$ was calculated equivalently to [161] using the toy model in the HERMES-MC engine. It was found to be

$$\mathcal{A}_{Z^*} = 0.73 \pm 0.04\,(\mathrm{stat.}) \qquad \mathcal{A}_{P^*} = 0.74 \pm 0.07\,(\mathrm{stat.}) \tag{4.9}$$

for the Z^* and P^* samples respectively. The final result of this search in the full range is

$$\mathcal{B}_{\mathrm{UL},Z^*} = 0.77 \pm 0.22\,(\mathrm{stat.}) \pm 0.17\,(\mathrm{syst.}) \qquad \mathcal{B}_{\mathrm{UL},Z^*} = 2.2 \pm 1.0\,(\mathrm{stat.}) \pm 0.5\,(\mathrm{syst.})\,, \tag{4.10}$$

taking the statistical errors from the fit on deuterium with the $D^* - D^0$ background shape, the statistical error from the acceptance ratio, a 20 % systematic error on $N^{pK^0_S}_{\Theta,\mathrm{obs}}$ and an approximated 10 % systematic error on $N^{\Lambda\pi^+}_{\Theta,\mathrm{UL}}$ due to the background model parametrization. The smaller systematic error for the background parametrization comes from the relatively smooth background shape in the $\Lambda\pi^+$ channel in the region of interest. A restriction to the Θ^+ signal region ($\sim \pm 2\,\sigma$ of the measured peak position on deuterium) yields

$$\mathcal{B}_{\mathrm{UL},Z^*} = 0.68 \pm 0.19\,(\mathrm{stat.}) \pm 0.15\,(\mathrm{syst.}) \qquad \mathcal{B}_{\mathrm{UL},P^*} = 1.4 \pm 0.6\,(\mathrm{stat.}) \pm 0.3\,(\mathrm{syst.})\,. \tag{4.11}$$

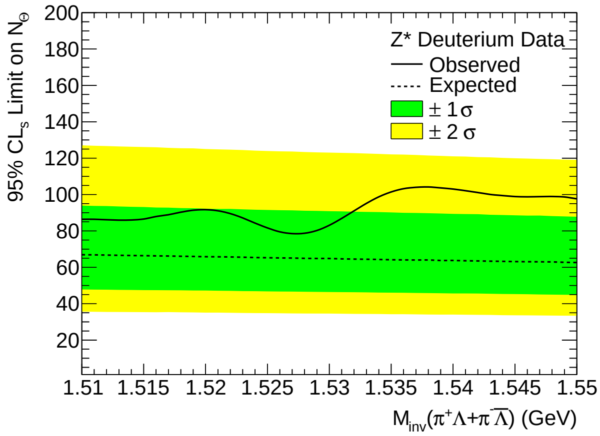

(a)

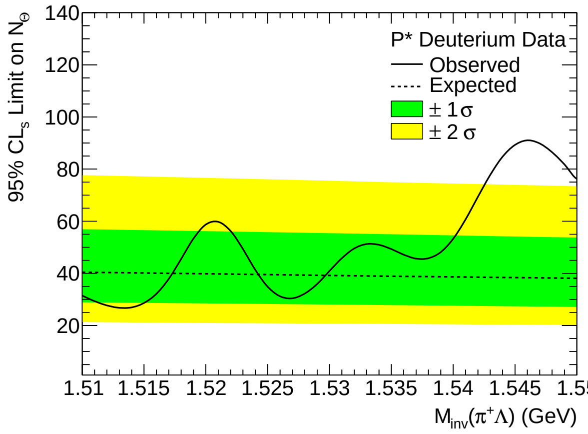

(b)

Figure 4.28: Observed 95 % CL$_s$ limits on the number of signal events N_Θ as a function of $M_{\text{inv}}(\Lambda\pi^+)$ (solid line) and the expectation (dashed line) under the background only hypothesis ($N_\Theta = 0$) for the Z^* $\Lambda\pi^+ + \bar{\Lambda}\pi^-$(a) and P^* $\Lambda\pi^+$ (b) data on deuterium. The green and yellow bands show the $\pm 1\sigma$ and $\pm 2\sigma$ uncertainties on the background only expectation.

In summary a signal similar to the bump in the pK^0_S-channel on deuterium is not seen in the $\Lambda\pi^+$-channel, but can also not be excluded at high confidence, so that the observed upper limits are still compatible to ratios of branching fractions of known excited Σ resonances. A narrow excited Σ baryon on the other hand is not expected by common quark models. The central value of the result can be interpreted as hint for an $S = +1$ assignment to the bump in the pK^0_S-channel. This statement is also supported by the preceding study in [161], where no momentum cut on the p candidate and no fiducial volume cuts were required. The loss in statistics of the fiducial volume cut on the pion from the Λ decay is 50-60 %[1], and with a cut on the proton momentum about 10 % is lost. These cuts were kept because the analysis in both channels were required to be compatible.

[1] Most pion tracks from a Λ decay have realtively low momentum and therefore hit the field clamps due to strong deflection in the spectometer magnet.

5 Summary and Conclusion

The analysis of resonant structures in the pK^0_S (and its charge conjugate) channel, associated with a search for the light pentaquark Θ^+, using HERMES data from quasi-real photoproduction off hydrogen and deuterium targets has been redone. The analysis included previously published (HERA I) and new (HERA II) data. The main improvement in the re-analyzed data, compared to the published data, were refined tracking and PID algorithms. The main improvements in the analysis itself were the usage of a blind technique, providing two different data samples with properties specified a priori, additional systematic studies and a statistical analysis based on the latest available tools. Selection criteria have been optimized, introduced or omitted in the course of maximizing the naive significance $Z = \frac{S}{\sqrt{S+B}}$ for K^0_S and protons separately and by systematic studies. The final spectra were selected following two different philosophies. One, called Z^*, aims for optimized statistic, while the other philosophy (P^*) intends a more careful approach reaching for higher purity. The two final spectra provided a benchmark to address systematic effects in the selection chain. Both spectra exhibit a bump at ~ 1522 MeV from deuterium data, but no structure is seen in hydrogen data. It is found that the Z^* and P^* deuterium spectra are statistically consistent, and that the significance of the bump in the Z^* spectrum is higher, while the purity of the bump in the P^* selection is higher, as it would be expected. Thus a systematic artifact introduced by selection criteria is ruled out with high confidence.

One focus of this work was the improvement of the proton identification in the RICH by optimization of the Λ signal yield. Four different PID methods and their parameters were used, namely EVT, IRT, DRT and OROR (OROR is the logical OR of the three other methods of proton identification). It turned out that an improvement of proton identification was possible. OROR gives the statistically best result and EVT yields the most pure Λ sample, but all methods yield a similar number of Λ signal events within about 25 %. The four methods were then applied to the pK^0_S-channel. Contrary to the proton selection for Λs, the selected pK^0_S spectra differ by up to a factor of ~ 2 in total statistics, which is not understood. As the proton identification may be degraded when additional pion tracks are in the same RICH half, the spectra were divided into four classes of event topologies (proton alone in one RICH-half, p and π^+, p and π^-, p and two πs in the same RICH-half). It turned out that the shape of the spectra in the pK^0_S-channel are very different for the four topologies. Unfortunately, the Θ^+-bump at ~ 1522 MeV coincides either with the onset or with the peak of the background spectrum.

In [149] a correlation between the intensity of the hypothetical Θ^+ peak and an angle θ was claimed. θ is the angle between the momentum of the pK^0_S system and the beam direction (taken as $\mathbf{e}_z$ for simplicity) in the lab frame. The claimed θ-dependence and the found correlation between the Λ contamination and $-\log\left(\text{prob}(\mathbf{V}_{\pi\pi})\right)$ in [148] triggered a systematic study of the $-\log\left(\text{prob}(\mathbf{V}_{\pi\pi})\right)$ cut on $\Lambda(1520)$, which subsequently led to a reexamination of the event topologies. A peak in the pK^0_S spectrum has eventually been found for a certain event topology. Since such a cut limits the kinematic phase space and artificially reduces background or pronounces an eventually fake peak, it is dangerous to make use of it. The existence of a signal in a certain region of the kinematic phase space could on the other hand be a hint why other experiments did not find a signal [110].

An extended statistical analysis of the final Z^* and P^* spectra has been carried out. The $pK^0_S + \bar{p}K^0_S$ Z^* selection on deuterium with the $D^* - D^0$ background parametrization yielded a global significance of $3.1\,\sigma$. The systematic uncertainty due to the background shape was approximated to be 20 %. This number was calculated from different signal yields of fits with $D^* - D^0$ and a 3rd order Chebyshev polynomial as background models.

The hydrogen spectra show no statistically significant excess and an upper limit on the ratio of signal events on hydrogen to deuterium has been calculated at the 95 % confidence level $\mathcal{R} = \frac{e^{\pm}p\rightarrow(pK_S^0)X}{e^{\pm}d\rightarrow(pK_S^0)X} = 0.39 \pm 0.11\,(\mathrm{stat}) \pm 0.08(\mathrm{syst})$, incorporating the approximated systematic error. In the statistical comparison between deuterium and hydrogen, two methods were used, yielding approximately the same results. The first method is a constant plus signal fit to the direct ratio of deuterium to hydrogen, where systematic effects are expected to cancel. The other is a Bayesian analysis based on the MARKOV-chain-Monte-Carlo technique, using the METROPOLIS-HASTINGS algorithm to obtain posterior distributions for the data sets of both targets, which are needed to calculate p values and the corresponding $\mathrm{CL_s}$ limits. The compatibility between deuterium and hydrogen with the $pK_S^0 + \bar{p}K_S^0\ Z^*$ selection yields a $\mathrm{CL_s}$ value of 0.0027, or a significance of $\approx 3\,\sigma$ when the hydrogen data is considered as background only hypothesis.
The strangeness of the bump was tested by a search for a similar bump in the $\Lambda\pi^+$-channel. No signal is seen at $\sim$ 1520 MeV in that channel and an upper limit on the branching ratio $\mathcal{B} = \frac{\Gamma(\Theta^+\rightarrow\Lambda\pi^+)}{\Gamma(\Theta^+\rightarrow pK_S^0)} = 0.68 \pm 0.19\,(\mathrm{stat.}) \pm 0.15\,(\mathrm{syst.})$ at 95 % confidence level has been calculated, using the $pK_S^0 + \bar{p}K_S^0\ Z^*$ selection. The observed upper limit is compatible to branching ratios of known excited Σ resonances, but a narrow excited Σ baryon is not expected by common quark models.
In conclusion the bump on deuterium is a hint that there might be a real signal in the data at $\approx$ 1522 MeV, but it is not strong enough to claim the observation of a particle. The result presented here is consistent with the published HERMES result from 2004 [81].

The statement about the existence of a signal in the pK_S^0-channel at HERMES at this stage is not definitive and therefore dissatisfying. The situation should best be regarded in the Bayesian notion of statistics. It allows to make a distinct yes or no decision based on data collected but biased to the subjective degree of belief[1]. My subjective view is, that the observed bump in deuterium is a real physical effect. I exclude that it is a systematic artifact due to the result obtained from hydrogen and the P^* selected data. I also doubt it to be a statistical fluctuation, since the selection of the event topology, whose kinematics were confirmed by the toy signal in the HERMES-MC, showed a clear and narrow bump whose purity increased with tighter cuts. This bump however, is not present in hydrogen data. Similar narrow structures in a certain region of the kinematic phase space were also observed at CLAS [97] and LEPS[2] [86], although the CLAS bump is displaced in mass. Assuming the signal to be caused by a physical process leads to the question after its nature. From my point of view, the question whether it is the claimed Θ^+ or not is secondary. First of all it would be helpful to reproduce and examine the observed kinematic dependence in more detailed studies at e.g. LEPS II or other high statistics experiments to verify or falsify its existence and possibly measure its properties to understand the effect. However, the situation at HERMES and also ongoing reports of evidence from other collaborations should be tried to be understood.

[1] The counterpart would be the frequentist notion, where the hypothesis is true with a probability of p.
[2] LEPS is limited by setup to the forward region.

Lists of Cuts

Pre-Selection

- Deuterium data (98e1, 99d1, 00e1, 06f1, 07d1)
- Hydrogen data (02d1, 03d1, 04d2, 05d1, 06f1, 07d1)
- Data quality mask 0x02780000
- All tracks are long tracks
- The number of tracks had to be at least 3 and at most 6
- All momenta < 15 GeV (HTC-momenta)
- The proton track candidate had to be a hadron ($-100 < \mathrm{PID3} + \mathrm{PID5} < 0$) with a HTC-momentum > 4 GeV
- The primary vertex $V_{p\mathrm{B}}$[1] had to be within the target cell (-20 cm $< V_{p\mathrm{B}} < 20$ cm for HERA I and 2 cm $< V_{p\mathrm{B}} < 22$ cm for HERA II)
- Cuts on the charge for the corresponding selection
- Fiducial volume cuts (HTC-parameters) [162]

HTC-parameters are used to be consistent with the rest of the analysis.

Z^* Selection for the pK^0_S-channel

- Vertex distance in beam direction $\left(\mathbf{V}_{\pi\pi} - \mathbf{V}_{p\mathrm{B}}\right)_z > 4.09$ cm
- Coplanarity angle $\varphi < 2.535°$
- K^0_S mass within the $2\sigma_{\mathrm{weighted}}$ window of the final fit to the K^0_S signal (486.241 MeV $< M_{\mathrm{inv}}(\pi\pi) <$ 508.555 MeV)
- K^0_S vertex probability $-\log\left(\mathrm{prob}(\mathbf{V}_{\pi\pi})\right) < 17.8$
- Transverse momentum of the pion candidates $p_T > 41$ MeV with respect to $\mathbf{p}_{K^0_\mathrm{S}}$
- No Λ cuts for the two π-candidates and the $p\pi^-_{K^0_\mathrm{S}} + \bar{p}\pi^+_{K^0_\mathrm{S}}$ system ($\notin [1111.85, 1119.45]$ MeV)
- Proton selection with the OROR method

[1] For the $\Sigma(1385)$ configuration $V_{p\mathrm{B}}$ is replaced by $V_{\pi\mathrm{B}}$.

P^* Selection for the pK^0_S-channel

- Vertex distance in beam direction $\left(\mathbf{V}_{\pi\pi} - \mathbf{V}_{p\mathrm{B}}\right)_z > 6.6$ cm
- Coplanarity angle $\varphi < 1.615°$
- K^0_S mass within the $2\sigma_{\text{weighted}}$ window of the final fit to the K^0_S signal (486.119 MeV $< M_{\text{inv}}(\pi\pi) <$ 508.712 MeV)
- K^0_S vertex probability $-\log\left(\text{prob}(\mathbf{V}_{\pi\pi})\right) < 7.8$
- Transverse momentum of the pion candidates $p_T > 41$ MeV with respect to $\mathbf{p}_{K^0_S}$
- No Λ cut for the two π-candidates ($\notin [1111.85, 1119.45]$ MeV)
- Proton selection with the EVT method
- Proton-beam vertex probability $-\log\left(\text{prob}(\mathbf{V}_{p\mathrm{B}})\right) < 1.2$

Z^* Selection for the $\Lambda\pi^+$-channel

- Vertex distance in beam direction $\left(\mathbf{V}_{p\pi} - \mathbf{V}_{\pi\mathrm{B}}\right)_z > 3$ cm
- Coplanarity angle $\varphi < 6.9°$
- No K^0_S cut for the two π-candidates ($\notin [486.241, 508.555]$ MeV)
- Proton selection with the OROR method
- Λ mass within $[1111.85, 1119.45]$ MeV
- Selection of the pion from the $\Sigma(1385)$ decay with the IRT method
- Pion-beam vertex probability $-\log\left(\text{prob}(\mathbf{V}_{\pi\mathrm{B}})\right) < 6$
- Ghost track cut (ratio of HTC-momenta $0.95 < p_{\pi^-}/p_{\pi^+} < 1.05$ if $1274 < M_{\text{inv}}(\Lambda\pi^+) < 1292$ MeV)

P^* Selection for the $\Lambda\pi^+$-channel

- Vertex distance in beam direction $\left(\mathbf{V}_{p\pi} - \mathbf{V}_{\pi\mathrm{B}}\right)_z > 9.5$ cm
- Coplanarity angle $\varphi < 1.22°$
- No K^0_S cut for the two π-candidates ($\notin [486.241, 508.555]$ MeV)
- Proton selection with the EVT method
- Λ mass within $[1111.85, 1119.45]$ MeV
- Selection of the pion from the $\Sigma(1385)$ decay with the IRT method
- Pion-beam vertex probability $-\log\left(\text{prob}(\mathbf{V}_{\pi\mathrm{B}})\right) < 1.2$
- Ghost track cut (ratio of HTC-momenta $0.95 < p_{\pi^-}/p_{\pi^+} < 1.05$ if $1274 < M_{\text{inv}}(\Lambda\pi^+) < 1292$ MeV)

Selection for a Pure $\Lambda(1520)$ Signal

- The first 7 criteria[1] from the pre-selected sample from the pK_S^0- and $\Lambda\pi^+$-channels were used (c.f. A)
- Fiducial volume cuts were applied to the p and K^- candidates
- The primary vertex of both, p and K^- candidates, had to be within the target cell ($\in [-20, 20]$ cm for HERA I and $\in [2, 22]$ cm for HERA II)
- Positive charge for the p and negative charge for the K^- candidates (no antiparticles)
- Event topology cut (p and K^- in the same detector half)
- No ϕ cut for p and K^- candidates ($\notin [1012.93, 1026.09]$ MeV)
- Vertex distance of the proton-beam crossing and the calculated pK^- vertex less than 0.5 cm in beam direction
- Kaon selection with the IRT method
- Proton selection with the ANDAND method (logical AND of the IRT, DRT and EVT methods)

Additional Figures

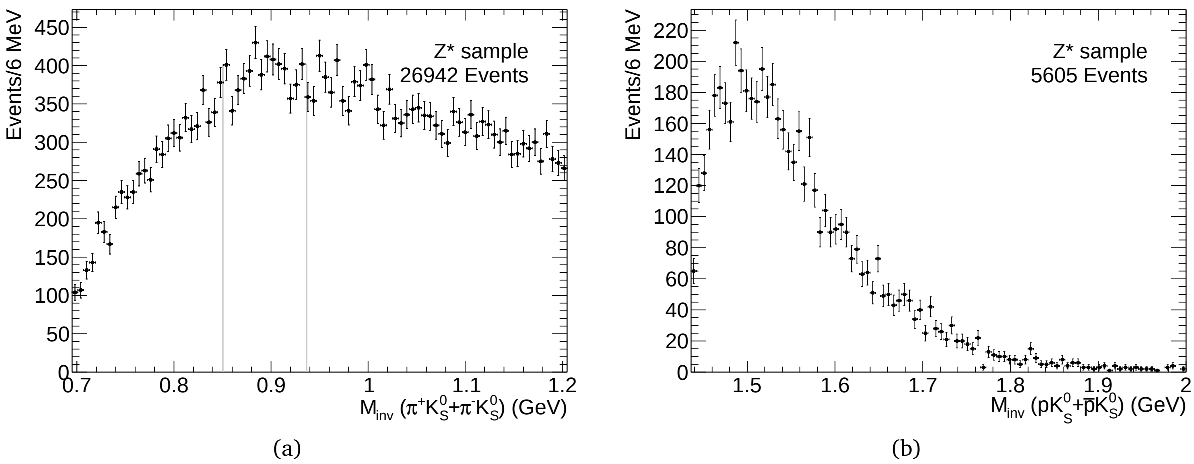

Figure B.1: (a) $\pi^+K_S^0 + \pi^-K_S^0$ invariant mass distributions from proton candidates with pion mass hypothesis for the Z^* sample. (b) Reflections in the pK_S^0-channel of events within the $K^*(892)$ signal region, illustrated by the gray line. All final cuts except the second Λ veto have been applied.

[1]but only deuterium data.

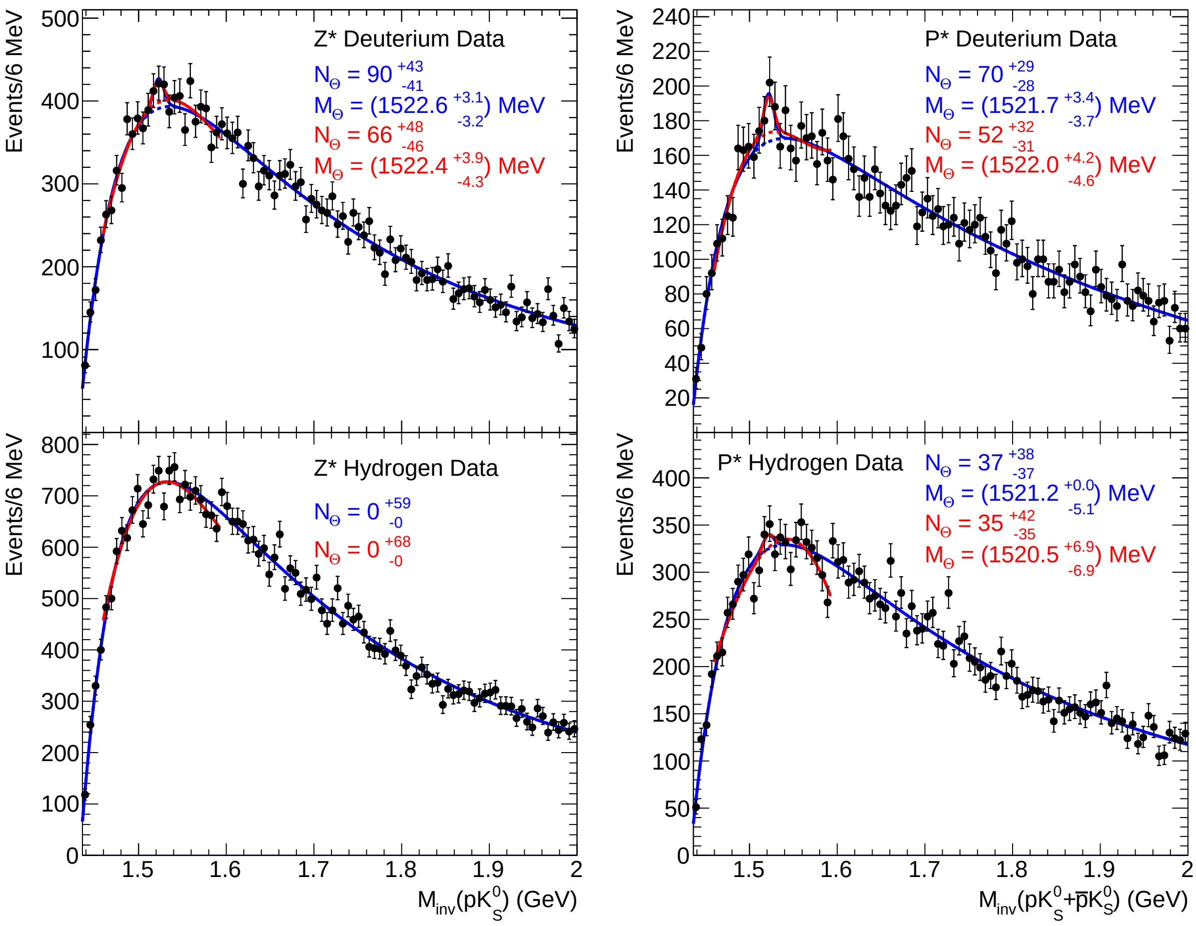

(a) (b)

Figure B.2: Fits to the final Z^* $M_{\mathrm{inv}}(pK^0_S)$ (a) and P^* $M_{\mathrm{inv}}(pK^0_S+\bar{p}K^0_S)$ spectra (b) with the RooFit `RooDstD0BG` (blue line and blue parameters) and 3rd order Chebyshev polynomial (red line and red parameters) as background model.

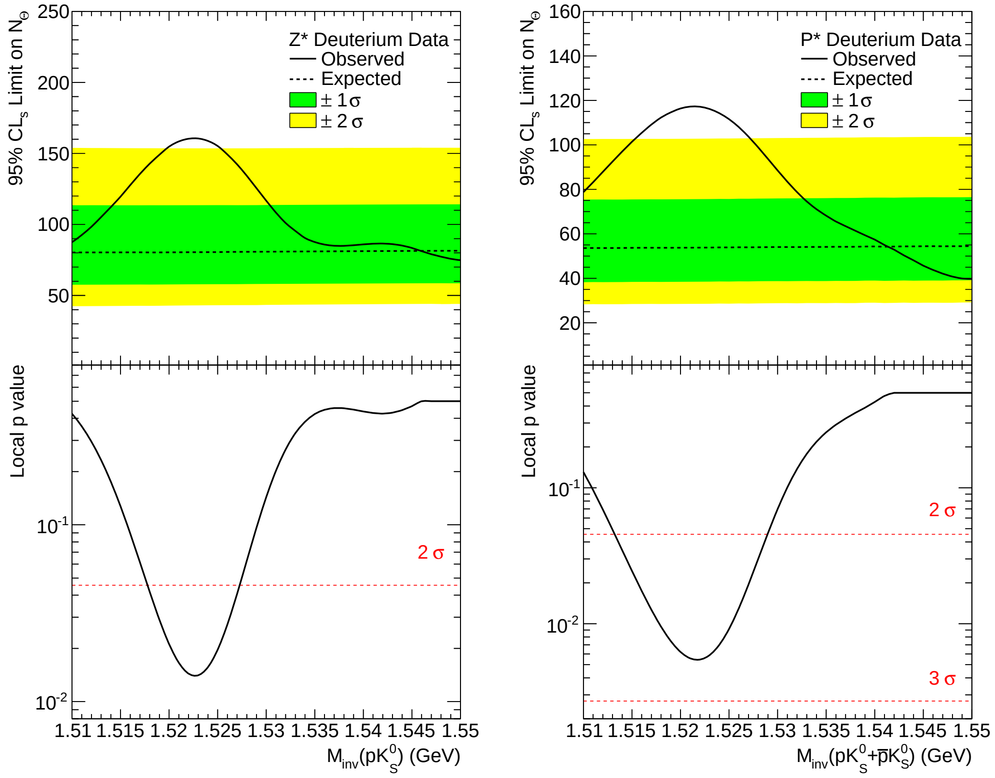

(a) (b)

Figure B.3: The upper panels show the observed 95 % $\mathrm{CL_s}$ limits on the number of signal events N_Θ as a function of $M_{\mathrm{inv}}(pK^0_S)$ (solid line) and the expectation (dashed line) under the background only hypothesis ($N_\Theta = 0$) for the particle only Z^* (a) and particle plus antiparticle P^* (b) data on deuterium. The green and yellow bands show the $\pm 1\sigma$ and $\pm 2\sigma$ uncertainties on the background only expectation. The observed local p values are plotted in the lower panels.

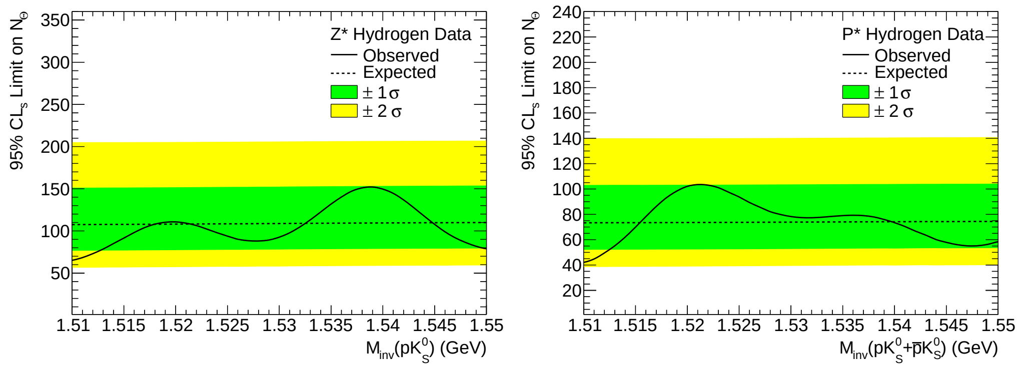

(a) (b)

Figure B.4: Observed 95 % $\mathrm{CL_s}$ limits on the number of signal events N_Θ as a function of $M_{\mathrm{inv}}(pK^0_S)$ (solid line) and the expectation (dashed line) under the background only hypothesis ($N_\Theta = 0$) for the particle only Z^* (a) and particle plus antiparticle P^* (b) data on hydrogen. The green and yellow bands show the $\pm 1\sigma$ and $\pm 2\sigma$ uncertainties on the background only expectation.

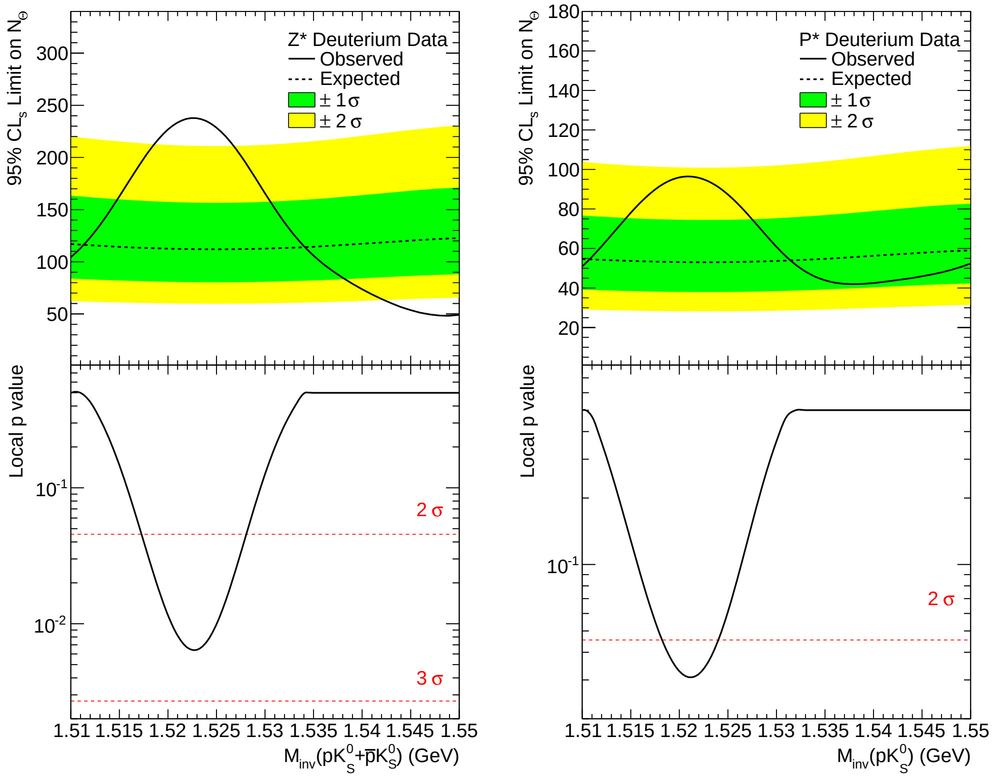

(a) (b)

Figure B.5: The upper panels show the observed 95 % CL$_s$ limits on the number of signal events N_Θ as a function of $M_{\mathrm{inv}}(pK^0_S)$ (solid line) and the expectation (dashed line) under the background only hypothesis ($N_\Theta = 0$) for the Z^* (a) and P^* (b) data on deuterium using a 3[rd] order CHEBYSHEV background. The green and yellow bands show the $\pm 1\sigma$ and $\pm 2\sigma$ uncertainties on the background only expectation. The observed local p values are plotted in the lower panels.

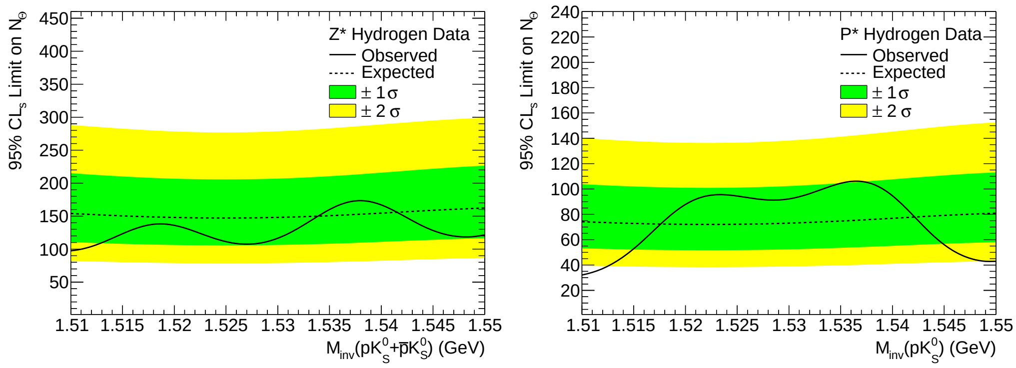

(a) (b)

Figure B.6: Observed 95 % CL$_s$ limits on the number of signal events N_Θ as a function of $M_{\mathrm{inv}}(pK^0_S)$ (solid line) and the expectation (dashed line) under the background only hypothesis ($N_\Theta = 0$) for the Z^* (a) and P^* (b) data on hydrogen using a 3[rd] order CHEBYSHEV polynomial as background model. The green and yellow bands show the $\pm 1\sigma$ and $\pm 2\sigma$ uncertainties on the background only expectation.

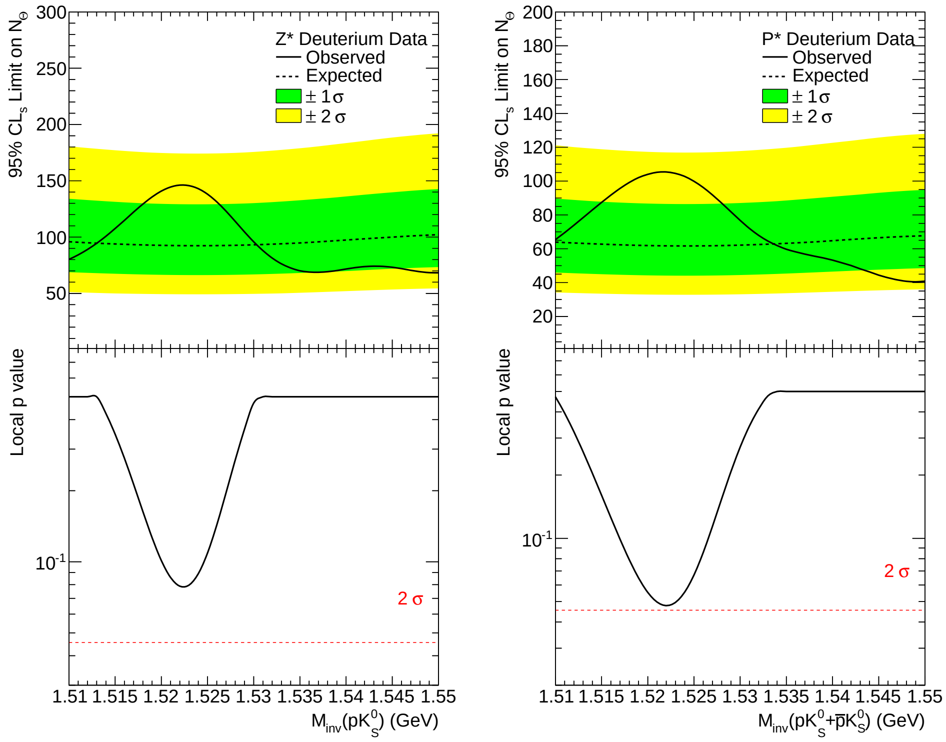

(a) (b)

Figure B.7: The upper panels show the observed 95 % CL$_s$ limits on the number of signal events N_Θ as a function of $M_{\mathrm{inv}}(pK^0_S)$ (solid line) and the expectation (dashed line) under the background only hypothesis ($N_\Theta = 0$) for the particle only Z^* (a) and particle plus antiparticle P^* (b) data on deuterium using a 3$^{\mathrm{rd}}$ order CHEBYSHEV background. The green and yellow bands show the $\pm 1\sigma$ and $\pm 2\sigma$ uncertainties on the background only expectation. The observed local p values are plotted in the lower panels.

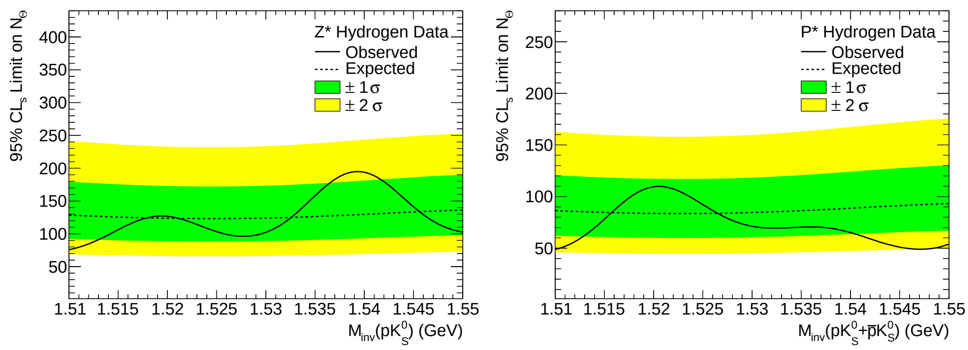

(a) (b)

Figure B.8: Observed 95 % CL$_s$ limits on the number of signal events N_Θ as a function of $M_{\mathrm{inv}}(pK^0_S)$ (solid line) and the expectation (dashed line) under the background only hypothesis ($N_\Theta = 0$) for the particle only Z^* (a) and particle plus antiparticle P^* (b) data on hydrogen using a 3$^{\mathrm{rd}}$ order CHEBYSHEV polynomial as background model. The green and yellow bands show the $\pm 1\sigma$ and $\pm 2\sigma$ uncertainties on the background only expectation.

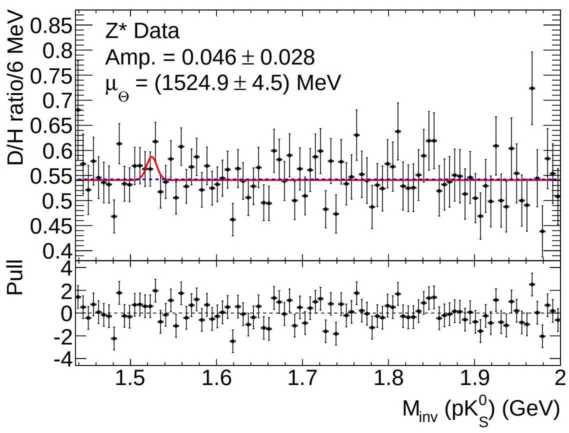

(a) (b)

Figure B.9: Deuterium to Hydrogen ratio for the Z^* (a) and P^* (b) samples with inverse charge selection. The ratio is fitted with the sum of a Gaussian signal and a constant background (red solid line) as signal plus background model and a constant (blue dashed line) as background only model. In the lower panels the pulls from the background only fit are plotted.

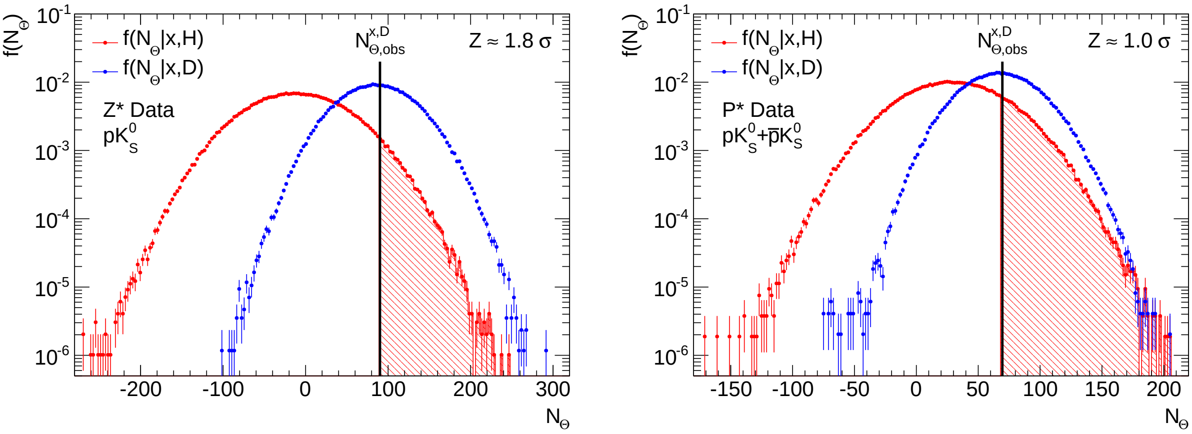

(a) (b)

Figure B.10: Posterior distributions of N_Θ from Z^* (a) and P^* (b) deuterium and hydrogen data with inverse charge selection. The observed value on deuterium is marked by the solid vertical line. The calculated p value corresponds to the hatched red area.

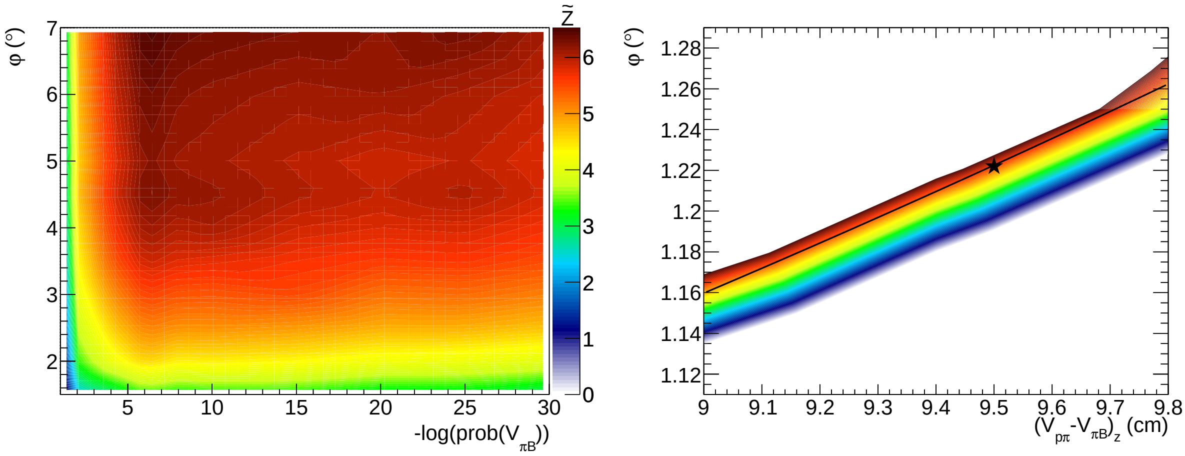

(a) (b)

Figure B.11: (a) 2-D scan profile of $-\log\left(\text{prob}(\mathbf{V}_{\pi\text{B}})\right)$ and φ for optimization of the $\Sigma(1385)$ cuts. (b) Purity scan profile of the $-\log\left(\text{prob}(\mathbf{V}_{\pi\text{B}})\right)$ and φ cuts for the $P^*\ \Lambda$ sample. The fitted 97 % purity contour is shown as solid black line. The naive significance Z is depicted by the colored band in arbitrary units.

References

[1] C. M. G. Lattes, H. Muirhead, G. P. S. Occhialini, C. F. Powell, *Processes Involving Charged Mesons*, Nature **159 (4047)**, 694-697 (1947), [doi:10.1038/2F159694a0]

[2] R. Bjorklund, W. E. Crandall, B. J. Moyer, H. F. York, *High Energy Photons from Proton-Nucleon Collisions*, Phys. Rev. **77 (2)**, 213-218 (1950), [doi:10.1103/PhysRev.77.213]

[3] O. Chamberlain, E. Segrè, C. Wiegand, T. Ypsilantis, *Observation of Antiprotons*, Phys. Rev. **100 (3)**, 947-950 (1955), [doi:10.1103/PhysRev.100.947]

[4] B. Cork, G. R. Lambertson, O. Piccioni, W. A. Wenzel, *Antineutrons Produced from Antiprotons in Charge-Exchange Collisions*, Phys. Rev. **104 (4)**, 1193-1197 (1956), [doi:10.1103/PhysRev.104.1193]

[5] C. L. Cowan *et al.*, *Detection of the Free Neutrino: a Confirmation*, Science **124 (3212)**, 103-104 (1956), [doi:10.1126/Fscience.124.3212.103]

[6] C. D. Anderson, S. H. Neddermeyer, *Cloud Chamber Observations of Cosmic Rays at 4300 Meters Elevation and Near Sea-Level*, Phys. Rev. **50 (4)**, 263-271 (1936), [doi:10.1103/PhysRev.50.263]

[7] G. D. Rochester, C. C. Butler, *Evidence for the Existence of New Unstable Elementary Particles*, Nature **160 (4077)**, 855-857 (1947), [doi:10.1038/160855a0]

[8] A. J. Seriff *et al.*, *Cloud-Chamber Observations of the New Unstable Cosmic-Ray Particles*, Phys. Rev. **78 (3)**, 290-291 (1950), [doi:10.1103/PhysRev.78.290]

[9] S. Sakata, *On a Composite Model for the New Particles*, Prog. Theor. Phys. **16 (6)**, 686-688 (1956), [doi:10.1143/PTP.16.686]

[10] M. Gell-Mann, *Symmetries of Baryons and Mesons*, Phys. Rev. **125 (3)**, 1067-1084 (1962), [doi:10.1103/PhysRev.125.1067]

[11] Y. Ne'eman, *Derivation of strong interactions from a gauge invariance*, Nucl. Phys. **26 (2)**, 222-229 (1961), [doi:10.1016/0029-5582(61)90134-1]

[12] M. Gell-Mann, Proceedings of the International Conference on High-Energy Nuclear Physics, Geneva, p. 805 (1962); published in M. Gell-Mann, Y. Ne'eman, *The Eightfold Way*, New York: Benjamin, 1964

[13] V. E. Barnes *et al.*, *Observation of a Hyperon with Strangeness Minus Three*, Phys. Rev. Lett. **12 (8)**, 204-206 (1964), [doi:10.1103/PhysRevLett.12.204]

[14] M. Gell-Mann, *A schematic model of baryons and mesons*, Phys. Lett. **8 (3)**, 214-215 (1964), [doi:10.1016/S0031-9163(64)92001-3]

[15] G. Zweig, *An* $SU(3)$ *model for strong interaction symmetry and its breaking*, CERN-Report **TH-401**, (1964)

[16] G. Zweig, *An* $SU(3)$ *model for strong interaction symmetry and its breaking II*, CERN-Report **TH-412**, (1964)

[17] O. W. Greenberg, *Spin and Unitary-Spin Independence in a Paraquark Model of Baryons and Mesons*, Phys. Rev. Lett. **13 (20)**, 598-602 (1964), [doi:10.1103/PhysRevLett.13.598]

[18] J. J. Aubert *et al.*, *Experimental Observation of a Heavy Particle* J, Phys. Rev. Lett. **33 (23)**, 1404-1406 (1974), [doi:10.1103/PhysRevLett.33.1404]

[19] J. E. Augustin *et al.*, *Discovery of a Narrow Resonance in* e^+e^- *Annihilation*, Phys. Rev. Lett. **33 (23)**, 1406-1408 (1974), [doi:10.1103/PhysRevLett.33.1406]

[20] B. J. Bjørken, S. L. Glashow, *Elementary particles and SU(4)*, Phys. Lett. **11 (3)**, 255-257 (1964), [doi:10.1016/0031-9163(64)90433-0]

[21] S. L. Glashow, J. Iliopoulos, L. Maiani, *Weak Interactions with Lepton-Hadron Symmetry*, Phys. Rev. D **2 (7)**, 1285-1292 (1970), [doi:10.1103/PhysRevD.2.1285]

[22] C. N. Yang, R. L. Mills, *Conservation of Isotopic Spin and Isotopic Gauge Invariance*, Phys. Rev. **96 (1)**, 191-195 (1954), [doi:10.1103/PhysRev.96.191]

[23] Y. Nambu, G. Jona-Lasinio, *Dynamical Model of Elementary Particles Based on an Analogy with Superconductivity. I*, Phys. Rev. **122 (1)**, 345-358 (1961), [doi:10.1103/PhysRev.122.345]

[24] J. Goldstone, *Field theories with "Superconductor" solutions*, Il Nuovo Cimento **19 (1)**, 154-164 (1961), [doi:10.1007/BF02812722]

[25] Y. Nambu, G. Jona-Lasinio, *Dynamical Model of Elementary Particles Based on an Analogy with Superconductivity. II*, Phys. Rev. **124 (1)**, 246-254 (1961), [doi:10.1103/PhysRev.124.246]

[26] G. Sterman *et al.* (CTEQ collaboration), *Handbook of perturbative QCD*, Rev. Mod. Phys. **67 (1)**, 157-248 (1995), [doi:10.1103/RevModPhys.67.157]

[27] J. Beringer *et al.* (Particle Data Group), *Review of Particle Physics*, Phys. Rev. D **86**, 010001 (2012), [doi:10.1103/PhysRevD.86.010001]

[28] W. Greiner, B. Müller, *Quantenmechanik - Symmetrien*, Harri Deutsch (2005)

[29] U. Mosel, *Fields, Symmetries and Quarks*, Springer (1999)

[30] T. Feldmann, P. Kroll, *Mixing of Pseudoscalar Mesons*, Phys. Scr. **2002 (T99)**, 13-22 (2002), [doi:10.1238/Physica.Topical.099a00013]

[31] N. H. Christ *et al.*, *η and η' Mesons from Lattice QCD*, Phys. Rev. Lett. **105 (24)**, 241601 (2010), [doi:10.1103/PhysRevLett.105.241601]

[32] C. Alexandrou, P. de Forcrand, B. Lucini, Evidence for Diquarks in Lattice QCD, Phys. Rev. Lett. **97 (22)**, 222002 (2006), [doi:10.1103/PhysRevLett.97.222002]

[33] Y. Oh, H. Kim, *Pentaquark baryons in the $SU(3)$ quark model*, Phys. Rev. D **70 (9)**, 094022 (2004), [doi:10.1103/PhysRevD.70.094022]

[34] M. E. Peskin, D. V. Schroeder, *An Introduction to Quantum Field Theory*, Perseus (1995)

[35] A. Manohar, *Equivalence of the chiral soliton and quark models in large N*, Nucl. Phys. B **248 (1)**, 19-28 (1984), [doi:10.1016/0550-3213(84)90584-4]

[36] M. Chemtob, *Skyrme model of baryon octet and decuplet*, Nucl. Phys. B **256**, 600-608 (1985), [doi:10.1016/0550-3213(85)90409-2]

[37] M. Praszałowicz, in: M. Jeżabek, M. Praszałowicz (Eds.), Workshop on Skyrmions and Anomalies, World Scientific, Singapore, 1987, p. 112.; Reprint: M. Praszalowicz, *Pentaquark in the Skyrme model*, Phys. Lett. B **575 (3-4)**, 234-241 (2003), [doi:10.1016/j.physletb.2003.09.049]

[38] T. H. R. Skyrme, *A unified field theory of mesons and baryons*, Nucl. Phys. **31**, 556-559 (1962), [doi:10.1016/0029-5582(62)90775-7]

[39] G. 't Hooft, *A planar diagram theory for strong interactions*, Nucl. Phys. B **72 (3)**, 461-473 (1974), [doi:10.1016/0550-3213(74)90154-0]

[40] G. 't Hooft, *A two-dimensional model for mesons*, Nucl. Phys. B **75 (3)**, 461-470 (1974), [doi:10.1016/0550-3213(74)90088-1]

[41] E. Witten, *Baryons in the $1/N$ expansion*, Nucl. Phys. B **160 (1)**, 57-115 (1979), [doi:10.1016/0550-3213(79)90232-3]

[42] G. Holzwarth, B. Schwesinger, *Baryons in the Skyrme model*, Rep. Prog. Phys. **49 (8)**, 825-871 (1986), [doi:10.1088/0034-4885/49/8/001]

[43] J. Schechter, H. Weigel, *The Skyrme Model for Baryons* (1999), arXiv:9907554 [hep-ph]

[44] T. H. R. Skyrme, *The Origins of Skyrmions*, Int. J. Mod. Phys. A **03 (12)**, 2745-2751 (1988), [doi:10.1142/S0217751X88001156]

[45] D. I. Diakonov, *Chiral Quark-Soliton Model* (1998), arXiv:9802298 [hep-ph]

[46] D. I. Diakonov, V. Y. Petrov, M. Polyakov, *Exotic Anti-Decuplet of Baryons: Prediction from Chiral Solitons*, Z. Phys. A **359**, 305-314 (1997), [doi:10.1007/s002180050406]

[47] D. I. Diakonov, V. Y. Petrov, P. V. Pobylitsa, *A chiral theory of nucleons*, Nucl. Phys. B **306 (4)**, 809-848 (1988), [doi:10.1016/0550-3213(88)90443-9]

[48] R. L. Jaffe, *Baryon Excitations in the Bag Model*, Proc. Topical Conference on Baryon Resonances, Oxford (1976), SLAC-PUB-1774

[49] A. Chodos *et al.*, *New extended model of hadrons*, Phys. Rev. D **9 (12)**, 3471-3495 (1974), [doi:10.1103/PhysRevD.9.3471]

[50] R. L. Jaffe, *Exotica*, Phys. Rep. **409 (1)**, 1-45 (2005), [doi:10.1016/j.physrep.2004.11.005]

[51] B. K. Jennings, K. Maltman, *Z^* resonances: Phenomenology and models*, Phys. Rev. D **69 (9)**, 094020 (2004), [doi:10.1103/PhysRevD.69.094020]

[52] A. Blotz *et al.*, *The SU(3) Nambu-Jona-Lasinio soliton in the collective quantization formulation*, Nucl. Phys. A **555 (4)**, 765-792 (1993), [doi:10.1016/0375-9474(93)90505-R]

[53] G.-S. Yang, H.-C. Kim, *Θ^+ baryon, $N^*(1685)$ resonance, and πN sigma term reexamined within the framework of a chiral soliton model*, Prog. Theor. Exp. Phys. **2013 (1)**, D01 (2013), [doi:10.1093/ptep/pts044]

[54] H. Weigel, *Radial excitations of low-lying baryons and the Z^+ penta-quark*, Eur. Phys. J. A **2 (4)**, 391-402 (1998), [doi:10.1007/s100500050136]

[55] T. D. Cohen, *Chiral soliton models, large N_c consistency and the Θ^+ exotic baryon*, Phys. Lett. B **581 (3-4)**, 175-181 (2004), [doi:10.1016/j.physletb.2003.11.065]

[56] R. L. Jaffe, *Life and Death Among the Hadrons*, AIP Conf. Proc. **792**, 97-106 (2005), [doi:10.1063/1.2122015]

[57] K. G. Wilson, *Confinement of quarks*, Phys. Rev. D **10 (8)**, 2445-2459 (1974), [doi:10.1103/PhysRevD.10.2445]

[58] F. Csikor, Z. Fodor, S. D. Katz, T. G. Kovács, *Pentaquark hadrons from lattice QCD*, JHEP **11**, 70-82 (2003), [doi:10.1088/1126-6708/2003/11/070]

[59] S. Sasaki, *Lattice Study of the Exotic $S = +1$ Baryon*, Phys. Rev. Lett. **93 (15)**, 152001 (2004), [doi:10.1103/PhysRevLett.93.152001]

[60] T. T. Takahashi, T. Umeda, T. Onogi, T. Kunihiro, *Search for the possible $S = +1$ pentaquark states in quenched lattice QCD*, Phys. Rev. D **71 (11)**, 114509 (2004), [doi:10.1103/PhysRevD.71.114509]

[61] T.-W. Chiu, T.-H. Hsieh, *Study of $\Theta^+(udud\bar{s})$ in lattice QCD with exact chiral symmetry*, Phys. Rev. D **72 (3)**, 034505 (2005), [doi:10.1103/PhysRevD.72.034505]

[62] B. G. Lasscock, D. B. Leinweber, A. G. Williams, *Exotic Hadrons on the Lattice*, Prog. Theor. Phys. Suppl. **168**, 36-44 (2007), [doi:10.1143/PTPS.168.36]

[63] K.-F. Liu, N. Mathur, *A Review of Pentaquark Calculations on the Lattice*, Int. J. Mod. Phys. A **21 (4)**, 851-858 (2006), [doi:10.1142/S0217751X06032162]

[64] A. S. B. Tariq, *Revisiting the pentaquark episode for lattice QCD*, PoS **LAT2007**, 136 (2007), [LAT2007_136]

[65] M. A. Shifman, A. I. Vainshtein, V. I. Zakharov, *QCD and resonance physics. theoretical foundations*, Nucl. Phys. B **147 (5)**, 385-447 (1979), [doi:10.1016/0550-3213(79)90022-1]

[66] R. D. Matheus, F. S. Navarra, M. Nielsen, *Rise and fall of pentaquarks in the QCD Sum Rules approach*, Braz. J. Phys. **36 (4)**, 1397-1409 (2006), [doi:10.1590/S0103-97332006000800014]

[67] C. Alt *et al.* (NA49 Collaboration), *Evidence for an Exotic $S = -2$, $Q = -2$ Baryon Resonance in Proton-Proton Collisions at the CERN SPS*, Phys. Rev. Lett. **92 (4)**, 042003 (2004), [doi:10.1103/PhysRevLett.92.042003]

[68] A. Aktas *et al.* (H1 Collaboration), *Evidence for a narrow anti-charmed baryon state*, Phys. Lett. B **588 (1-2)**, 17-28 (2004), [doi:10.1016/j.physletb.2004.03.012]

[69] P. Gubler *et al.*, *Spin-3/2 pentaquark in QCD sum rules*, Phys. Rev. D **79 (11)**, 114011 (2009), [doi:10.1103/PhysRevD.79.114011]

[70] R. L. Jaffe, F. Wilczek, *A perspective on pentaquarks*, Eur. Phys. J. C **33 (s01)**, s38-s42 (2004), [doi:10.1140/epjcd/s2004-03-1696-8]

[71] T. G. Trippe *et al.* (Particle Data Group), *Review of particle properties*, Rev. Mod. Phys. **48 (2)**, S1-S245 (1976), [doi:10.1103/RevModPhys.48.S1]

[72] M. Aguilar-Benítez *et al.* (Particle Data Group), *Review of particle properties*, Phys. Lett. B **170**, 2-350 (1986), [doi:10.1016/0370-2693(86)91663-1]

[73] K. H. Hicks, *On the conundrum of the pentaquark*, Eur. Phys. J. H **37 (1)**, 1-31 (2011), [doi:10.1140/epjh/e2012-20032-0]

[74] T. Nakano *et al.* (LEPS Collaboration), *Evidence for a Narrow $S = +1$ Baryon Resonance in Photoproduction from the Neutron*, Phys. Rev. Lett. **91 (1)**, 012002 (2003), [doi:10.1103/PhysRevLett.91.012002]

[75] C. Amsler *et al.* (Particle Data Group), *Review of particle physics*, Phys. Lett. B **667 (1-5)**, 1-1340 (2008), [doi:10.1016/j.physletb.2008.07.044]

[76] J. Pochodzalla, *Pentaquarks - Facts and Mysteries or Sisyphus at Work*, PANDA Physics Workshop (2004), arXiv:hep-ex/0406077

[77] V. V. Barmin *et al.* (DIANA Collaboration), *Observation of a baryon resonance with positive strangeness in K^+ collisions with Xe nuclei*, Phys. Atom. Nucl. **66 (9)**, 1715-1718 (2003), [doi:10.1134/1.1611587]

[78] S. Stepanyan *et al.* (CLAS Collaboration), *Observation of an Exotic $S = +1$ Baryon in Exclusive Photoproduction from the Deuteron*, Phys. Rev. Lett. **91 (25)**, 252001 (2003), [doi:10.1103/PhysRevLett.91.252001]

[79] A. E. Asratyan, A. G. Dolgolenko, M. A. Kubantsev, *Evidence for formation of a narrow $K^0_S p$ resonance with mass near 1533 MeV in neutrino interactions*, Phys. Atom. Nucl. **67 (4)**, 682-687 (2004), [doi:10.1134/1.1707127]

[80] J. Barth *et al.* (SAPHIR Collaboration), *Evidence for the positive-strangeness pentaquark Θ^+ in photoproduction with the SAPHIR detector at ELSA*, Phys. Lett. B **572 (3-4)**, 127-132 (2003), [doi:10.1016/j.physletb.2003.08.019]

[81] A. Airapetian *et al.* (HERMES Collaboration), *Evidence for a narrow $|S|=1$ baryon state at a mass of 1528 MeV in quasi-real photoproduction*, Phys. Lett. B **585 (3-4)**, 213-222 (2004), [doi:10.1016/j.physletb.2004.01.079]

[82] M. Abdel-Bary *et al.* (COSY Collaboration), *Evidence for a narrow resonance at 1530 MeV/c^2 in the K^0p-system of the reaction $pp \to \Sigma^+K^0p$ from the COSY-TOF experiment*, Phys. Lett. B **595 (1-4)**, 127-134 (2004), [doi:10.1016/j.physletb.2004.05.067]

[83] S. Chekanov *et al.* (ZEUS Collaboration), *Evidence for a narrow baryonic state decaying to $K^0_S p$ and $K^0_S \bar{p}$ in deep inelastic scattering at HERA*, Phys. Lett. B **591 (1-2)**, 7-22 (2004), [doi:10.1016/j.physletb.2004.04.024]

[84] A. Aleev *et al.* (SVD Collaboration), *Observation of a narrow baryon resonance decaying to pK^0_S in proton-nucleus interactions at 70 GeV/c with the SVD-2 setup*, Phys. Atom. Nucl. **68 (6)**, 974-981 (2005), [doi:10.1134/1.1954823]

[85] T. Nakano *et al.* (LEPS Collaboration), *Evidence for the Θ^+ in the $\gamma d \to K^+K^-pn$ reaction by detecting K^+K^- pairs*, Phys. Rev. C **79 (2)**, 025210 (2009), [doi:10.1103/PhysRevC.79.025210]

[86] M. Niiyama, *Recent results from LEPS and prospects of LEPS II at SPring-8*, Nucl. Phys. A **In Press**, corrected proof (2013), [doi:10.1016/j.nuclphysa.2013.03.013]

[87] K. Abe *et al.* (Belle Collaboration), *Search for the $\Theta^+(1540)$ pentaquark using kaon secondary interactions at Belle*, Phys. Lett. B **632 (2-3)**, 173-180 (2006), [doi:10.1016/j.physletb.2005.10.077]

[88] V. V. Barmin *et al.* (DIANA Collaboration), *Further evidence for formation of a narrow baryon resonance with positive strangeness in K^+ collisions with Xe nuclei*, Phys. Atom. Nucl. **70 (1)**, 35-43 (2007), [doi:10.1134/S106377880701005X]

[89] V. V. Barmin *et al.* (DIANA Collaboration), *Formation of a narrow baryon resonance with positive strangeness in K^+ collisions with Xe nuclei*, Phys. Atom. Nucl. **73 (7)**, 1168-1175 (2010), [doi:10.1134/S1063778810070100]

[90] V. V. Barmin *et al.* (DIANA Collaboration), *Observation of a narrow baryon resonance with positive strangeness formed in K^+Xe collisions* (2013), arXiv:1307.1653v1 [nucl-ex]

[91] B. McKinnon *et al.* (CLAS Collaboration), *Search for the Θ^+ Pentaquark in the Reaction $\gamma d \to pK^-K^+n$*, Phys. Rev. Lett. **96 (21)**, 212001 (2006), [doi:10.1103/PhysRevLett.96.212001]

[92] S. Niccolai *et al.* (CLAS Collaboration), *Search for the Θ^+ Pentaquark in the $\gamma d \to \Lambda n K^+$ Reaction Measured with the CLAS Spectrometer*, Phys. Rev. Lett. **97 (3)**, 032001 (2006), [doi:10.1103/PhysRevLett.97.032001]

[93] O. Samoylov *et al.* (NOMAD Collaboration), *Search for the exotic Θ^+ resonance in the NOMAD experiment*, Eur. Phys. J. C **49 (2)**, 499-510 (2006), [doi:10.1140/epjc/s10052-006-0080-y]

[94] V. Kubarovsky *et al.* (CLAS Collaboration), *Observation of an Exotic Baryon with $S = +1$ in Photoproduction from the Proton*, Phys. Rev. Lett. **92 (3)**, 032001 (2004), [doi:10.1103/PhysRevLett.92.032001]; erratum - ibid. **92 (4)**, 049902 (2004), [doi:10.1103/PhysRevLett.92.049902]

[95] M. Battaglieri *et al.* (CLAS Collaboration), *Search for $\Theta^+(1540)$ pentaquark in high statistics measurement of $\gamma p \to \overline{K}^0K^+n$ at CLAS*, Phys. Rev. Lett. **96 (4)**, 042001 (2006), [doi:10.1103/PhysRevLett.96.042001]

[96] R. De Vita *et al.* (CLAS Collaboration), *Search for the Θ^+ pentaquark in the reactions $\gamma p \to \overline{K}^0K^+n$ and $\gamma p \to \overline{K}^0K^0p$*, Phys. Rev. D **74 (3)**, 032001 (2006), [doi:10.1103/PhysRevD.74.032001]

[97] M. J. Amaryan *et al.*, *Observation of a narrow structure in ${}^1H(\gamma, K_S^0)X$ via interference with ϕ-meson production*, Phys. Rev. C **85 (3)**, 035209 (2012), [doi:10.1103/PhysRevC.85.035209]

[98] M. Anghinolfi *et al.* (CLAS Collaboration), *Comment on "Observation of a narrow structure in ${}^1H(\gamma, K_S^0)X$ via interference with ϕ-meson production"*, Phys. Rev. C **86 (6)**, 069801 (2012), [doi:10.1103/PhysRevC.86.069801]

[99] K. Gotzen, *Search for pentaquarks at* BaBar, Nucl. Phys. B Proc. Suppl. **164**, 117-120 (2005), [doi:10.1016/j.nuclphysbps.2006.11.107]

[100] M. Abdel-Bary *et al.* (COSY Collaboration), *Improved study of a possible Θ^+ production in the $pp \to pK^0\Sigma^+$ reaction with the COSY-TOF spectrometer*, Phys. Lett. B **649 (4)**, 252-257 (2007), [doi:10.1016/j.physletb.2007.04.023]

[101] A. Aktas *et al.* (H1 Collaboration), *Search for a narrow baryonic resonance decaying to K_S^0p or $K_S^0\overline{p}$ in deep inelastic scattering at HERA*, Phys. Lett. B **639 (3-4)**, 202-209 (2006), [doi:10.1016/j.physletb.2006.06.055]

[102] Y. M. Antipov *et al.* (SPHINX Collaboration), *Search for $\Theta(1540)^+$ in the exclusive proton-induced reaction $p + C(N) \to \Theta^+\overline{K}^0 + C(N)$ at the energy of 70 GeV*, Eur. Phys. J. A **21 (3)**, 455-468 (2004), [doi:10.1140/epja/i2004-10062-4]

[103] I. Abt *et al.* (HERA-B Collaboration), *Limits for the central production of Θ^+ and Ξ^{--} pentaquarks in 920 GeV pA collisions*, Phys. Rev. Lett. **93 (21)**, 212003 (2004), [doi:10.1103/PhysRevLett.93.212003]

[104] M. J. Longo *et al.* (HyperCP Collaboration), *High statistics search for the $\theta^+(1.54)$ pentaquark state*, Phys. Rev. D **70 (11)**, 111101(R) (2004), [doi:10.1103/PhysRevD.70.111101]

[105] A. Aleev *et al.* (SVD Collaboration), *New analysis on narrow baryon resonance decaying into pK^0_S in pA-interactions at 70GeV/c with SVD-2 setup* (2008), arXiv:0803.3313v2 [hep-ex]

[106] R. N. Cahn, G. H. Trilling, *Experimental limits on the width of the reported $\Theta(1540)^+$*, Phys. Rev. D **69 (1)**, 011501(R) (2004), [doi:10.1103/PhysRevD.69.011501]

[107] L. Camilleri, *Precision Measurements in Neutrino Interactions*, Nucl. Phys. B Proc. Suppl. **143**, 129-136 (2005), [doi:10.1016/j.nuclphysbps.2005.01.097]

[108] S. V. Chekanov, B. B. Levchenko, *Influence of experimental resolution on the statistical significance of a signal: Implication for pentaquark searches*, Phys. Rev. D **76 (7)**, 074025 (2007), [doi:10.1103/PhysRevD.76.074025]

[109] A. Aleev *et al.* (SVD Collaboration), *Further study of narrow baryon resonance decaying into $K^0_S p$ in pA-interactions at 70 GeV/c with SVD-2 setup*, NPI-MSU-2005-22-788 (2005), arXiv:hep-ex/0509033

[110] Ya. Azimov, K. Goeke, I. Strakovsky, *Explanation why the Θ^+ is seen in some experiments and not in others*, Phys. Rev. D **76 (7)**, 074013 (2007), [doi:10.1103/PhysRevD.76.074013]

[111] M. Düren, *The HERMES Experiment: From the Design to the First Results*, Habilitation Thesis (1995), DESY-HERMES 95-02

[112] K. Ackerstaff *et al.* (HERMES collaboration), *The HERMES spectrometer*, Nucl. Instr. Meth. A **417 (2-3)**, 230-265 (1998), [doi:10.1016/S0168-9002(98)00769-4]

[113] B. Sobloher, *Polarisation and Polarimetry at HERA* (2012), arXiv:1201.3836v1 [physics.ins-det]

[114] J. Buon, K. Steffen, *Hera variable-energy "mini" spin rotator and head-on ep collision scheme with choice of electron helicity*, Nucl. Instr. Meth. A **245 (2-3)**, 248-261 (1986), [doi:10.1016/0168-9002(86)91257-X]

[115] A. Airapetian *et al.*, *The HERMES polarized hydrogen and deuterium gas target in the HERA electron storage ring*, Nucl. Instr. Meth. A **540 (1)**, 68-101 (2005), [doi:10.1016/j.nima.2004.11.020]

[116] M. Düren *et al.*, *Test of a polarized hydrogen gas target based on the storage cell technique*, Nucl. Instr. Meth. A **322 (1)**, 13-19 (1992), [doi:10.1016/0168-9002(92)90352-5]

[117] C. Baumgarten *et al.*, *The storage cell of the polarized H/D internal gas target of the HERMES experiment at HERA*, Nucl. Instr. Meth. A **496 (2-3)**, 277-285 (2003), [doi:10.1016/S0168-9002(02)01752-7]

[118] A. Nass *et al.*, *The HERMES polarized atomic beam source*, Nucl. Instr. Meth. A **505 (3)**, 633-644 (2003), [doi:10.1016/S0168-9002(03)00986-0]

[119] C. Baumgarten *et al.*, *An atomic beam polarimeter to measure the nuclear polarization in the HERMES gaseous polarized hydrogen and deuterium target*, Nucl. Instr. Meth. A **482 (3)**, 606-618 (2002), [doi:10.1016/S0168-9002(01)01738-7]

[120] C. Baumgarten *et al.*, *A gas analyzer for the internal polarized target of the HERMES experiment*, Nucl. Instr. Meth. A **508 (3)**, 268-275 (2003), [doi:10.1016/S0168-9002(03)01702-9]

[121] `https://hermes-wiki.desy.de/Triggers`

[122] J. T. Brack *et al.*, *The HERMES forward tracking chambers: construction, operation, and aging effects*, Nucl. Instr. Meth. A **469 (1)**, 47-51 (2001), [doi:10.1016/S0168-9002(01)00710-0]

[123] A. Andreev *et al.*, *Multiwire proportional chambers in the HERMES experiment*, Nucl. Instr. Meth. A **465 (2-3)**, 482-497 (2001), [doi:10.1016/S0168-9002(01)00691-X]

[124] S. Bernreuther *et al.*, *The HERMES back drift chambers*, Nucl. Instr. Meth. A **416 (1)**, 45-58 (1998), [doi:10.1016/S0168-9002(98)00674-3]

[125] W. Wander, *Reconstruction of High Energy Scattering Events in the HERMES Experiment*, PhD Thesis (1996), HERMES Thesis **97-031**

[126] W. Wander *et al.*, *DAD - Distributed ADAMO Database system at HERMES*, CHEP 95 Proc. 349-353 (1995), DESY-HERMES-**95-40**

[127] `https://hermes-wiki.desy.de/HTC`

[128] A. Airapetian *et al.*, *The HERMES recoil detector*, JINST **8**, P05012 (2013), [doi:10.1088/1748-0221/8/05/P05012]

[129] R. E. Kalman, *A New Approach to Linear Filtering and Prediction Problems*, J. Basic Eng. **82 (1)**, 35-45 (1960), [doi:10.1115/1.3662552]

[130] N. Akopov *et al.*, *The HERMES dual-radiator ring imaging Cherenkov detector*, Nucl. Instr. Meth. A **479 (2-3)**, 511-530 (2002), [doi:10.1016/S0168-9002(01)00932-9]

[131] D. M. Thiessen, *The Gas System for the HERMES Transition Radiation Detector*, Master Thesis (1995), HERMES Thesis **96-028**

[132] H. Avakian *et al.*, *Performance of the electromagnetic calorimeter of the HERMES experiment*, Nucl. Instr. Meth. A **417 (1)**, 69-78 (1999), [doi:10.1016/S0168-9002(98)00540-3]

[133] E. Cisbani, *The dual radiator RICH for the HERMES experiment at DESY* Nucl. Phys. B Proc. Suppl. **78 (1-3)**, 366-371 (1999), [doi:10.1016/S0920-5632(99)00572-1]

[134] R. Kaiser, *Likelihood Analysis for the RICH IRT Method* (2000), HERMES Internal Report **00-026**

[135] R. Lamb, A. Hillenbrand, *Event Level RICH algorithm: An explanation and user guide* (2007), HERMES Internal Note **07-017**

[136] J. R. Klein, A. Roodman, *Blind analysis in nuclear and particle physics*, Ann. Rev. Nucl. Part. Sci. **55**, 141-163 (2005), [doi:10.1146/annurev.nucl.55.090704.151521]

[137] `http://root.cern.ch`

[138] W. Verkerke, D. Kirkby, *The RooFit toolkit for data modeling* (2003), arXiv:physics/0306116 [physics.data-an]

[139] L. Moneta *et al.*, *The RooStats Project* (2011), arXiv:1009.1003v2 [physics.data-an]

[140] A. Airapetian, *MC studies on trigger 17/27 efficiency* (2005), talk at HERMES Collaboration meeting

[141] S. Wang *et al.* (Drafting Committee 75 of the HERMES Collaboration), *Search for a $|S| = 1$ baryon state with Improved HERMES Data, version 1.10* (2012), HERMES Internal Draft

[142] J. Podolanski, R. Armenteros, *Analysis of V-events*, Phil. Mag. Series 7 **45 (360)**, 13-30 (1954), [doi:10.1080/14786440108520416]

[143] S. Wang *et al.* (Drafting Committee 75 of the HERMES Collaboration), *Release report associated with search of hypothetic Θ^+ resonance decaying into proton and K_s*, (2010), HERMES Internal Report

[144] A. Airapetian *et al.* (Drafting Committee 75 of the HERMES Collaboration), *Additional evidence for a narrow $|S| = 1$ baryon state in quasi-real photoproduction* (2011), HERMES Internal Draft

[145] L. Felawka, *Using Hypothesis Testing for Theta+ Yield Consistency Checks* (2011), HERMES Internal Note **11-001**

[146] W. Yu *et al.*, *Study on Pentaquark State Θ^+* (2004), HERMES Internal Note **04-018**

[147] L. Rubáček, *Search for the Pentaquark States in Lepton-Nucleon Scattering at HERMES*, PhD Thesis (2006), HERMES Thesis **06-071**

[148] S. Wang, Y. Mao, B. Ma, *Detail Steps to Understand the Bump @1520 MeV on Invariant Mass* $M(pK_S^0)$ (2013), talk at HERMES Collaboration meeting

[149] S. Wang, Y. Mao, B. Ma, *Understanding the* Θ^+ *Resonance in HERMES* (2013), HERMES Working Plot

[150] M. Stahl, *Comments on the recently proposed cut on the angle* θ (2013), HERMES Working Plot

[151] M. Stahl, *Statistische Methoden zum Testen von Hypothesen mit RooStats am Beispiel eines Pseudo-*Θ^+*-Signals im* $\Lambda\pi^+$*-Kanal bei HERMES*, Studienarbeit (2013)

[152] G. Cowan, K. Cranmer, E. Gross, O. Vitells, *Asymptotic formulae for likelihood-based tests of new physics*, Eur. Phys. J. C **71 (2)**, 1554 (2011), [doi:10.1140/epjc/s10052-011-1554-0]

[153] A. L. Read, *Presentation of search results: the* CL_s *technique*, J. Phys. G **28 (10)**, 2693 (2002), [doi:10.1088/0954-3899/28/10/313]

[154] M. Stahl, *Particle-antiparticle-ratios* (2012), HERMES Working Plot

[155] G. Aad *et al.* (ATLAS Collaboration), *Observation of a new particle in the search for the Standard Model Higgs boson with the ATLAS detector at the LHC*, Phys. Lett. B **716 (1)**, 1-29 (2012), [doi:10.1016/j.physletb.2012.08.020]

[156] S. Chatrchyan *et al.* (CMS Collaboration), *Observation of a new boson at a mass of 125 GeV with the CMS experiment at the LHC*, Phys. Lett. B **716 (1)**, 30-61 (2012), [doi:10.1016/j.physletb.2012.08.021]

[157] E. Gross, O. Vitells, *Trial factors for the look elsewhere effect in high energy physics*, Eur. Phys. J. C **70 (1-2)**, 525-530 (2010), [doi:10.1140/epjc/s10052-010-1470-8]

[158] E. Gross, O. Vitells, *Statistics Challenges in High Energy Physics Search Experiments*, PoS **ACAT2010**, 007 (2010), [ACAT2010_007]

[159] W. K. Hastings, *Monte Carlo Sampling Methods Using Markov Chains and Their Applications*, Biometrika **57 (1)**, 97-109 (1970), [JSTOR:2334940]

[160] A. Gelman, W. R. Gilks, G. O. Roberts, *Weak convergence and optimal scaling of random walk Metropolis algorithms*, Ann. Appl. Prob. **7 (1)**, 110-120 (1997), [doi:10.1214/aoap/1034625254]

[161] M. Stahl, *Is there a* Θ^+ *in the* $\Lambda\pi^+$*-channel?* (2012), talk at HERMES Collaboration meeting

[162] `https://hermes-wiki.desy.de/Standard_Cuts#Fiducial_volume_cut`

Additional helpful literature for the first chapter of this thesis:

[163] D. J. Griffiths, *Introduction to Elementary Particles*, John Wiley & Sons (1987)

[164] I. J. R. Aitchison, A. J. G. Hey, *Gauge Theories in Particle Physics*, Institute of Physics Publishing (2004)

[165] A. Pich, *Quantum chromodynamics* (1995), arXiv:9505231 [hep-ph]

[166] W. Cassing, *Quantenchromodynamik und Näherungen*, Lecture notes (2012)

List of Figures

List of Tables

Acknowledgements

First I would like to thank Michael Düren for the opportunity to work on and study this interesting subject at such a diverse and complex experiment. He has given me the freedom to chose the direction of my studies on my own account and was always open to discussions. I would especially like to thank him for all the support of my work and the opportunity to continue my studies on the pentaquark at a time when the subject seemed to be concluded at HERMES.

I would also like to express my gratitude to Avetik Hayrapetyan who answered a huge amount of questions I had with a lot of patience, and was always able to spur my ambition on this particular and other interesting subjects in physics. We spent numerous hours on discussions about the pentaquark and the analysis, recent arXiv preprints, HERMES history and also lots of non-physics related subjects like Hessian and Armenian culture.
Շատ շնորհակալ եմ Ավետի՛ք։

Further I would like to thank the people at HERMES. I was only able to meet them a few times during my occasional stays at Hamburg (or Bilbao), but I always hat the feeling to be welcome and that my work is appreciated despite my level of education. I especially would like to thank the members of DC75 for fruitful discussions, and Gunar Schnell for reviewing this thesis.

I want to thank the members of our group here in Gießen. It was a pleasure to work in such a cordial and productive atmosphere. Moreover I would like to thank my friends and office mates Daniel, Erik and Julian for their help with formal programming knowledge or yielding physics discussions and of course for the spare time we spent together. My thanks also go to Marcel and Wayne for a "jävligt bra" semester in Umeå and some nice parties at home.

Zu guter Letzt möchte ich mich bei meinen Freunden und meiner Familie in und um Griedelbach bedanken. Danke für all die Unterstützung die ich von Euch erfahren habe und für das Verständnis, dass ich gerade in den letzten Wochen und Monaten wenig Zeit mit Euch verbringen konnte. Ein besonders herzlicher Dank gilt meinen Eltern, die mich immer gefördert, und mir das Leben erleichtert haben.

Erklärung

Ich versichere, dass ich diese Arbeit selbstständig geschrieben und deren Inhalt wissenschaftlich erarbeitet habe. Außer der angegebenen Literatur habe ich keine weiteren Hilfsmittel benutzt.

Gießen, den 29.07.2013 Marian Stahl